WESTERN SYDNEY
UNIVERSITY

Generation of human pluripotent stem cell-derived micro-lenses to investigate lens development and lens toxicity

by

Michele Elizabeth Mason

B Medical Science (Advanced)

A thesis submitted to Western Sydney University
to fulfil the requirements for the degree of
Master of Philosophy (Medicine)

School of Medicine
Western Sydney University (Australia)

Supervisor: Dr Michael O'Connor
Co-supervisors: Dr Patrice Castignolles and Dr Marion Gaborieau

Statement of authentication

I hereby declare that this thesis contains no material that has been accepted for the award of any other degree or diploma and that, to the best of my knowledge and belief, this thesis contains no material previously published or written by another person, except where due reference has been made in the text of this thesis.

Michele Elizabeth Mason

Date: 28 March 2018

Acknowledgements

This thesis is the product of the work of one and the work of many. This project would not have been possible if not for the developmental work that preceded my involvement in it. Likewise, I could not have done this work alone. I acknowledge those who had a key contribution to my completion of this project and thesis. In particular, some technical aspects of the project required assistance, and I thank Dr David Harman (Western Sydney University, WSU) for his assistance with mass spectrometry analyses; Chitra Umala Dewi (WSU) for assistance generating the ROR1-enriched lens cells used in Chapter 3; and Prof Traian Chirila (Queensland Eye Institute, Australia) for provision of the silk fibroin.

Thank you to my primary supervisor, Michael O'Connor, for your guidance, helping me understand what is and is not possible, and for providing the opportunity for me to practice my resilience, patience, and determination. This project has been a valuable learning experience.

Many thanks to my co-supervisors, Marion Gaborieau and Patrice Castignolles, as you have always been there with advice and support when I needed you.

To all of my lab mates. Seaky and Mel, you guys rock. Thank you for all your support and for always having the time to share your lab hacks with me. Szeifoul, Chitra and Humayun, thank you for your friendship and for making every day at uni a pleasure. I have enjoyed your company and will miss you all very much.

Thank you also to the 'behind the scenes' crew who have been fundamental to my progress:

Sabine, my motorcycling buddy. We have been through so much together. I could not have gotten through this without you. You have always been there for me with support, advice, and hugs. David; Your encouragement, advice, and guidance have been invaluable, I am grateful that you have always had time for me when I needed you. Wendy; you always made me feel like I could do this. You never doubted me, and have always been there to celebrate or commiserate at every step along the way. For this, I am eternally grateful.

To my Friday Night Cheer Squad™; for always lifting my spirits at the end of the week and providing support, love, and humour, as required. To my offspring; William, David, Erin and Patrick; you have given me inspiration and motivation to keep going, no matter what. I wanted to show you that when you set your mind to something, you should do everything you can to reach your goal.

Mum, I know you would have been proud of me.

To you all. Thank you.

Table of Contents

List of Figures

List of Tables

List of Abbreviations

2D two-dimensional

3D three-dimensional

°C degrees Celsius

µL microliter

µm micrometer

ACN acetonitrile

AggreWell AggreWell 400™

Al aluminium

ARN age-related nuclear

BSA bovine serum albumin

BMP bone morphogenetic protein

Ca calcium

Cd cadmium

CO_2 carbon dioxide

CRYAA α-crystallin A chain

CRYAB α-crystallin B chain

CRYBA1 isoform A1 of β-crystallin A3

CRYBA2 β-crystallin A2

CRBA4 β-crystallin A4

CRYBB1 β-crystallin B1

CRYBB2 β-crystallin B2

CRYBB3 β-crystallin B3

CRYBB4 β-crystallin B4

CRYBS crystallin beta S

CRYGC crystallin gamma C

CRYGS crystallin gamma S

Cu copper

DAPI 4',6-diamidino-2-phenylindole

DG de-gassed

DMEM Dulbecco's Modified Eagle Medium

DMSO dimethyl sulfoxide

E3 a medium defined by the O'Connor laboratory for maintenance of lens epithelial cells in culture

EDTA ethylene diamine tetraacetic acid

ES embryonic stem

FACS fluorescent activated cell sorting

FGF fibroblast growth factor

g gravitational force

IOL intra-ocular lens

iPS induced pluripotent stem

ITS insulin-transferrin-selenium

LEC lens epithelial cell

LF lens fiber

LMP low melting point

MACS magnetic activated cell sorting

Mg magnesium

mL milliliter

mm millimeter

mM millimole per liter

MMP matrix metalloproteinase

NBF neutral buffered formalin

NGS normal goat serum

Nd:YAG neodymium-doped yttrium aluminium garnet

OFZ organelle free zone

PBS phosphate buffered saline

PCR polymerase chain reaction

PEG poly(ethylene glycol)

PEGSSDA poly(ethylene glycol) thiol-modified diacrylate

PS pluripotent stem

PTM post-translational modification

RNA ribonucleic acid

ROCK inhibitor Rho kinase inhibitor

ROR1 receptor tyrosine kinase like orphan receptor 1

Se selenium

SNP Single nucleotide polymorphism

SPE solid phase extraction

TFA trifluoroacetic acid

V vanadium

vol/vol volume per volume

WHO World Health Organisation

w/v weight per volume

Abstract

Cataract is an opacification of the eye's lens. It is the leading cause of blindness and causes life-impacting vision loss for millions of people worldwide. Currently the only treatment is surgical implantation of an intra-ocular lens. Due to the number of annual surgeries this approach is expensive and can result in a range of sight-affecting complications. Difficulties arise in accessing vision-restoring surgery for people with cataract living in developing countries due to inadequate access to cataract surgery. Greater understanding of cataract molecular mechanisms is required for development of anti-cataract drugs that may be easier to access than surgery. Several cataract risk factors have been postulated; however, their specific molecular mechanisms are poorly identified. This is due largely to a lack of functional human lens tissue available for studying cataract. Previous investigations of cataract have used animal models to study lens development and cataract; however, there are significant differences between humans and animal lenses including protein expression and cell membrane composition. Human pluripotent stem (PS) cells are a potential source of human lens cells and an elegant 3-stage protocol for generating lens cells and rudimentary lens tissue was published in 2010. Several groups have attempted to refine this protocol with varying success. Nevertheless, all of these approaches suffer from three main issues: i) production of heterogeneous cultures of human lens and non-lens cells; ii) poorly- or uncontrolled-production/loss of rudimentary lens tissue; and iii) limited or no evidence that the stem cell-derived lens tissues have focusing ability (a defining property of the lens). Very recent work in our laboratory overcame the first of these issues, allowing simple and large-scale production of purified, ROR1-positive human lens epithelial cells (LECs) from heterogeneous cell cultures generated from PS cells. This ROR1^{+} LEC purification protocol provided a starting point for this thesis to investigate conditions for generating light-focusing human lens tissue *in vitro*.

The studies presented here resulted in a method to produce tens-of-thousands of uniform, transparent and light-focusing human PS cell-derived lens organoids, termed micro-lenses. These micro-lenses appear able to model a clinically-relevant cataract associated with exposure to the cystic fibrosis drug Vx-770. These functional human micro-lenses represent a useful tool for drug discovery and toxicity.

In addition to the successes of producing the world-first human PS cell-derived micro-lenses, there were several lessons learned during this project. Repeated failures of the cells to survive and proliferate on RGDS-chitosan film negated some of the first approaches at human lens regeneration (i.e., attempts at producing a chitosan-based explant pair system); these difficulties required consideration of an alternate approach. A wider understanding of lens biology gave rise to the idea of trying to mimic non-human lens developmental in the lab, inspired by teleost lens development. This LEC aggregation method was made possible by thinking laterally and using simple, available, materials to replicate embryonic aspects of teleost lens development. This method ultimately proved successful in producing human PS cell-derived micro-lenses. Furthermore, the rapid assessment lesson learned by experiencing some unworkable situations in the course of the project were then applied during the hydrogel 3D growth environment trials. Repeatable aggregate loss in some hydrogels confirmed that the agarose-based gels best supported the developing micro-lenses and facilitated progression of investigation of micro-lenses derived from enriched ROR1 cells. Additionally, this project was not without its share of failures. Reflection upon these challenges and ascertaining the reasons for (and ways to move beyond) them have changed my approach to managing difficulties and improved my analytical abilities. These skills will be applied to my future undertakings.

Chapter 1

General introduction

1.1 Cataract

The eye's lens must be transparent with a high refractive index in order to focus light onto the retina. Cataract is a pathological condition that results in loss of transparency due to increased light scatter in the lens, resulting in impaired vision or blindness. Cataract is prevalent in our ageing population and the leading cause of preventable blindness worldwide (1). Cataract accounts for 35% of blindness globally, affecting approximately 12.6 million people in 2015 (2). By 2020 the estimated number of people worldwide to be blinded by cataract is 13.4 million (2). A further 57.1 million people worldwide are predicted to have moderate to severe visual impairment resulting from cataract (2). This continues a decades-long trend of increasing blindness/low vision due to cataract from 50.5 million combined in 1990 to 65.2 million in 2015, and 70.5 million predicted in 2020 (2).

Currently, the only treatment available for cataract is surgical implantation of a plastic intra-ocular lens (IOL), and this surgery is increasing in demand by an ageing population. Cataract surgery is one of the most commonly performed surgical procedures in the world yet the current levels of surgery are too low to cope with the load of patients with cataract (3). Additionally, due to population ageing, it is expected that there will be and increased demand for cataract surgeries; the number of people with moderate to severe visual impairment due to cataract is expected to increase by 8% between 2015 to 2020 (2) due to increased life expectancy and growth in ageing populations (4). The World Health Organization (WHO) global action plan (5) aims to decrease preventable blindness by 25% between 2010 and 2019, prioritizing cataract (4). Countries with a low human development index and lower gross domestic product per capita have a strong correlation with low numbers of cataract surgery (6). In developing countries, it can be difficult to access cataract surgery; for instance, many patients are hindered by poverty and/or the difficulty travelling to cities from rural areas (7). Additionally, a large backlog for cataract surgery exists due to both low available resources, and time taken to train surgeons (8).

In developing countries, such as Bangladesh and the Philippines, the economic burden of cataract is not limited to a decreased ability of the patient to work (9). Often, a secondary consequence of cataract-induced vision loss or blindness is the loss of income for a second, otherwise productive, family member, who is required to become a full-time carer for the untreated cataract patient (9). In addition to direct costs of cataract, loss of productivity (10) and social isolation (11) negatively affects the quality of life for the cataract patient (8).

Good quality vision is usually restored immediately after cataract surgery, though posterior capsule opacification (PCO) is a common side-effect that often appears after 2 or more years in a large number of patients and requires additional treatment to maintain visual acuity. The costs of treating cataract worldwide are increasing annually due to an increasing ageing population (4). The direct cost of cataract treatment was $326 million in Australia in 2004 (1). Internationally, billions of dollars are spent each year on cataract surgery. Identification of risk factors for cataract and and understanding of their molecular mechanisms could lead to identification of strategies that prevent or delay cataract, thereby minimising the debilitating effects and high costs of cataract-related vision loss.

Cataract surgery involves the removal of the cataract-affected lens from the eye – via phacoemulsification – followed by implantation of an IOL within the remaining lens capsular bag (a thin, transparent membrane that surrounds the lens). As mentioned, PCO is a prevalent complication that can follow IOL implantation (12). PCO occurs when lens cells not removed during primary cataract surgery proliferate and migrate to the posterior lens capsule and cause abnormal lens capsule wrinkling (13). The overall incidence of secondary cataract has been reported to be 28% at 5 years after cataract surgery (14). However, this increases to up to 70% in patients under 40 years of age (13) and 90% of pediatric cataract patients when the posterior capsule remains intact (15). Treatment of PCO generally involves posterior capsulotomy using a neodymium-doped yttrium aluminium garnet (Nd:YAG) laser (16). Hydrophobic IOL implants may reduce or delay the incidence of PCO compared to hydrophilic IOLs (14,17). However, any intervention after the primary cataract surgery leads to higher overall monetary cost preceded by a period of increasing functional vision impairment for the patient over the course of a few years.

Despite cataract being prevalent in the ageing population, congenital and childhood cataract can also occur with devastating effects, particularly on the social and intellectual development of the patient (10). Pediatric cataract is one of the most common causes of blindness in children, particularly in the developing world (18). Early recognition and treatment of lens opacity is essential to avoid deprivation amblyopia (18) whereby loss of vision in critical neurological developmental periods can cause permanent blindness. Congenital cataract requires early intervention to prevent amblyopia and surgery often takes place as early as 8 to 12 weeks of age (19). Infants may be implanted with an IOL at this stage (if access to follow-up surgery is limited; in these cases, the children require corrective spectacles initially before the child 'grows into' the corrective power of the IOL). Alternately, and more typically in developed countries, the childhood cataract patient does not undergo IOL implantation after cataract removal. Instead, the child remains aphakic for up to 2 to 10 years to allow the child's eye to grow. During this time, visual correction is provided by aphakic glasses or contact lenses (when environmentally appropriate, e.g. not in the Middle-East) until IOL implantation at a later date (19). These approaches all require multiple surgical interventions and the glasses/contact lens management techniques are often difficult and/or highly traumatic for the patients and their families (20).

1.1.1 Cataract risk factors

Cataract can be classified in a number of ways, including the location in the lens and the characteristics of the opacified area. The most common cataract type is age-related nuclear cataract (ARN) (21,22). Other types of cataract such as cortical cataract demonstrate a variety of forms including radial, dot and spoke shaped opacities (23). Multiple cataract risk factors (Table 1.1) have been postulated for age-related cataract; however, their mechanisms of action are yet to be fully established. Examples of end-point molecular changes thought to be responsible for disruption of light transmission through the lens include misfolding and aggregation of lens crystallin proteins in the lens (24-27) and the development of multi-lamellar membrane bodies (28). Color changes of the lens can also occur, termed brunesence, that have been attributed to crystallin glycation and the Maillard reaction of sugars in the lens (23,29). Single nucleotide polymorphisms (SNPs) have also been correlated with cataract in gene-gene and gene-environmental analyses (30). Difficulties arise in determining the causative mechanisms of cataract in human lenses due to severe difficulties in accessing useful quantities of intact/non-phacoemulsified human lenses or lens material across the timeframe of cataract development (particularly the early stages).

Table 1.1 Cataract types and risk factors

Risk factor	Type	Proposed mechanism
metal ion and tryptophan metabolites (31)	nuclear	crystallin cross-linking
cigarette smoking (32,33)	nuclear, posterior subcapsular	metal ions
hyperglycaemia (34,35)	nuclear, posterior subcapsular, cortical	glycation of crystallin
radiation: UV, electromagnetic, ionizing (36-38)	posterior subcapsular, cortical	includes instantaneous, long and short-term exposure
drugs (39)	posterior subcapsular	long term use of corticosteroids
alcohol (40)	age-related	cytochrome-induced oxidation / increased Ca permeability
age (41)	age-related nuclear	multilamellar bodies
age (42)	age-related	post-translational modification - methylation
multifactorial (32)	age-related	both multiple genes and environmental factors
oxidative stress (29,43)	age-related	miRNA regulation of oxidative stress genes, Maillard reaction
altered crystallin transcriptional activity (30,44)	age-related	CRYAA polymorphisms SNPs in ARC-susceptible Han population

Ideally, investigation of cataract risk factors requires a suitable 3-dimensional (3D) human lens model – capable of light transmittance and focusing ability - in order to examine how the molecular mechanisms of cataract formation lead to loss of lens function. Such a model must be accessible at every stage of cataract development and available in sufficient quantities to enable analysis of multiple replicates of exposure to suspected cataract causing agents via a range of detection techniques. The ability to test cataract risk factors such as smoking (33,45), oxidation (21,23,33,46,47), diabetes (34,35), electromagnetic radiation (48-50), ageing (23,29,51), UV light (24,38) and drugs in an *in vitro* human lens model would provide much-needed insight into the mechanisms operating at all stages of cataract formation – with concomitant identification of candidate pharmacological targets to delay or treat risk factor-specific cataract types.

1.2 Lens biology as a template for *in vitro* lens generation

Typical approaches to enabling investigation of cataract risk factors have been *in vivo* and/or *in vitro* analysis of animal lens models. These studies require detailed comprehension of lens anatomy, molecular biology and development and have provided further understanding of human lens biology. The following section reviews what is known about these processes.

1.2.1 Lens anatomy

Anatomically, the lens is a transparent, biconvex, avascular and non-innervated tissue located near the anterior of the eye, posterior to the cornea and iris (Figure 1.1). After light enters the eye through the cornea, the lens focuses it onto the retina. Lens function is intimately linked to its anatomical features. Postnatally, the lens consists of two cell compartments, lens epithelial cells (LECs) and lens fiber (LF) cells (Figure 1.2). The LECs form an anterior monolayer of cuboidal cells that are normally quiescent in the postnatal period apart from a ring of cells anterior to the lens equator (27). The progeny of these cells then gave rise to immature LF cells. Lens growth occurs through addition of new 'shells' of 'secondary' LF cells around previously generated LF cells. The oldest (i.e., primary) LF cells are located within the center (or nucleus) of the lens and, as described in more detail in Section 1.3, these oldest of LF cells are formed during embryonic development (52). The production of secondary LF cells involves extensive cell elongation to create highly ordered and tightly-packed concentric shells of cortical LF cells that have flattened hexagonal cross-sections (53) that overlay the older cells of the lens nucleus (54). The apical tips of the elongated lens cells typically have an apical-apical interaction with other lens cells, forming the anterior lens suture. In contrast, the basal tips of the LF cells maintain attachment to the lens capsule until they reach and contribute to the posterior lens suture (55). The lens sutures in primates have more complex branching than in other animals, over 12 branches in adult humans (56,57). Lens sutures are thought to allow for the ends of the LF cells to controllably realign when the lens accommodates, i.e. changes shape to focus (56).

Other key features of LF cell differentiation include: expression of large amounts of crystallin proteins (that provide the lens with its required refractive index); and the establishment of an organelle free zone (OFZ) via controlled degradation of all organelles (thereby increasing lens transparency by removing potentially light-scattering particles from the light path of the lens including the cell nucleus) (58-60). Nuclear degradation is a key process that contributes to maximal light transmission and reduced light scatter. Establishment of the OFZ occurs in the pre-natal period; however, this process has not been well documented in humans (60,61). Studies of early lens development have relied mainly on embryonic and postnatal chick, or mouse and rat lenses to examine nuclear and/or organelle degradation (58,62-65). Denucleation and organelle loss occurs may involve autophagy (58); however, the mechanisms involved are not fully clear.

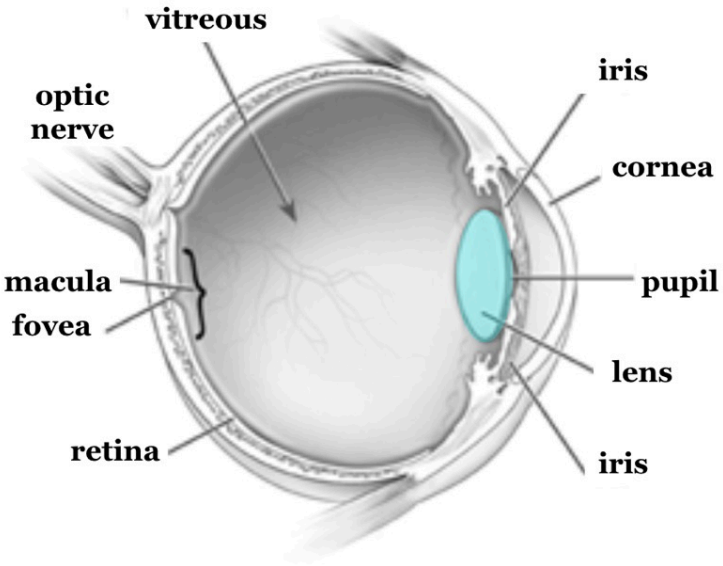

Figure 1.1 Structure of the eye

A cross-sectional diagram of the eye showing the location of the lens and other primary eye structures, as indicated. The lens is shown in blue (modified from (66)).

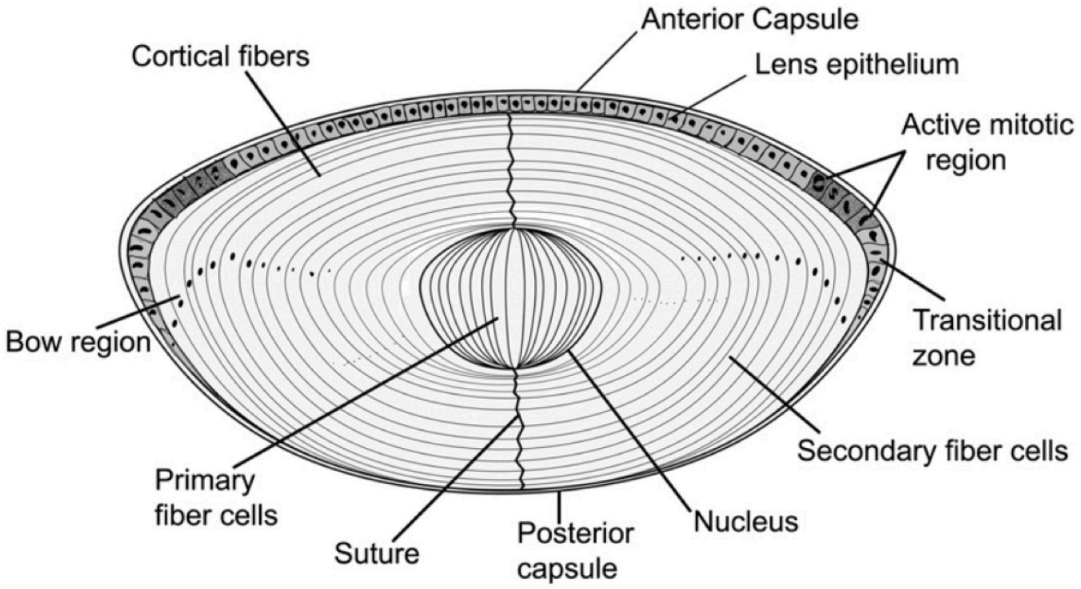

Figure 1.2 Structure of the mammalian lens

This diagram indicates the location of the anterior lens epithelial monolayer, transitional zone where LF cell differentiation begins, the lens nucleus (containing the primary LF cells), and the layers of secondary LF cells overlaying lens nucleus (54).

The predominant proteins within the lens are the abundantly expressed crystallins (67). LF cells express α-, β- and γ-crystallin proteins, whereas LECs express only α-crystallin protein (68). A marker of LF cells undergoing elongation is expression of β- and γ-crystallin proteins, concomitant with abundant production of α- crystallin (69,70). The high concentration of crystallin in the lens, approximately 50% of the wet weight, and the high refraction of the amino acids that compose γ-crystallin (71) contribute to the high light transmission properties of the lens. Interestingly, the crystallin proteins of the lens nucleus are present at birth and exist throughout life without being replaced (as terminally differentiated cells have lost their transcriptional machinery) (65). They are therefore amongst the longest-lived proteins in the body (72). Likewise, LF cells do not turn over, and the lens continues to grow throughout life by addition of LF cell layers (52). The longevity of crystallin proteins makes them susceptible to loss of solubility, aggregation and post-translational modifications that are among the speculated mechanisms of cataract formation.

The lens capsule (that surrounds the lens) is the thickest basement membrane in the body (73,74) and contributes to its ellipsoidal shape (53,75). The lens capsule also has a role in cell signalling in the developing and mature lens (73). Lens capsule proteins are secreted by both LECs and LF cells (73) and include collagen IV (the most abundant), laminin, perlecan and entactin/nidogen (76). These proteins provide protection and structure to the lens (73) while still providing permeability to nutrients and growth factors (77).

1.3 Mechanisms of lens development

1.3.1 Mammalian lens development

The structure of the mature lens described above is a consequence of a series of events that occur during embryonic development. In mammals, lens development begins with a thickening of the lens placode (Figure 1.3), a section of surface ectoderm in the early embryo (78). The cells of the lens placode proliferate, invaginate, then close and separate from the lens placode to form the lens vesicle (78). Cells in the posterior section of this spherical monolayer of lens progenitor cells then differentiate into primary LF cells in response to relatively high concentrations of fibroblast growth factor (FGF) present in the vitreous humour (Figure 1.1) (75,79,80). Elongation of the primary LF cells fills the lumen of the lens vesicle, generating the basic lens structure. Maturation of the primary LF cells involves nuclear and organelle degradation and expression of specific β- and γ-crystallin proteins (27). Mammalian lens development reflects genetic similarities with other species, including some invertebrates, even though the resulting lenses exhibit distinct morphological differences (81). There are a number of conserved genes and gene regulatory networks that are highly conserved in both mammals and other species (81). For example, transcription factors *Pax6* and the *Sox* family is conserved in invertebrates such as *Drosophila* in addition to vertebrates and mammals functioning in both as induction of the lens placode and LF cell differentiation (81). Regulatory signalling pathways involving Wnt and BMP are conserved across vertebrate species (81,82). Likewise, cell adhesion molecules E-cadherin and N-cadherin are expressed in both invertebrate and vertebrate lenses (81). Additionally the predominant lens protein crystallin is highly conserved at the gene level and have widespread expression in the lens among species (71,82-85). Lens growth continues throughout life as a result of LEC proliferation at the lens equator, followed by differentiation to secondary LF cells that form layers of tightly packed, elongated, LF cells that overlay the older cells of the lens nucleus (Figure 1.2) (53).

1.3.2 Teleost lens development

Like early mammalian lenses, lens development in teleost species such as the Zebrafish (*Danio rerio*) commences with a thickening of the lens placode and proliferation of these lens progenitor cells (86). However, in contrast to mammalian lens development, these proliferating lens progenitor cells form a solid aggregate of cells (87) called a lens cell mass (i.e., not a lens vesicle with an acellular lumen). This lens cell mass separates from the lens placode (Figure 1.3), after which cells within the lens cell mass differentiate to form primary LF cells. Secondary LF cells are added in a concentric arrangement similar to the process described above for mammalian lenses. The mature Zebrafish lens structure is almost spherical during prenatal development (rather than ellipsoid as in humans) yet the final lens shape has distinct and recognizable similarities to a mammalian embryonic lens (88).

Figure 1.3 Comparative development of mammalian and teleost lenses

The mammalian lens (left) is formed from a thickened lens placode (left, top) that extends and invaginates to form a vesicle lined with a monolayer of LECs that differentiate, at the equator of the vesicle, to produce LF cells that fill the vesicle (left, bottom). The Zebrafish lens (right) commences development with a thickening of the lens placode (right, top) that continues to thicken and form a ball-like mass that separates as LF cells are added in a concentric configuration (right, bottom). (Modified from (87)).

The differing early developmental structures of mammalian and teleost lenses result in broadly similar lens structures and functions. In the laboratory, formation of a lens vesicle-like structure comprised of paired rat LEC explants (Figure 1.4) has been used to generate functional (Figure 1.5), physiologically-sized rat lenses (89). The time and labor-intensive nature of that system restricts its capacity to generating only small numbers of rat lenses *in vitro* for studies of cataract development (89). Also, it still represents an animal-based model of lens function. A simple and robust system for reproducibly generating large numbers of light-focusing human lenses, perhaps by gaining insight from an aspect of the teleost developmental morphology and arranging a quantity of $ROR1^+$ LECs into a spherical shape that resembles the ball-like mass of teleost lenses to produce human lens tissue *in vitro*, could benefit study of lens development and cataract.

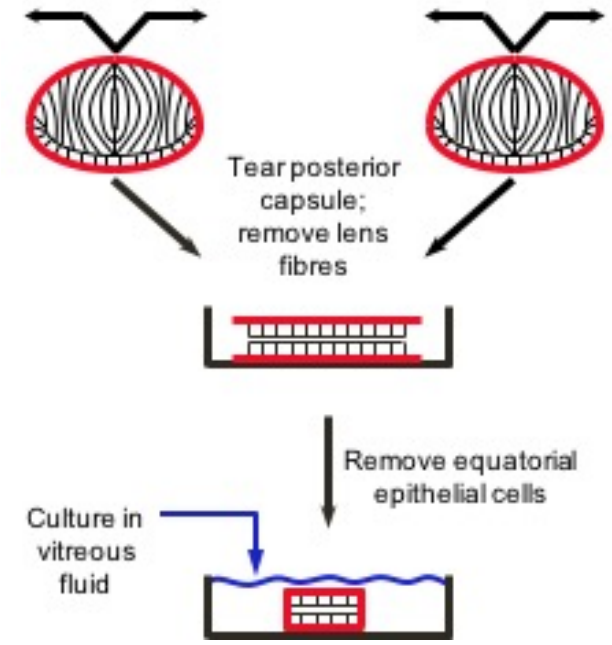

Figure 1.4 Rat explant pair-based lens regeneration

Schematic diagram showing how the anterior epithelial monolayer of rat lenses were harvested, trimmed to remove partly differentiated equatorial LF cells then paired to simulate the lens vesicle *in vitro*. Placement of the bottom LEC monolayer in contact with the plastic culture dish provided an approximation of the polarized exposure to vitreous fluid seen *in vivo.* (89).

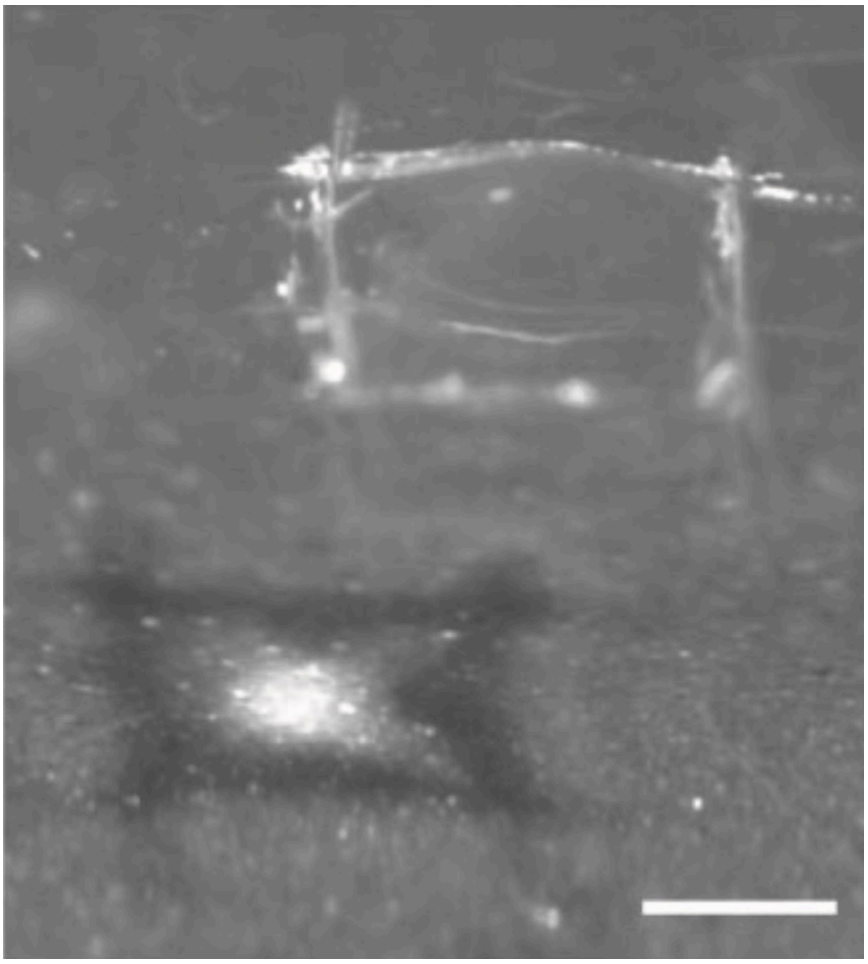

Figure 1.5 Rat lens explant pair produced a lens that had focusing ability

A light-focusing *in vitro* rat lens generated from paired rat LEC explants demonstrating the ability of these *in vitro* generated tissues to focus light. Scale bar 500 µm (89)

1.4 The necessity for an *in vitro* human lens model

Morphological and genetic differences between species mean that the current use of animal lens models may be insufficient to address the need for research on human lens tissue (22). Likewise, human lens tissue from the embryonic developmental phase or healthy and light-focusing adult human lens tissue are difficult to procure (22). Human pluripotent stem (PS) cells are an emerging technology that enables large-scale production of normal or diseased human cells or tissue. Development of a human lens model that possesses similar functional, anatomical and molecular properties to normal human lenses - particularly the ability to focus light - as well as the ability to be produced in large quantities could fulfil the need for studies of lens development, assessment of cataract risk factors, clinically relevant toxicity assays and anti-cataract drug screening. Candidate drugs that can cause cataract could be utilized to validate a lens tissue model.

Encouragingly, human PS cells can be differentiated via a 3-stage protocol into heterogeneous populations containing lens cells (90). Several groups have attempted to produce human lens-like tissues after generating lens cells following the 3-stage method (91-93). However, rudimentary lens tissues produced using any of these methods have key limitations, including abnormal surface attachment and lack of demonstrated light focusing ability (91). Functional human lens tissue would be an invaluable aid to further lens biology research and gain a better understanding of molecular mechanisms of cataract, particularly if human lens tissue models could be generated simply and efficiently in large numbers.

1.5 The role of pluripotent stem cells in *in vitro* lens production

Much of our understanding of early lens development has been obtained by investigating animal models that have developmental and physiological similarities to humans. However, the development of human PS cell technology offers the opportunity to generate large numbers of normal (or diseased) human cells *in vitro*. This is because human PS cells can differentiate into any cell type in the body, given the appropriate spatio-temporal combination of growth factors. Human PS cells are able to indefinitely self-renew due to high levels of telomerase expression that maintains the telomere length and is associated with human cell line immortality (94). The most commonly used human PS cells are embryonic stem (ES) cells and induced pluripotent stem (iPS) cells.

Human ES cells are obtained from surplus preimplantation stage blastocysts (5 to 14 days post-fertilisation) (94-96), donated with informed consent from *in vitro* fertilisation programs (97). Human ES cells are obtained from the inner cell mass (94,96) of human blastocysts 5 to 14 days post fertilisation. At this stage, the embryo is composed of the trophoblast that forms the outer layer (cytotrophoblast for attachment to the uterine wall) and placenta (syncytiotrophoblast), and the inner cell mass that undergoes gastrulation to form the embryo (95). Human PS cell lines can be also be derived from a single cell blastomere that is removed during preimplantation genetic diagnosis (PGD) (98). Notably, human ES cell lines can be derived from normal embryos, or embryos containing disease-causing congenital mutations identified via PGD.

In contrast, human iPS cells are somatic cells that have been reprogrammed to a pluripotent, embryonic-like state by forced expression of transcription factors involved in pluripotency (99,100). Human iPS cells can be used to generate normal or patient/disease specific pluripotent cell lines with which to study the mechanisms of the disease in an *in vitro* model (101). Human iPS cells avoid some of the ethical issues associated with the derivation of human ES cells and can also provide the ability for disease modeling without the need for PGD.

1.5.1 Production of lens cells from human PS cells *in vitro*

The 3-stage growth factor method for generating heterogeneous populations of LECs and subsequently, LF cells, from human ES cells was published in 2010 (Figure 1.6) (90). The method involves exposure to a progressive sequence of growth factors that regulate cell fate chosen to mimic aspects of embryonic lens development *in vitro.* The first stage introduces Noggin for 6 days to inhibit Bone Morphogenic Protein (BMP) signalling and thus differentiate the human ES cells towards a neuroectoderm fate (90). The 12-day long second stage introduces BMP4 and BMP7, as well as Fibroblast Growth Factor 2 (FGF2) to induce production of lens placodal cells (i.e., LEC progenitor cells) (90). A third stage that uses FGF2 and WNT3a stimulates differentiation of LECs to LF cells (85,90).

This 3-stage method represents a simplification of the growth factor regulation of the lens developmental process. First the development of neuroectoderm is prompted by Noggin, an antagonist of BMP (102), followed by induction of LECs. The growth factors FGF and BMP interplay to promote LEC differentiation, with a low concentration of FGF encouraging proliferation of LECs (103). The final stage represents the most complex growth factor relationships. Wnt regulates embryonic lens formation and is a highly conserved molecule amongst different species (104). Wnt is important for elongation and primary LF cell differentiation (102,104) as it is implicated in cytoskeletal arrangement (103) and migration; explanted LECs migrate along a Wnt gradient (75). The growth factor FGF is required for induction of LF cell fate from LECs (104) with a dose dependent respose; low concentratons of FGF promote proliferation of LECs and a higher dose promotes LF differentiation (75,103). Together with FGF, Wnt modulates the transition of LECs to LF cells using the aforementioned 3-stage method (90), although the mechanisms of Wnt and FGF signalling together remain unclear (102). The effectiveness of this 3-stage protocol is demonstrated by the fact that it has been replicated by a number of research groups using a variety of human PS cells (91-93).

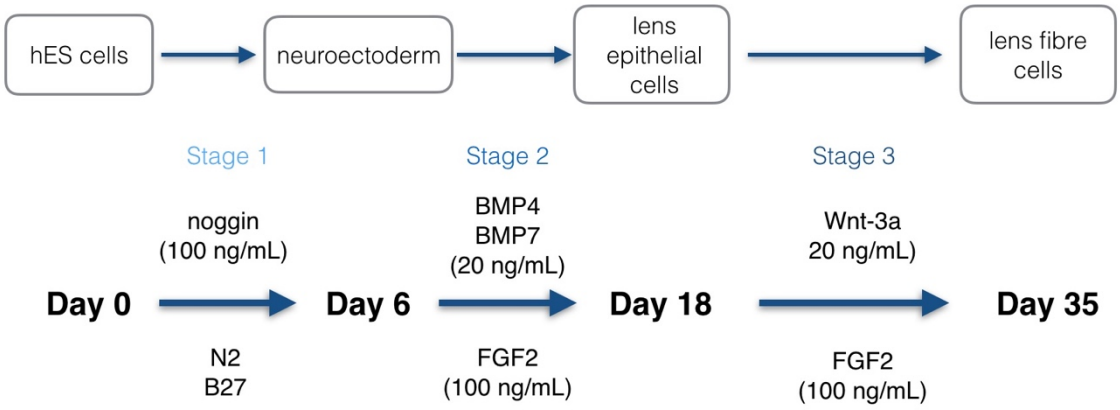

Figure 1.6 Generation of lens cells from human PS cells

The 3-stage process introduces a sequence of growth factors that stimulate human PS cells towards a neuroectoderm fate followed by lens cell production, resulting in a heterogeneous mixture of non-lens cells and spontaneously generated 'lentoids' that contain LECs and LF cells. Adapted from (90).

Whilst this elegant 3-stage lens differentiation method (90) does produce LECs and LF cells, the method does have some important limitations. The resulting cell population is a heterogeneous mixture of LECs, LF cells and non-lens cells. An impure population of cells gives uncertainty as to the cell type obtained when harvesting the cells for downstream applications. The inability to selectively harvest pure LECs or LF cells from the originally published differentiation method can make interpretation of data from this system challenging.

Additionally, random production of lens-like tissue occurs in the later stages of cell cultures following the 3-stage method (90). Production of abnormally adherent lens-like clusters - called lentoids - occurs randomly in the culture dish. The lentoids produced are then frequently observed to be lost from the culture surface into the culture medium (90). Furthermore, the lentoids have no reported ability to focus light, a fundamental requirement of the lens (105). This is unsurprising given the highly organized nature of the lens and the relatively disorganized structure of these spontaneously generated lentoids. Similar data have been obtained by other groups. For example, Qiu *et al,* (106) recently harvested lens cells from a cataract patient, reprogrammed them to a pluripotent state, then differentiated the resulting iPS cells to become lens cells. As with Yang *et al*, this approach yielded a mixed cell population of non-lens cells, LECs and LF cells (90). Comparably, Li and colleagues (93) harvested cells from the anterior LECs of lenses removed from cataract patients. These cells were induced to pluripotency then, following the 3-stage protocol (90), differentiated back into a (mixed population of) LECs (93). Whilst these studies demonstrated the possibility of generating lens cells from iPS cells, with or without a genetic-based disease state, the methods were insufficiently developed to yield either pure LEC populations or produce discrete and light-focusing lens tissue.

1.5.2 Improvements to lens cell production from human PS cells

Attempts at purifying lens cells from mixed cultures of differentiating human PS cells have seen variable success. Adopting an approach alternative to the Yang method, Mengarelli and Barberi (107) cultured human ES cells in insulin-transferrin-selenium (ITS) medium and separated the resulting mixture of cells via fluorescent activated cell sorting (FACS). Adult lens surface markers, c-Met/HGFR and CD44 were used to positively select and separate lens cells that were then cultured (107). However further culture of these cells revealed that the population was impure and included neuronal cells (107). Furthermore, the lens cell population had poor survival and proliferation, demonstrating the necessity for a more appropriate lens culture medium capable of retaining the morphology of the LECs.

More recently, Fu and colleagues (91), generated tens of lens-like tissues in a highly manual and semi-controlled manner. While these structures developed a small amount of magnifying ability, they remained abnormally attached to the cell culture dish. More recently, our group developed a method of producing large numbers of purified human LECs via magnetic-activated cell sorting (MACS) using an embryonic lens cell-specific marker, the ROR1 (receptor tyrosine kinase like orphan receptor 1) surface antigen identified by a previous PhD student from our laboratory using a bioinformatic approach (108). These ROR1^{+} LECs displayed similar morphology, gene expression and protein expression to human fetal LECs (108). A subsequent combinatorial growth factor screening approach identified a medium capable of proliferating the ROR1^{+} human cells while maintaining their LEC-like features. This large-scale source of purified human LECs raised the possibility of developing a highly controlled 3D culture system capable of generating light-focusing human lens tissue.

1.5.3 Organoids as model tissues

While the generation of human cell types from PS cells has advantages over studies of animal tissues, investigation of cell monolayers cannot replicate the finely-tuned and complex interactions produced by cells within organs. Recent advances in stem cell manipulations *in vitro* have seen development of miniature-sized organ counterparts called organoids. These *in vitro* organoids resemble their full-size *in vivo* counterparts in terms of cell type, cellular organisation and function. They have become an increasingly utilized tool for the study of organ development and for producing tissues for disease-in-a-dish models (109). Organoids may be derived from tissue specific adult stem (AS) cells (110,111), human ES cells or iPS cells (101,112,113).

Organoids have been developed for several tissue types thus far including liver (114), brain (115), intestine (116), lung (117) and kidney (118-120). Rudimentary eye-related organoids have also been developed including the lentoids described above, as well as retina and optic cups (121). These organoids are being used to study normal organ development and diseased-state organs. For example, gut organoids have been used for investigation of the effects of rotavirus infection in the intestine (122) and brain organoids have been used to help understand the effect of Zika virus (that can cause microcephaly in the fetus) on the brain (123). Moreover, organoids have the potential to be useful for drug toxicity and therapeutic drug screening, particularly if produced in large quantities (111). Due to the specialized and intensive nature of culturing stem cell-derived organoids, production of large quantities of organoids is not always possible. The ability to simply and reproducibly generate large numbers of light-focusing human lenses from human PS cells in a controlled manner would overcome many of the limitations inherent to the existing lens differentiation protocols, thereby offering detailed molecular insights into human lens and cataract formation.

1.6 Hypothesis and aims

1.6.1 Hypothesis

That aggregation of human PS cell-derived purified ROR1^{+} LECs to mimic a teleost lens cell mass, can produce large numbers of light-focusing human micro-lenses, suitable for studies of lens development and cataract formation.

1.6.2 Aims

1. To examine whether human PS cell-derived purified ROR1^{+} LECs can generate large numbers of functional micro-lenses *in vitro.*

2. To test the capacity of human PS cell-derived micro-lenses to evaluate clinically-relevant drug-induced lens toxicity (by assessing the effects of the cystic fibrosis drug Vx-770).

3. To investigate possible improvements to micro-lens production by assessing alternative starting cells and growth conditions.

Chapter 2

Generation of *in vitro* human micro-lenses

2.1 Introduction

2.1.1 Limitations of current lens-like models

The breakthrough method to produce lens cells from human PS cells by Yang et al. (90) provided a means to generate lens cells and lentoids *in vitro*. Whilst this elegant 3-stage lens differentiation method (90) produced lens cells, the method has some important limitations. The cell population produced was a heterogeneous mixture of LECs, LF cells and non-lens cells, with up to 59% of cells not expressing αA-crystallin. Use of such an impure population of cells gives uncertainty about the cell types being assessed and the responses detected in downstream applications. Additionally, within this 3-stage lens cell differentiation protocol, the lentoids produced are of variable size, non-adherent and are lost into the culture medium and subsequently removed during medium changes. These properties make them difficult to capture and investigate. Moreover, these lentoids have not been shown to have measurable light transmission or focusing capacity. These factors limit the usefulness of the produced lentoids to be harnessed for studying lens development or as a model for investigation of cataract. As a result, several groups have attempted to improve the method to produce more normal lens-like tissues from human PS cells (91-93).

A useful system for studying lens development or for high-throughput drug screening would have the ability to produce large quantities of non-adherent, uniform, light-focusing lens-like tissues. A recently described (91) effort to produce lens organoids utilized mechanical separation of lens epithelial-like cells, cultured to produce a 3D structure surrounded by non LF-like cells. This was the “fried egg” lentoid body structure described by Fu (91). The “fried egg” lentoids demonstrated magnification properties; however, they remained adherent to a two-dimensional (2D) culture surface. The generation of “fried egg” lentoid bodies using iPS cells was highly manual and laborious, and produced few lens-like structures (91) therefore is impractical for use as a high throughput drug screening tool.

2.1.2 Mimicking cross-species development to produce an *in vitro* lens

There are several obstacles evident when devising a method to replicate human lens development in an *in vitro* environment. The mammalian lens development process involves the formation of a lens vesicle, a hollow ball of LECs. In turn, this vesicle is exposed to a gradient of growth factors (including FGF signaling) (75,124) that polarise the lens to produce an anterior LEC monolayer and a large posterior fiber cell compartment.

A previous attempt at an *in vitro* lens generation by our group revealed that by mimicking aspects of embryonic lens development *in vitro,* production of correctly organized, light focusing lens tissue was possible (89,125). Key lens features of the rat LEC-derived 'paired explant' *in vitro* lenses included transparency, light focussing, expression of mature lens proteins, β-crystallin and γ-crystallin and organelle loss consistent with terminal LF cell differentiation. The rat lens explant pair demonstrated that taking an approach that replicated mammalian lens development *in vitro* was sufficient to produce *de novo* lens tissue. However, as mentioned above, the manual nature of this process means it is not amenable to generation of large numbers of lenses for high-throughput studies. While a method for generating large numbers of mouse lens vesicles *in vitro* has recently been developed, this process is highly complex and time consuming (126). Interestingly, differences in early developmental pathways, as previously shown in teleost and mammalian lenses, can result in both a functionally and structurally similar lens. Both mammalian and teleost lenses retain similar crystallin proteins (83,127), despite demonstration of different lens precursor structures (Figure 1.3) (87).

Recently, our group recently published a method for purification of ROR1$^+$ LECs from human PS cell cultures (108). The aim of the work in this Chapter was therefore to test whether these ROR1$^+$ cells could be used to generate uniformly sized, non-adherent light-focusing human lens tissue *in vitro,* suitable for lens toxicity screening and drug discovery. Therefore, aggregation of human PS cell-derived ROR1$^+$ lens cells into a ball-like mass to replicate teleost lens development was tested for production of functional human lens-like tissue *in vitro* (128). This approach was chosen as it held the potential to generate large numbers of similarly-sized, and similarly developmentally-staged micro-lenses suitable for high throughput drug screening. A commercial product, AggreWell, was used to aggregate the purified ROR1$^+$ lens cells to replicate the teleost-like lens ball-like mass. Using an AggreWell, it was possible to generate up to 1200 similarly-sized cell aggregates at once within each well of a 24-well plate.

2.1.3 Lens generation requires a 3D culture environment

Development and implementation of a 3D growth environment is a vital to provide non-adherent support for aggregate to micro-lens growth. When cell culture is performed on a 2D flat culture surface, the majority of the surface area of the cell is either attached to the culture vessel or exposed to the medium and only a small surface area of each cell is in contact with surrounding cells. Cell-cell signalling is essential for normal cellular processes including proliferation and differentiation (129). Furthermore, responses to stimuli are more predictable with 3D organoid forms than in 2D culture (129), as 3D cell culture more accurately reflects the *in vivo* environment (130). Therefore, producing lens-like tissue in a 3D environment is a natural progression from, and improvement to, 2D culture.

An advantage that the aggregated lens cell ball-like mass has over an explant-pair monolayer is the 3D cell-cell contact that results from forced aggregation of the cells. Several benefits apply when cells are cultured in 3D rather than traditional 2D culture. The aggregated LEC model replicates the *in vivo* teleost lens development environment, whereby the majority of aggregated cells in 3D culture are surrounded by and interacting with other cells (131). This cell-cell interaction is possible in 3D culture, but less so in 2D culture, therefore aggregates in 3D culture may have greater similarity to *in vivo* counterparts (132).

A suitable 3D growth environment must have several properties that allow for culture of the lens cell aggregates. The 3D growth environment is required to support and contain the aggregates (without them attaching to the culture vessel) and allow for nutrient and gas exchange. Likewise, it must be sufficiently permeable to growth factors to allow the correct cell-signalling for differentiation of LECs to LF cells to occur. The 3D growth environment must be adequately transparent to allow visualisation of the aggregates as they develop. Ideally, the 3D growth environment will enable an FGF gradient to occur. This would mimic the posterior-to-anterior gradient of high-to-low concentration, that occurs in the human eye, to control the differentiation of LF cells in a polarized manner (75).

2.1.4 Simple, relevant quantifiable assay for cataract research

Validation of any human lens organoid developed for cataract research requires the ability to induce cataract in the resulting tissue. A drug that has recently commenced use in treating cystic fibrosis, the chloride channel gating potentiator, Vx-770 (also known as Ivacaftor, Kalydeco) has been associated with non-congenital cataract in rat pups and long-term recipients of Vx-770 treatment (133,134). Due to the risk of cataract development, ophthalmological examinations of patients taking Vx-770 were recommended by the manufacturer (135) and recommendations to monitor ocular health were made during an efficacy and safety study over long-term use (136). The acknowledged risk of developing non-congenital cataract upon exposure to Vx-770 indicated that this drug was worthwhile investigating for cataract formation. Many of the patients with cystic fibrosis are young children, for whom development of a cataract would have adverse social and developmental effects (18).

Exposure of the aggregated lens cells to clinically-relevant doses of Vx-770 (137) during their developmental period may enable elucidation of induction of cataract by this drug. Additionally, candidate drugs that are known to cause cataract, such as corticosteroids (39), or are associated with cataract could be utilized to induce cataract and validate a lens tissue model. Once it is known that cataract may be induced, drugs currently considered to reverse cataract (138,139) may be tested directly in a human lens model. Measurement of light transmission and focusing ability of lens organoids could form a quantifiable assay for the effect of drugs on exposed lens organoids.

The addition of a human lens organoid to other currently developed human organoid tissues could also benefit drug-screening applications. Intestinal organoids were used to test the effects of Vx-770 on the *CFTR* gene (*CFTR F508del*) mutated chloride channel function. Interestingly, these intestinal organoids were derived from rectal biopsies from cystic fibrosis patients for the purpose of a drug screening assay (110). If Vx-770 can induce cataract in lens organoids, testing the toxicity of drugs on different types of organoid tissues becomes more relevant. Drug effects may be variable between different tissue types; determining which drugs benefit one system but damage another before they reach clinical trials in people is an ideal outcome.

The aims for this chapter include determination whether human PS cell-derived purified ROR1^{+} LECs can be aggregated to mimic the ball-like mass similar to teleost lens development and generate large numbers of functional micro-lenses *in vitro*. Additionally, such functional micro-lenses may be used to evaluate clinically-relevant drug-induced lens toxicity by assessing the effects of the cystic fibrosis drug Vx-770 on micro-lens development, light transmission, and light focusing properties.

2.2 Methods

2.2.1 Reagents and consumables

Reagents used for cell culture including mTeSR1, Dulbecco's Modified Eagles Medium (DMEM), and Dispase (Cat no. 07923) were acquired from Stem Cell Technologies (Melbourne, Australia). Reagents used in cell harvesting and antibody staining, including TryPLE Express and Dulbecco's Phosphate Buffered Saline (PBS) (Gibco Life Technologies, Cat no. 14190-250), were acquired from Invitrogen Corporation (Mulgrave, Australia), unless stated otherwise. Matrigel to coat tissue culture plates was acquired from BD Biosciences (North Ryde, Australia). Rho-kinase inhibitor (ROCK inhibitor) (Merck, Kilsyth, Australia) was used as an anti-apoptotic agent during cell passaging and experiment set up. DMEM:F12 (Thermo Fisher, North Ryde NSW, Cat no. 11330-057) was the base medium for all differentiation experiments.

All tissue culture plates (6-well, 96-well, 35 mm and 60 mm, T175 flask) and pipette tips used for general cell culture were acquired from Greiner Bio-one (Frickenhausen, Germany). General laboratory equipment included light microscope (Olympus CKX41 inverted microscope and accompanying digital camera (Olympus, Macquarie Park, Australia). A Beckman Coulter Allegra® X - 15R Centrifuge (Gladesville, Australia) was used for volumes from 1.5 mL to 50 mL. Volumes lower than 1.5 mL were centrifuged using a Beckman Coulter Microfuge 22R Centrifuge or QikSpin Personal Microfuge (Edwards Instrument Co., Narellan, Australia). Cells were incubated in a Heracell 150 CO_2 incubator at 37 °C, 5 % (vol/vol) CO_2 (Thermo Fisher Scientific). Non-sterile pipettes tips and glasswares were sterilized in a Tuttnauer 3150EL autoclave (Tuttnauer, Breda, Netherlands). All culture work was carried out in a Gelaire BH - EN 2000 D Series Class II Biological Safety Cabinet (Seven Hills, Australia) with surfaces disinfected with 70% ethanol prior to and after use.

2.2.2 Human PS cell maintenance and harvest

The human PS cell line CA1 was used (provided by Prof. Andras Nagy, Toronto, Canada) (108). Approval for use of these cells was obtained from the Western Sydney University Human Research Ethics Committee (approval number H10950).

CA1 cells were cultured in mTeSR1 and passaged every 7 days as clumps using 1 mg/mL dispase (140) on tissue culture dishes pre-coated with Matrigel (0.1 mg/mL in DMEM) for 30 minutes (min) minimum, after which the Matrigel was removed. CA1 cells were harvested for differentiation by making a single-cell suspension from 60 mm maintenance plates. In preparation, CA1 maintenance plates were incubated with 10 μM of ROCK inhibitor in mTeSR1 for 1 h minimum at 37 °C, 5% (vol/vol) CO_2. A single cell suspension was generated using 2 mL TrypLE for 7 min at 37°C, 5% (vol/vol) CO_2. The cells were removed from the culture plastic with a cell scraper and pipetted into a 15 mL tube. The plates were washed with 3 mL of PBS (-Ca/-Mg) and the wash added to the 15 mL tube. The tubes were centrifuged at 300 x *g* for 5 min, the supernatant removed and discarded. The cells were resuspended in 1 mL mTeSR1 containing 10 μM ROCK inhibitor. Cells were counted by placing 10 μL of the single cell suspension into a well of a 96 well plate and adding 40 μL of trypan blue (Gibco, Cat no. 15250061). The cell and trypan blue mixture was added to a haemocytometer (Bright-Line; Hausser Scientific, Pennsylvania, USA) and the cells were counted using an inverted light microscope.

2.2.3 Generation of heterogeneous cell population containing lens cells

Single cell suspensions of CA1 cells were cultured on a Matrigel-coated T175 flask in mTeSR1 medium until a tightly packed confluent monolayer was obtained. The culture medium was changed to Stage 1 medium: DMEM:F12 containing 100 ng/mL noggin (Miltenyi Biotech, Cat no. 130-103-456), 1x N2 supplement (Gibco Life Technologies, Cat no. 17502-048) and 1x B27 (Gibco Life Technologies, Cat no. 17504-044) with daily medium change for 6 days. The culture medium was then changed to Stage 2 medium: DMEM:F12 containing 100 ng/mL FGF2 (Miltenyi Biotech, Cat no. 130-093-842), 20 ng/mL BMP4 (Miltenyi Biotech, Cat no. 130-098-787) and 20 ng/mL BMP7 (Miltenyi Biotech, Cat no. 130-103-436) for at least 12 days with daily medium changes. The published 3-stage process was modified (Figure 2.1) so that on or near Day 18, the cells were harvested for purification by magnetic assisted cell sorting (MACS).

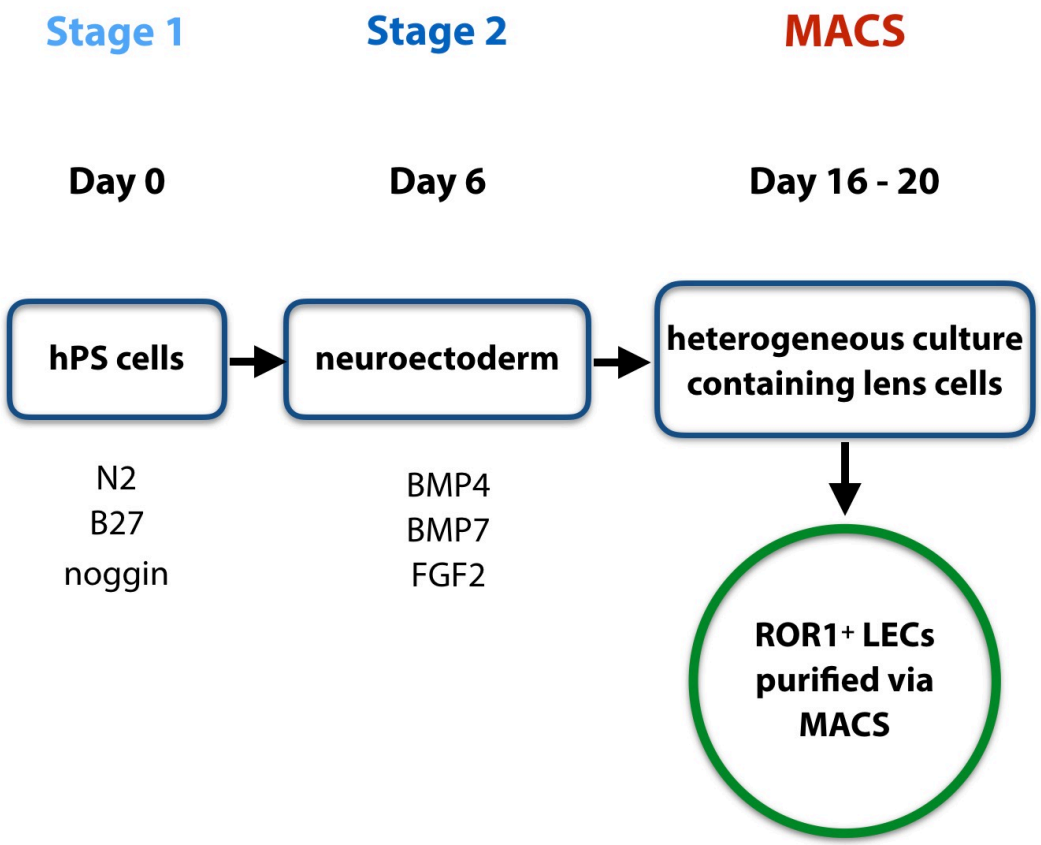

Figure 2.1 Modified 3-step human PS cell differentiation process

Schematic diagram showing the 3-stage process that induced PS cells towards the neuroectoderm fate then supplied growth factors that promote differentiation into lens cells. This process was modified so that between day 16 to 20, purified ROR1^{+} lens cells were extracted from the cell mixture. Adapted from (90).

2.2.4 Harvesting differentiated cells for MACS

Differentiating human PS cells in T175 flasks were incubated for 60 min with 10 μM ROCK inhibitor in cell culture medium. The cell culture medium was removed and 10 mL TrypLE added and the flask was incubated for 7 to 10 min until the majority of cells were dissociated. Remaining attached cells were removed from the culture surface with a cell scraper and the cell suspension removed by pipette to a 50 mL tube. The flask was rinsed with 12 mL PBS (-Ca/-Mg) and the PBS collected into the same 50 mL tube. The cell suspension was passed through a 40 μm nylon cell strainer (BD Biosciences) into a 50 mL tube. The cell suspension was equally divided between two 15 mL tubes then centrifuged at 300 x *g* for 5 min. The supernatant was removed and discarded, and the pellets resuspended each in 1 mL of cold MACS blocking buffer (2% (vol/vol) bovine serum albumin (BSA) (Miltenyi biotech, Cat no.130-091-376) and 2 mM ethylenediamine tetraacetic acid (EDTA). 10 μL of resuspended cells were removed for a cell count.

2.2.5 ROR1 antibody staining and MACS

Biotinylated antibody was prepared in advance. Anti-ROR1 antibody (R&D Systems, Cat no. AF2000) was diluted and biotinylated (Miltenyi Biotech, Cat no. 130-093-385) following the respective manufacturer's protocols. The 15 mL tubes were centrifuged at 300 x *g* for 5 min. The supernatant was removed and discarded, and the pellets resuspended each in 60 μL of cold MACS buffer (0.5% (vol/vol) BSA, 2 mM EDTA) and 40 μL of biotinylated ROR1 antibody per approximately 3 x 10^6 cells, at ice bath temperature. The cell and biotinylated antibody mixture were incubated at 4 ^oC for 20 min. 1 mL of cold MACS buffer was added to each 15 mL tube before the tubes were centrifuged (300 x *g,* 5 min). The supernatant was removed and discarded, and the pellets resuspended each in 80 μL cold MACS buffer and 20 μL of anti-biotin microbeads (Miltenyi, Cat no. 130-090-485) per 3 x 10^6 cells. Cells were then incubated at 4 ^oC for 15 min, after which 1 mL of cold MACS buffer was added to each 15 mL tube, followed by centrifugation (300 x *g*, 5 min). The supernatant was removed and discarded, and the pellets resuspended in 500 μL cold MACS buffer.

The cells were separated with the Miltenyi autoMACS Pro Separator (Miltenyi Biotec, Cat no. 130-092-545) with positive selection program (Figure 2.2). The collected cells were centrifuged (300 x *g*, 5 min), the supernatant removed and discarded, and the pellets resuspended in 1 mL E3 medium (108) with 10 μM ROCK inhibitor. The cells were counted and then plated on Matrigel-coated wells of a 6 well tissue culture plate (6wp) at 10^5 cells/ cm^2 in 2 mL E3 medium (with 10 μM ROCK inhibitor for the first 24 h only) then maintained in an incubator at 37 ^oC, 5% (vol/vol) CO_2. The E3 medium was changed daily thereafter until the $ROR1^+$ cells were confluent.

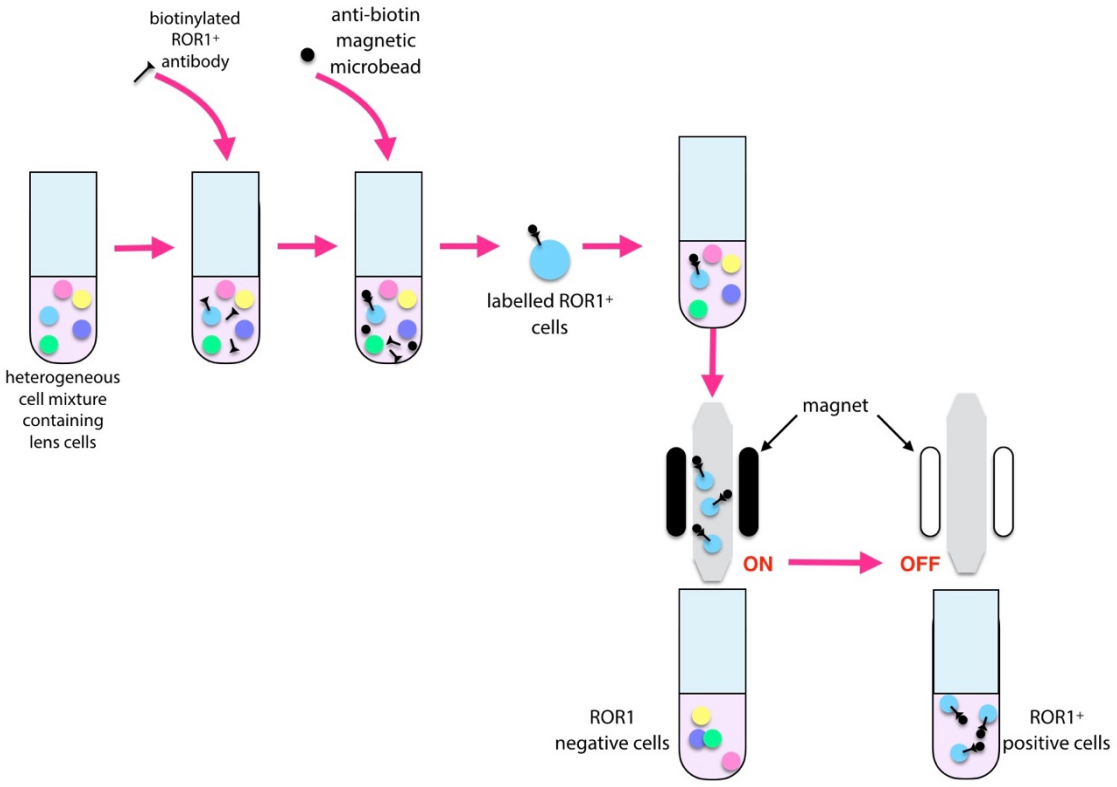

Figure 2.2 AutoMACS separation of ROR1$^+$ cells from lens cell mixture

The heterogeneous cell mixture containing ROR1$^+$ cells was mixed with biotinylated ROR1 antibody then anti-biotin microbeads. The mixture was passed through a magnetized column that retained labelled cells. The non-labelled cells were collected and discarded. The magnet is deactivated then the ROR1$^+$ cells are eluted and collected for culture.

2.2.6 Cell culture on silk fibroin and chitosan films

The procedure for mixing and casting chitosan films was adapted from (135). Chitosan powder 1.7 % (by weight) (medium molecular weight, lot number MKBH1108V, average degree of acetylation, DA, of 24 % of monomer units and viscosity of 563 cP in 1 % acetic acid) was mixed with a 2 % (by weight) acetic acid aqueous solution at room temperature (protected from light by wrapping in aluminium foil) for 5 days. The dispersion was centrifuged at 1076 ×g and 23 °C for 1 h. 10 mL aliquots were placed in a 9 cm Petri dish and dried at room temperature to form clear, colorless chitosan films. Briefly, 1 cm^2 sections of chitosan film were stirred with EDC-HCl (3 mg, 3.13 mM), NHS (2 mg, 3.48 mM), and peptide (RGDS, 1 mg, 0.46 mM) in PBS then placed on a shaker for up to 18 h then rinsed with PBS and ultrapure water, dried and stored at -20^{o}C (135).

The silk fibroin (courtesy of Prof Traian Chirila, Queensland Eye Institute, Australia), and RGDS grafted chitosan films (with a maximum of 5600 RGDS peptide units per nm^2 (135)), were prepared for cell culture by soaking overnight in PBS, coating with 1 mg/mL of Matrigel in DMEM and exposing to UV light for 1 h inside the biological safety cabinet. The silk fibroin was treated identically; however, it did not tolerate handling during this process and was eliminated from further testing. 5 x 10^5 purified ROR1$^+$ cells were added to each 3mm diameter sections of chitosan film, incubated at 37^{o}C for 30 min or until cells attached to chitosan film, then E3 medium was gently added to the culture vessel to submerge the chitosan films. Purified ROR1$^+$ cells were cultured on chitosan films from at least three separate differentiation experiments and they repeatedly failed to attach and proliferate.

2.2.7 Harvesting ROR1$^+$ cells and preparing aggregates

Briefly, AggreWell plates (Stem Cell Technologies, Cat no. 27845) were prepared as per the manufacturer's instructions (141) before ROR1$^+$ cells were collected via TrypLE. ROR1$^+$ cells were seeded into the AggreWell plates at 5 x 10^5 cells/well and aggregated by centrifugation at 300 x *g*, 5 min. The aggregates were cultured in the AggreWell plate for 24-48 h, then collected and embedded in 0.25% (w/v) agarose in M199 in 24 well plates. Aggregates were cultured in Stage 3 medium for up to 28 days, with daily medium changes.

2.2.8 Agarose embedding of ROR1$^+$ aggregates

A 1 L glass beaker containing 400 mL of sterile water, magnetic stirrer and thermometer was covered with aluminium foil. Two aliquots of 9 mL M199 (Gibco Life Technologies, Cat no.11150-059) was added to two separate 15 mL tubes and placed in the beaker. The agarose suspension was prepared by placing 0.5 g agarose powder (Amresco Agarose 1, Cat no. 0710-500G) in 50 mL M199 medium before heating in a microwave oven. To make 0.25% (w/v) agarose, 3 mL of 1% (w/v) agarose was added to the pre-warmed 9 mL M199, in the biosafety cabinet. The 15 mL tubes were returned to a beaker of 37^{o}C water before harvesting the ROR1$^+$ aggregates commenced. The agarose did not exceed 37^{o}C at the time of embedding to prevent the potential of heat exposure to change protein structure or gene expression of the aggregates.

2.2.9 Harvesting and embedding ROR1$^+$ aggregates

The aggregates in the AggreWell plate were gently triturated with a 2 mL pipette then carefully collected and placed in a 15 mL tube. Wells were washed with 1 mL E3 medium, the collection process repeated and the medium added to the tubes containing the aggregates. The aggregates were allowed to settle via gravity for 10-20 min. The supernatant was carefully removed leaving the calculated volume in the bottom of the tube sufficient to provide 50 μL of aggregates for each subsequent desired treatment.

A similar volume of PBS was placed in a second 15 mL tube to provide a visual guide to the final volume required in the aggregate-containing tube. To check the efficiency of the settling process, the removed supernatant was placed into a 35 mm or 60 mm dish and checked under the microscope for aggregates.

The settled aggregates were resuspended in the remaining volume before 50 μL aliquots were placed in the desired number of 24-well plate wells. Once this was done, 300 μL of 0.25% (w/v) agarose was added to each well. When the 0.25% (w/v) agarose was completely gelled, 500 μL of Stage 3 medium (DMEM:F12 containing 100 ng/mL FGF2 and 20 ng/ mL Wnt3a (R&D Systems Cat no. 1324-WN/CF) 20 ng/mL) was added to each well on top of the 0.25% (w/v) agarose. The cell culture medium was changed daily thereafter.

2.2.10 Measuring light transmission and light focusing ability

The aggregates were assessed at various times during the culture period for light transmission and light focusing ability. Images of each aggregate were taken at 5 positions. Using a light microscope and accompanying digital camera the aggregates were brought into focus and an image taken using the imaging software Q Capture Pro v6 (Q Imaging, Brisbane, Australia). Noting the number of rotations of the fine focus knob, the objective was moved to the point of maximal light focus and another image was taken. The objective was moved in the same direction for the same number of turns of the fine focus knob and another image taken. The objective was then raised to midway between each of the previously taken images and two other images taken (providing 5 images in total). Measurements of light transmitted and focal point intensity were obtained using the quantification function of Fiji ImageJ software, by quantifying approximately the central quarter diameter of the aggregate, and a similar measurement taken from the surrounding media. The data were analysed using the Kolmogorov-Smirnov test for normal distribution then subsequently analysed using the Student's t-test.

2.2.11 Mass spectrometry analysis of micro-lenses

Minimal sized segments of 0.25% (w/v) agarose containing micro-lenses were mechanically separated from the remaining 0.25% (w/v) agarose. The segments were homogenized using a micro-pestle (SSBio, Cat no. 1005-39) in 0.5% (w/v) RapiGest SF (Waters, Cat no. 186001861) on ice before reduction in 100 µL of 5 mM dithiothreitol (Calbiochem) in 50 mM NH_4HCO_3 then placed in a heating block for 1 h at 60 °C. Samples were then alkylated with 100 µL of 15 mM iodoacetamide at room temperature for 1 h then 200 ng trypsin (Promega, Cat no. V5280) in 75 mM NH_4HCO_3 added for protein digestion and placed in a heating block for 16 h, or overnight, at 37 °C.

The peptides were purified by solid phase extraction (SPE) using Waters Oasis HLB cartridges (Waters, Cat no. 186003908). The cartridges were washed with 1 mL acetonitrile (ACN) then 0.1% (vol/vol) trifluoroacetic acid (TFA) placed into the cartridge to condition the environment. The sample was acidified by adding 250 µL 0.4% (vol/vol) aqueous TFA to neutralize the buffer and deactivate the trypsin, then loaded into the extraction cartridge. Samples were washed with 1 mL 0.1% (vol/vol) TFA to remove salts then 1 mL ultrapure water to remove aqueous soluble unwanted material and TFA. Samples were eluted with 500 µL of 70% (vol/vol) ACN to 650 µL low binding collection tubes (Simport, Cat no. T330-6LST). ACN was evaporated from the collection tubes to dryness using rotational vacuum concentrator (Christ RVC 2-25 CD plus) for 3 h. 15 µL of 0.1% (vol/vol) formic acid was added to acidify peptide, rested for 30 min, triturated, then centrifuged (Dynamica Velocity 14R) for 10 min at 20 290 x *g*.

The formic acid solution containing the peptides was collected in glass vials and analyzed by LC-MS/MS using a nanoAcquity UPLC and Xeno QtoF mass spectrometer (Waters) using a nanoelectrospray source implementing a glass emitter tip which tapers to 10 µm (New Objective, Woburn MA). The analysis was carried out by Dr David Harman. The MS/MS data files were analyzed with Mascot Daemon and checked with SwissProt database with Homo sapiens-specific searches.

2.2.12 Immunofluorescence analysis of micro-lenses

Cultured micro-lenses were fixed within the surrounding agarose inside the 24-well plates using 10% (vol/vol) neutral-buffered formalin (NBF) (Sigma), then placed on a rocker for up to 48 h. Afterwards, the NBF was removed and the samples washed three times for 1 h each time with PBS. The 24-well plates were sealed with Parafilm and stored at 4^{o}C until processing. Minimal sized segments of 0.25% (w/v) agarose containing micro-lenses were mechanically separated from the remaining 0.25% (w/v) agarose, embedded in 2% (w/v) agarose and placed in tissue processing cassettes. The samples were dehydrated in a Micro STP-120 Tissue Processor (Thermo Fisher Scientific) in 50% (vol/vol), 70% (vol/vol) and 80% (vol/vol) ethanol for 60 min each then 95% (vol/vol) and 100% (vol/vol) ethanol for 2 x 90 min each, xylene for 3 x 90 min then paraffin for 1 x 60 min then 1 x 90 min. Samples were manually embedded in paraffin and cut into 5 µm thick sections using an Microm HM325 microtome before being mounted on glass microscope slides.

The following solutions were prepared for immunofluorescence analysis.

0.1% (vol/vol) BSA in PBS: 2.3 mL of 10% (vol/vol) BSA (Miltenyi Biotech) was placed in a glass measuring cylinder and made up to 230 mL with PBS (+Ca/+Mg).

10% (w/v) Tween20 stock solution: 3 g of Tween 20 (Amresco, Cat no. M147) was added to 27 mL of PBS (+Ca/ +Mg) in a 50 mL tube and mixed on a roller, to prevent bubbles forming.

Wash buffer: 2.3 mL of 10% (vol/vol) (Miltenyi Biotech) and 2.3 mL of 10% (w/v) Tween20 was placed in a glass measuring cylinder and made up to 230 mL with PBS (+Ca/+Mg).

The following primary antibodies were prepared to a concentration of 4 to 5 μg/mL in wash buffer: αA-crystallin Rabbit IgG (Santa Cruz, Cat no. sc-22743), β-crystallin Rabbit IgG (Santa Cruz, Cat no. sc-22745), γ-crystallin Rabbit IgG (Santa Cruz, Cat no. sc-22746) and Rabbit IgG control (Innovative research, Cat no. 121266101). Sections to be stained were outlined on the underside of the slide with a Stat marker (Statmark, Trajan Scientific) before slides were rehydrated in glass Coplin jars with 35 mL each of the following solutions in sequential order: 10 dips in xylene wash then immersed 2 x 10 min; 2 x 5 min in 100% (vol/vol) ethanol; 1 x 5 min in 95% (vol/vol) ethanol; 1 x 5 min in 70% (vol/vol) ethanol; 1 x 5 min in 50% (vol/vol) ethanol; 1 x 5 min in 30% (vol/vol) ethanol; 1 dH_2O rinse; 2 x 5 min in wash buffer.

Slides were then placed on a Teriwipe and the Stat marker lines visible through the slide were used to guide separation of each section using hydrophobic solution provided by a Pap Pen (Trajan Scientific). Sections were blocked with approximately 100 μL of 10% (vol/vol) Normal Goat Serum (NGS) (Life Technologies, Cat no. 50062Z) for 10 min at room temperature, after which the NGS was tapped off onto a Kimwipe. The blocked slides were placed in a plastic embedding mould inside a small, sealable container lined with water-dampened sponges to create and maintain a humid environment. 100 μL of diluted primary antibody or control was added to each section. The container was sealed and placed in the 4^{o}C cool room overnight, after which the primary antibody solutions were removed. All subsequent steps used wash buffer 0.1% (vol/vol) BSA and 0.1 % (w/v) Tween 20 in PBS (+ Ca/+Mg): 100 μL of wash buffer was added to each section for 2 × 10 min then slides were placed in 35 mL wash buffer in Coplin jar for 10 min. Diluted goat anti-rabbit AlexaFluor488 (Invitrogen, Cat no. A11078) secondary antibody was diluted to 1/1000 in wash buffer and 100 μL was added to each section and incubated at room temperature in a dark cupboard for 1 h. The secondary antibody was then removed and slides washed for 2 x 10 min in 35 mL in wash buffer in a Coplin jar.

Slides were then placed in a 1/1000 dilution of the nuclear stain DAPI (Invitrogen, Cat no. D3571) in wash buffer, in a foil-wrapped Coplin jar for 10 min. The slides were rinsed in 35 mL wash buffer in a foil-wrapped Coplin jar for 10 min then mounted gently dried by tapping on to a Kimwipe then mounted with DPX solution (Trajan Scientific, Cat no. 1.00579.0500) before being imaged using a CKX41 microscope with an Olympus ORFLT50 camera and Q Capture Pro 6.

2.2.13 Vx-770 toxicity assay

Commencing on the day of embedding, ROR1^{+} aggregates in 0.25% (w/v) agarose were treated with Stage 3 medium with either dimethyl sulfoxide (DMSO) (Sigma Aldrich, Castle Hill, Australia) or Vx-770 (Selleckchem, Cat no. S1144) in the dose range between 200 and 2000 ng/mL. DMSO had been shown not to cause cataract (142) so was used as the vehicle for dispersing the Vx-770 into aqueous medium.

Stock solutions were made for each dose as shown in Table 2.1.

Table 2.1 Vx-770 dose stock solutions

Desired final concentration Vx-770 (ng/mL)	dilution Vx-770 : DMSO	DMSO (µL)	Vx-770 (2 mg/mL stock concentration) (µL)	Vx770:DMSO added to 2mL stage 3 medium (µL)
0	0:1	50	0	2
200	1:10	5	45	2
500	1:4	12.5	37.5	2
1000	1:2	25	25	2
1500	3:4	37.5	12.5	2
2000	1:0	0	50	2

Aggregates were exposed to the dose of Vx-770 for up to 28 days. Light focusing and light transmittance was measured at regular intervals and samples were collected for analysis by mass spectrometry at days 7, 18 and 27, as described above.

2.3 Results

2.3.1 Generation of purified ROR1$^+$ LEC cultures

To generate lens cells, a published modification (Figure 2.1) of the 3-stage lens differentiation protocol was used (108). As previously reported, the initial stages of this protocol generated a heterogeneous mixture of cells and lentoids (Figure 2.3A). Dissociation of these heterogeneous cultures at approximately day 16 was followed by ROR1-based MACS, and subsequent culture produced a homogeneous population of LEC-like cells with similar morphology (Figure 2.3B) to human PS cell-derived lens cells (108) and human fetal lens cells (143). Purified ROR1$^+$ cells were cultured until confluence in a published medium, E3, shown to maintain LEC-like polygonal morphology (108).

2.3.2 ROR1$^+$ LEC aggregation to form thousands of teleost-like lens cell masses

Initial attempts made during the early experimental phase of this project to replicate the LEC monolayer and subsequently the lens vesicle using human PS cell-derived lens cells were ultimately unsuccessful. The premise was to culture a monolayer of LECs on peptide-grafted chitosan film (functionalized for LEC attachment) (144) or a silk fibroin membrane (145,146). Ultimately, the silk fibroin did not withstand handling during Matrigel coating. The purified ROR1$^+$ cells did not attach or proliferate sufficiently to the RGDS-grafted chitosan films (data not shown) for a paired-explant type system to be a viable method in this case. Chitosan film is biocompatible and remains a suitable substrate for future investigation of lens cell culture. However, work to improve surface and peptide grafting homogeneity, and biodegradability, was outside the focus of this thesis. Therefore, a different approach to forming the lens-like tissue *in vitro* was investigated, specifically, identifying lens formation in other species and determining whether these may be adapted, or mimicked, for use with human PS cell derived lens cells.

To mimic the ball-like masses of early teleost lens development, the ROR1$^+$ cells were aggregated using commercially available AggreWell plates (Figure 2.4A). The resultant aggregates were fairly uniformly-sized spheroids of approximately 400-500 tightly packed cells, roughly 80-100 μm in diameter (Figure 2.4B). These ball-like aggregates appeared less dark under phase imaging than the surrounding agarose 3D growth environment (Figure 2.4C). This simple method yielded up to 1200 aggregates per well of the AggreWell plate. By using several wells simultaneously, production of tens-of-thousands of similarly-sized ROR1$^+$ aggregates could be generated. The agarose gel 3D growth environment supported the aggregates and effectively prevented their attachment to the culture plastic or to each other (Figure 2.4C).

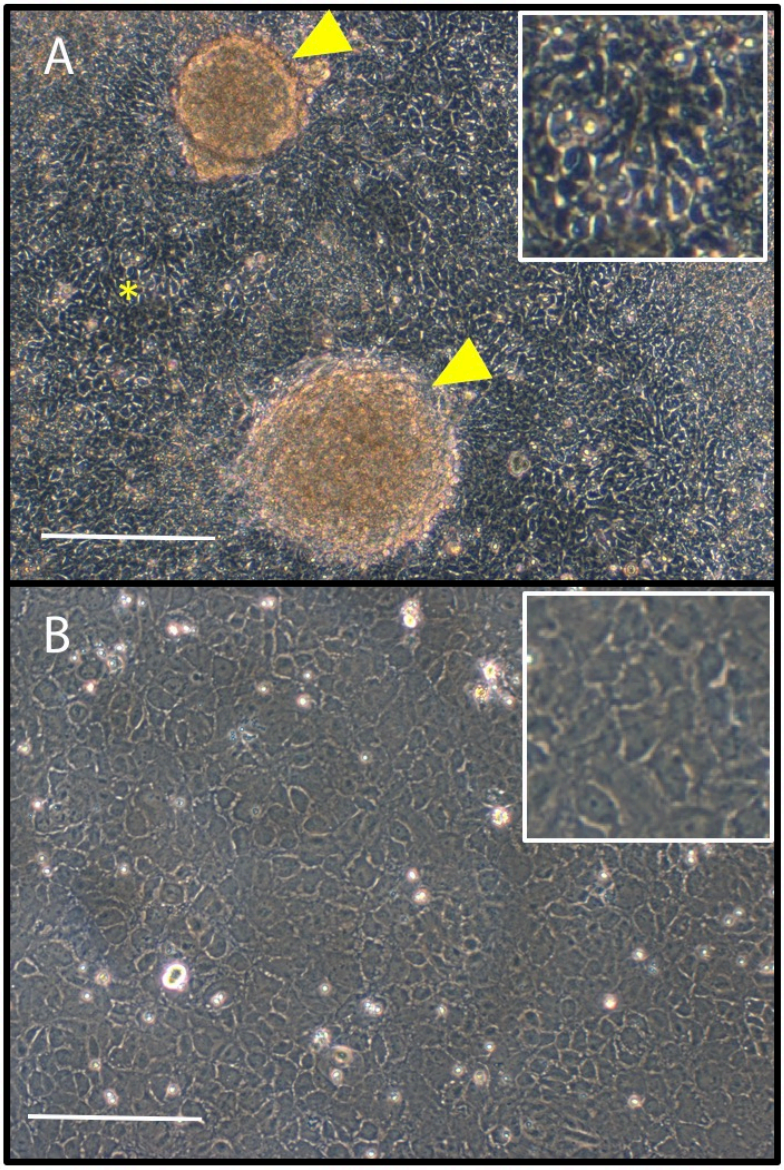

Figure 2.3 Generation of purified cultures of ROR1^{+} lens epithelial cells

(A) human PS cell culture in Stage 2 medium on Day 13 showing variable-sized lentoids (arrowheads; ultimately lost from culture) and polygonal cells (asterisk, inset), comparable to those described in the published protocol (90,108). (B) Homogeneous population of tightly-packed polygonal LEC-like cells (inset; magnified) obtained via ROR1-based MACS. Scale bars (A, B) 200 µm

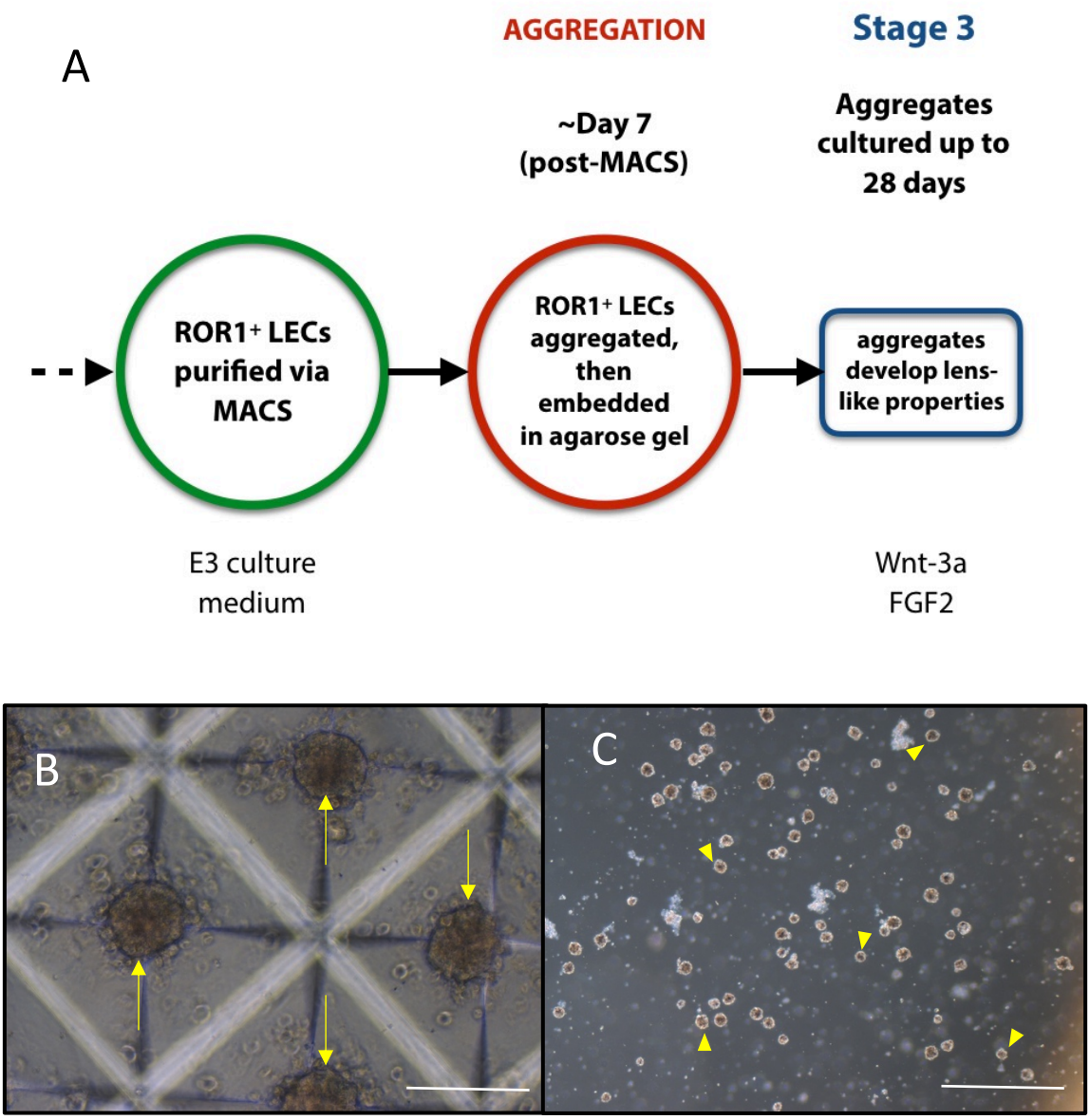

Figure 2.4 Aggregation of ROR1$^+$ lens epithelial cells

(A) Schematic diagram showing the aggregation and embedding step of ROR1$^+$ cells into ball-like masses before initiation of Stage 3 of the lens cell differentiation protocol (90,108). (B) Aggregated ROR1$^+$ cells (arrows) within micro-wells of an AggreWell plate showing the majority of input cells were incorporated into clearly-defined aggregates. (C) Low magnification image of ROR1$^+$ aggregates (arrowheads) embedded in agarose. Scale bars (B) 200 µm; (C) 1 mm

2.3.3 Maturation of aggregates into micro-lenses

On day 1 of aggregate culture (i.e., the day of embedding), spheroidal aggregates of ROR1$^+$ cells (Figure 2.5A-E) transmitted less light than the surrounding 3D growth environment (Figure 2.5K). At this stage, the aggregates also had minimal light focusing ability, indicating the spheroidal shape alone was insufficient for marked focusing ability (Figure 2.5C).

After 24 days in stage 3 culture, the ROR1$^+$ cell aggregate had developed increased light transmission as well as the ability to focus light, with tracking of individual aggregates showing a marked increase in both light transparency (Figure 2.5A vs F) and focusing ability (Figure 2.5C vs H). Light transmission measurements indicated that by approximately day 24 of aggregate culture, the light transmission ability of the aggregates had reached that of the background culture medium (Figure 2.5F, K). These data were found to normally distributed with the Kologorov-Smirnov test, therefore the parametric T-test was applied. The light focusing ability of the micro-lenses also increased markedly over this period (Figure 2.5H, L).

2.3.4 Human PS cell-derived micro-lenses express LF cell proteins

Analysis by mass spectrometry demonstrated that LF cell crystallin proteins became increasingly expressed at later stages of culture; α-crystallins were present in early culture and LF cell-like β-crystallins were detected by approximately day 1 (Figure 2.6 and Table 2.2). This detection of α- and β-crystallins by mass spectrometry was supported by immunofluorescence on micro-lenses at day 24 (Figure 2.7). The α- and β-crystallins were expressed uniformly across the micro-lens sections (Figure 2.7A, B). Whilst γ-crystallin was not detected by mass spectrometry on the samples tested, immunofluorescence showed variable expression across the micro-lens (Figure 2.7C). Immunofluorescence analysis confirmed the presence and location of crystallin proteins detected during mass spectrometry analysis. Analyses of other lens epithelial cell markers were outside the scope of this thesis. These data indicated that purified ROR1^{+} LECs, when aggregated, can be induced to form thousands of uniform ball-like masses that develop light transmission and light focusing as they increase expression of LF cell crystallin proteins.

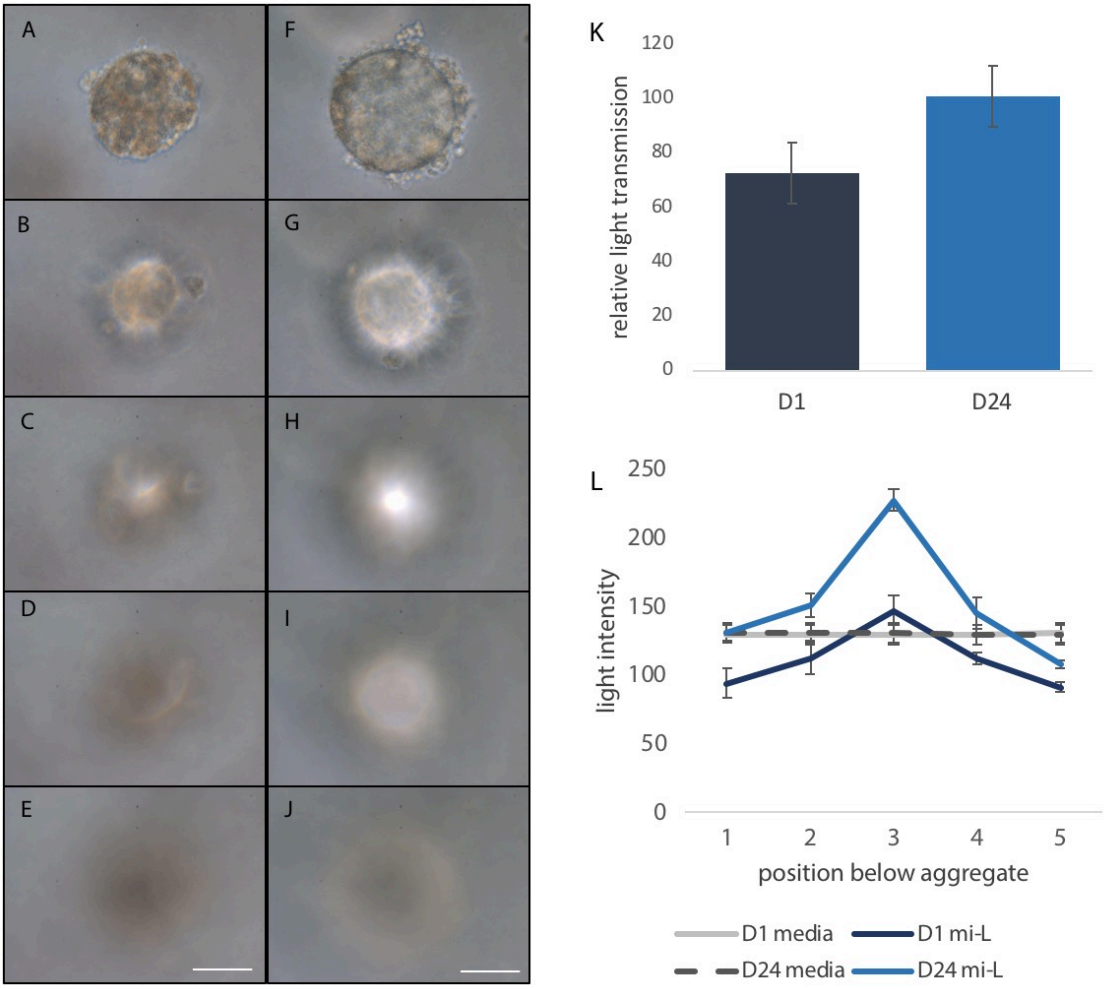

Figure 2.5 Aggregated ROR1^{+} cells develop into light-transmitting micro-lenses with significant light focusing capacity

(A-E) Light microscopy images taken at identical incremental distances below the aggregates on day 3 post-aggregation demonstrated the aggregates transmitted less light than the culture medium (A) and possessed limited capacity to focus light (C). (F-J) Micro-lenses on day 27 typically transmitted equivalent levels of light compared to the culture medium (F) and focused light to an intense point (H). (K) Quantification of the increase in light transmission of the aggregates relative to the background on day 3 and day 24. (L) Quantification of the increase in light focusing ability on day 3 and day 24. The representative images in Figure 2.5A-E and Figure 2.5F-J were the taken from the same aggregate at the different time points indicated. Scale bar (A-J) 50 µm

Table 2.2 Micro-lens proteins identified by mass spectrometry

Analysis by mass spectrometry identified α-crystallin in micro-lenses cultured in stage 3 medium at days 7, 18 and 27; LF cell β-crystallins were identified at approximately day 18 and day 27. The number of peptides identified and the percent sequence coverage for example crystallin peptides are indicated (e.g. 5, 28%, respectively).

Lens proteins identified	Day 7	Day 18	Day 27
CRYAA	1, 6%	8, 30%	8, 35%
CRYBB1	-	5, 28%	9, 34%
CRBA1	-	-	1, 6%
CRBA4	-	-	4, 13%

A

```
  1 MDVTIQHPWF  KRTLGPFYPS RLFDQFFGEG LFEYDLLPFL  SSTISPYYRQ
 51 SLFRTVLDSG _ISEVRSDRDK FVIFLDVKHF SPEDLTVKVQ DDFVEIHGKH
101 NERQDDHGYI SREFHRRYRL PSNVDQSALS CSLSADGMLT FCGPKIQTGL
151 DATHAERAIP VSREEKPTSA PSS
```

B

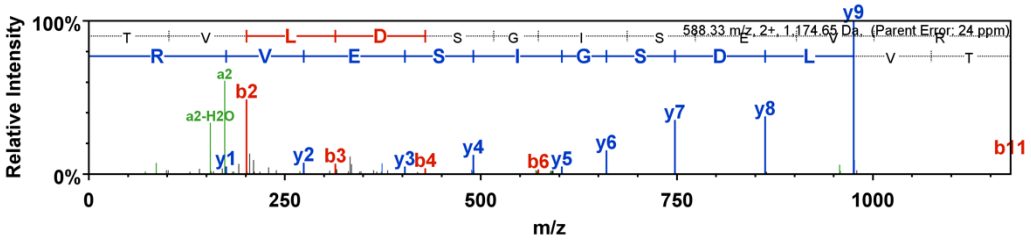

C

```
  1 MSQAAKASAS _ATVAVNPGPD TKGKGAPPAG TSPSPGTTLA PTTVPITSAK
 51 AAELPPGNYR LVVFELENFQ GRRAEFSGEC SNLADRGFDR VRSIIVSAGP
101 WVAFEQSNFR GEMFILEKGE YPRWNTWSSS YRSDRLMSFR PIKMDAQEHK
151 ISLFEGANFK GNTIEIQGDD APSLWVYGFS DRVGSVKVSS GTWVGYQYPG
201 YRGYQYLLEP GDFRHWNEWG AFQPQMQSLR RLRDKQWHLE GSFPVLATEP
251 PK
```

D

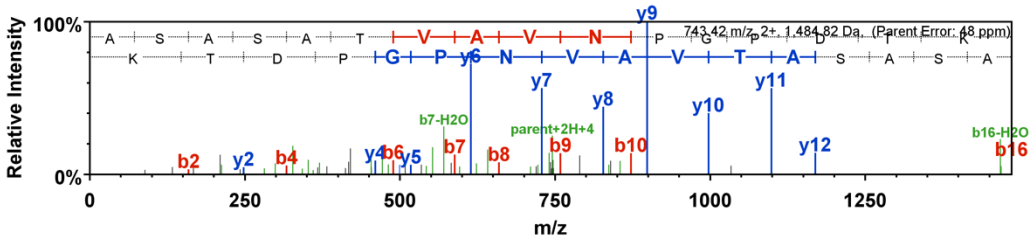

Figure 2.6 Representative mass spectrometry data demonstrating micro-lenses express α-and β-crystallin proteins

(A, B) MS/MS analysis showed 35% sequence coverage of CRYAA at day 18 (A), with example raw data peptide identification of sequence TVLDSGISEVR (A, underlined and B). (C, D) MS/MS analysis showed 39% sequence coverage of CRYBB1 at day 27 (C), with example raw data peptide identification of sequence ASASATVAVNPGPDTK (C, underlined and D).

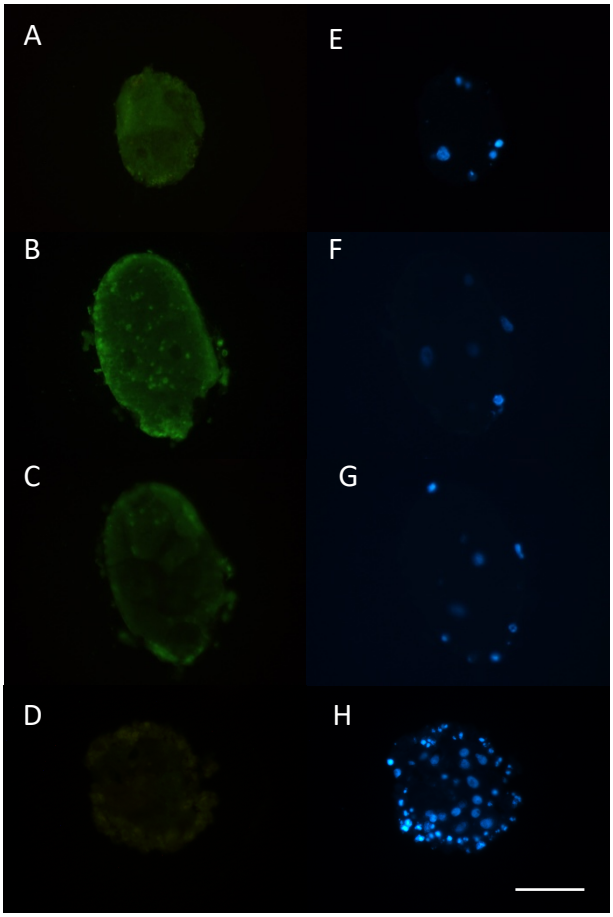

Figure 2.7 Cultured micro-lenses express LF cell-like crystallins

(A-C, E-G) Immunofluorescence staining showed uniform expression of αA-crystallin (A) and β-crystallin (B) after culture in Stage 3 media for 24 days. Expression of γ-crystallin was detected by day 24 (C). Control immunofluorescence image showing non-specific staining (D). The corresponding images of DAPI-stained nuclei are shown (E-H). Scale bar 50 µm

2.3.5 Treatment with Vx-770 reduced micro-lens function

To test whether the micro-lens system was suitable for drug toxicity assays, the developing micro-lenses were exposed to clinically relevant doses of Vx-770. Aggregates were dosed in the range of 0 ng/mL (vehicle only) to 2000 ng/mL which corresponds to the range of clinical doses of Vx-770 in pediatric cystic fibrosis patients (137). After 23 days, the vehicle-only treated micro-lenses (Figure 2.8A to E) had developed light transmission and focusing capability similar to the functional micro-lenses generated in stage 3 media only (Figure 2.5F to J). In contrast, the ROR1^{+} aggregates treated with 500 ng/mL and higher doses of Vx-770 did not develop into functioning micro-lenses. Light microscopy observation showed that these ROR1^{+} aggregates lost the initial defined-edge and did not develop the same level of light transmission and focusing ability that micro-lenses treated with lower doses did (Figure 2.8K, L). Quantification of these observations showed a significant difference between the relative light transmission and relative focal intensity of the vehicle-only treated aggregates compared to treatments of 500 ng/mL and higher.

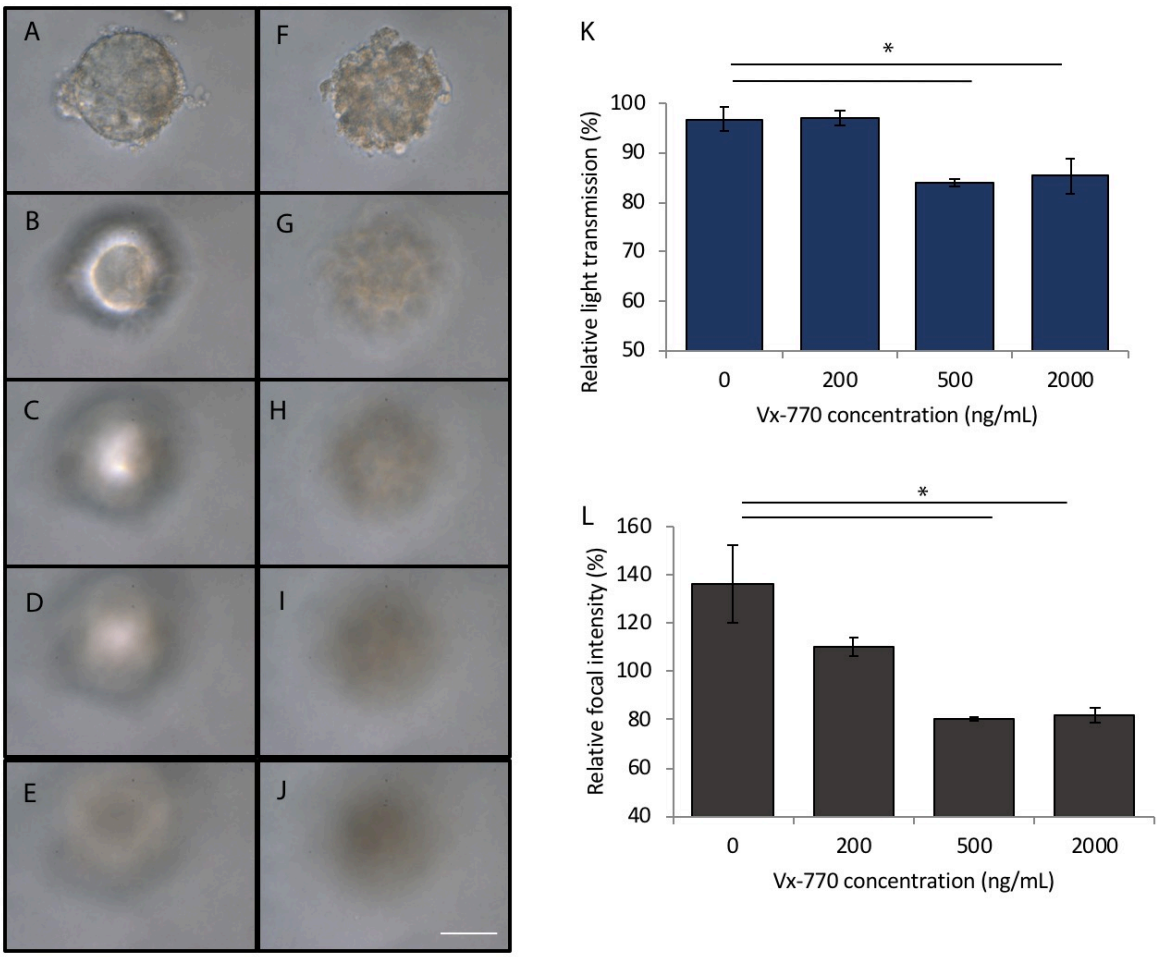

Figure 2.8 Development of micro-lens function is reduced by treatment with Vx-770

(A to E) Representative images of a micro-lens treated with 0 ng/mL Vx-770 (vehicle only control) for 23 days of culture shows the aggregate developed similar light transmission (A) and focusing capability (C) to untreated micro-lenses (i.e., compared with Figure 2.5C). (F to J) Representative images of a micro-lens treated for 23 days with 2000 ng/mL Vx-770 shows the aggregate lost the defined-edge and did not develop light transmission (F) or focusing ability (H). (K, L) The response to Vx-770 was dose-dependent; micro-lenses developed light transmission ability (K) and focusing ability (L) with control and 200 ng/mL treatments but did not at doses at or above 500 ng/mL (*$p \leq 0.05$; day 23 of culture). Scale bar 50 µm

2.4 Discussion

2.4.1 Mimicking cross species development for 3D tissue regeneration

Previous attempts to produce mammalian micro-lenses *in vitro* included harvest of LEC monolayers via rat lens explants which were then paired to mimic the hollow lens vesicle (125). That rat lens explant pair lens model demonstrated light transmission and focusing ability (125). Furthermore, a cataract developed in this model (125), indicating that such a lens model could be used for investigating cataractogenesis. Chitosan film is biocompatible and bacteriostatic and remains a suitable substrate for future investigation of lens cell culture. However, the $ROR1^{+}$ LECs did not attach and/or proliferate well on the initial chitosan preparations. As the research required to improve the surface homogeneity and peptide grafting efficiency was outside the focus of this thesis, an alternative approach was investigated. Animal models have been widely used in cataract studies (22) and while they are useful, they are not human tissue. Indeed, there are differences between the cell membrane composition of human lenses and those from other animals (147) as well as growth characteristics, for example, human lenses have a greater proportion of growth in the pre-natal period compared to other species (69). Moreover, expression of γ-crystallin homologs between species differs; human expression of γS-crystallin differs from fish (γM-crystallin), bovine (γB, γE-crystallin) and mouse (γ-crystallin) (71,148).

Differences in lenses between species are not limited to differences in crystallin expression and cell membrane composition. They also include the physical variations of lens organogenesis. For example, mammalian lenses arise from a LEC-lined vesicle and teleost lenses arise from a ball-like mass of LECs. By forming mammalian cells into a teleost-inspired ball-like mass, human micro-lenses were produced from ROR1^{+} cells. Thus, mimicking the physical pathway of teleost lens development enabled production of uniform, light transmitting, light focusing human micro-lens tissue. Developmental studies of other species and their organ development pathways may provide further insight and alternate, perhaps simpler, means of producing human PS cell-derived organoids for other (i.e., non-lens) tissues in the future.

2.4.2 Human micro-lenses can be produced *in vitro* in large quantities

The original 3-stage process to differentiate lens cells from human PS cells (90) was capable of producing hundreds-to-thousands of lentoid bodies during the 3-stage process. As the lentoids were lost to the culture medium, they were unable to have light focusing or light transmitting capacity measured, and they were not readily available for downstream analysis. Consequently, lentoids produced via the unmodified 3-stage differentiation method have had relatively limited utility as an *in vitro* human lens model to study lens development or cataract.

Attempts to improve on this human PS cell lens model have been recently published (91,93). Fu and colleagues (91) produced tens-to-hundreds of lentoids that possessed magnification ability. These lentoids had properties indicative of their lens-like nature, (91) including an increase in relative expression of LF cell genes *CRYBB2* and *CRYG*. However, this "fried-egg" process of generating these lentoids is complex and labour intensive, and therefore, unsuitable for large-scale production of lens organoids. Moreover, the electron microscopy images obtained from these "fried-egg" lentoids in the literature revealed internal structures that appear to less closely resemble that of a normal lens compared to the ROR1^{+} micro-lenses produced here. The micro-lenses produced during these experiments demonstrated characteristics of LF cells. Indicators of terminal LF cell differentiation included a peripheral LEC monolayer degrading nuclei, and development of LF cell membrane interdigitations (108). These physical characteristics of micro-lenses generated within our laboratory were examined by electron microscopy and published (Appendix A) along with data generated by myself and others, however analysis of these images were undertaken by others and thus excluded from this thesis (108).

A more useful system of large-scale human lens organoids, for example for drug screening assays, requires generation of tens-to-hundreds of thousands of uniform lens-like tissues with clearly demonstrated lens functional abilities. The ROR1 cell-based system described here can produce such numbers of uniform micro-lenses in a highly controlled manner. These lentoids are not randomly lost from the culture system, and they express known lens fiber cell proteins. In addition to the drug screening, these properties of the ROR1^{+} micro-lenses could be used specifically for studying human lens development. These micro-lenses derived from human PS cells could facilitate insight into the key time points that α-, β- and γ-crystallin commence and cease expression in the lens, and how this correlates with development of light focusing ability. This could facilitate investigation of the molecular aspects of gene regulatory networks and their controls, organelle loss and nuclear degradation during lens development, which have typically only been observed in non-human models. These human PS cell-derived micro-lenses are the first of their kind that provide large amounts of *in vitro* human lens tissues suitable for investigation of development and for drug toxicity screening.

2.4.3 Clinical utility of the micro-lenses

Changes in light transmission and light focusing during micro-lens development were measured in the micro-lens generation system described in this chapter. Initially aggregated ROR1$^+$ cells did not transmit light at a greater intensity than the background medium. However, after culture with growth factors that induced LF cell development, the aggregates transmitted greater light than previously, and similar to that of the background medium. Likewise, light focusing, a key characteristic of the lens, was an important indicator that the micro-lenses generated possessed functional properties similar to larger *in vivo* lens tissue. The intensity of the light focused was quantified, and therefore, able to form the basis of an assay to investigate light focusing changes related to cataract and drug response.

Cataracts are opacities that cause light scatter in the lens, thereby impairing vision by reducing light transmission to the retina. The cystic fibrosis drug Vx-770 was chosen to model cataract formation in the micro-lenses as it is suspected of causing cataract in young cystic fibrosis patients who have received the drug (133,134). Diminished vision resulting from childhood cataract has long-term social, emotional and developmental consequences (10). An inability to develop light transmission and light focusing ability, conceptually similar to cataract, was induced by exposing aggregates to 500 ng/mL and higher doses of Vx-770 from the beginning of micro-lens culture. These data suggest that the micro-lens system may be useful for defining the molecular mechanisms responsible for the formation of human cataract thought to be caused by Vx-770. More generally, the micro-lenses could reduce the necessity for animal-based toxicity testing of emerging drugs (22).

The micro-lenses could also provide a platform for further discovery of the molecular mechanisms of cataract caused by other risk factors, such as hyperglycemia (34) and smoking (149). For example, protein ageing and subsequent instability (150) as well as glycation of crystallins (21,72) are postulated risk factor mechanisms of cataract formation that could be investigated using the micro-lens system. Similarly, changes in protein aggregation or other post-translational modifications (PTMs), such as methylation (42,151), could be identified. In turn, this could lead to investigation and development of potential patient-specific (i.e., risk factor-specific) anti-cataract drugs.

2.4.4 Limitations of the agarose 3D growth environment

The relative simplicity of the micro-lens system means that other laboratories can replicate the differentiation, purification, aggregation and embedding protocols and generate many thousands of micro-lenses for cataract research. The 3D growth environment that agarose provided had several advantages for use as a first embedding medium. Agarose is inexpensive and readily available; it did not require specialized equipment in order to produce the growth environment for the aggregates. The micro-lenses were supported in a 3D growth environment allowing the spheroidal shape of the micro-lens to be maintained; this is difficult, if not impossible to maintain if aggregates are attached to a hard culture plastic surface (that also doesn't reflect normal lens biology). Moreover, agarose is transparent at the concentrations used here and thus allowed for quantification of light transmission and light focusing of the micro-lenses.

In addition to these positive physical properties, the agarose gel conceivably provided a concentration gradient for the growth factors FGF2 and Wnt3a to mimic the lens forming gradient thought to occur *in vivo* (75). Nevertheless, there were some inherent difficulties being certain that this was the case. The pore sizes within the agarose gel were almost certainly heterogeneous and it could not be certain that a growth factor concentration gradient was established. Additionally, harvesting and processing of the micro-lenses in the manner described did not ensure that situational polarity was maintained, therefore the effect of a theoretical gradient by establishing a definite apical-basal relationship between LECs and LF cells could not be determined.

Despite the success of generating these micro-lenses in agarose, there were some limitations associated with this system. Firstly, the 0.25% (w/v) agarose has a narrow temperature range at which it will gel. This means that the timing of aggregate harvesting and embedding must perfectly align with the point at which the gel has cooled and the precise temperature cannot be measured at the time of embedding due to sterility issues that might contaminate the culture. If left too long, the aggregates risk clumping together or attaching to the culture surface before embedding is completed. Secondly, obtaining the correct temperature for embedding is challenging: if the agarose is too hot, it can cause damage to the aggregates, for example, by changing the tertiary structure of α-crystallin, or gene expression of the aggregates. If it is too cool it before embedding has been completed. Thirdly, there is a risk of contamination during the embedding process when heating/cooling the agarose.

Further drawbacks of the agarose system include difficulty harvesting micro-lenses for physical investigations. Both imaging by electron microscopy and immunofluorescence required thin sections of tissue to be cut using a microtome. The micro-lenses are very small and are held in a relatively large volume of the 3D growth environment. This made harvesting and sectioning difficult as there were often few, if any, micro-lenses present in any given section, making the sectioning process extremely time-consuming. Increasing the ratio of micro-lenses to 3D growth environment would be advantageous. This can be achieved in either of two ways. The first way is to increase the number of micro-lenses in the 3D growth environment (which risks individual micro-lenses not receiving sufficient nutrients or growth factors). A second approach would be to remove part or all of the 3D growth environment once the developmental phase is complete but without damaging or compromising the structural or molecular integrity of the micro-lenses.

A 3D growth environment that retains the positive properties of the current system, i.e., transparent, permeable and able to withstand handling during long-term culture with daily medium changes - but is degradable for harvesting the micro-lenses – would be more desirable. The following chapter assesses agarose alternatives in an attempt to further improve the utility of the micro-lens system.

Chapter 3

Evaluation of an alternative 3D growth environment for micro-lenses and assessment of ROR1-enriched vs purified ROR1^{+} cell derived micro-lenses

3.1 Introduction

3.1.1 Alternative 3D growth environments

As described in Chapter 2, the production of thousands of human PS cell-derived light-focusing micro-lenses was achieved by culturing aggregated ROR1$^+$ cells in an agarose 3D growth environment. While this approach was effective, two key steps are subject to significant challenges that could limit routine application: handling difficulties with the use of the agarose for embedding the micro-lenses, and time, labour and financial costs associated with production of ROR1$^+$ cells.

Firstly, as previously mentioned, agarose supported production of the micro-lenses by ensuring that: they were rarely in contact with each other or the plastic ware; they were not lost or damaged during daily media changes for several weeks; and that nutrients and lens-inducing growth factors were accessible to ROR1$^+$ cells. Secondly, some challenges were noted including the narrow working temperature range during embedding, the risk of contamination, and difficulties upon harvesting the micro-lenses for downstream analysis. Due to these difficulties, alternative commercially-available physiologically relevant hydrogel 3D growth environments were investigated (152). Desirable properties of an alternative to agarose include rapid setting (so that aggregates would remain suspended), a working temperature range close to 37^{o}C, permeability to nutrients and growth factors, mechanical stability to allow routine media changes and the ability to dissociate the embedding material to harvest micro-lenses for downstream analysis.

The options available were to either produce an artificial extracellular matrix, the most promising of which was a complex to produce poly(ethylene glycol) (PEG)-peptide conjugated hydrogel (153,154), or to use a commercially-available hydrogel product. A disulphide-containing poly(ethylene glycol) diacrylate (PEGSSDA) based hydrogel may be cross-linked (polymerised) in the presence of hyaluronic acid to produce a hydrogel (155). Non-enzymatic dissolution of the hydrogel matrix takes place by dissociation of the thiol bonds in the presence of *N*-acetyl-L-cysteine (155). To both maintain the simplicity of the micro-lens system and ensure testing of quality controlled agarose alternatives, only commercially-available products were assessed here. Numerous commercially-available hydrogel matrices have been reported to replicate the tissue growth environment allowing culture of tissues in a 3D growth environment (152). Three commercially available hydrogel products were identified as potentially possessing the desirable criteria (Table 3.1); the hyaluronic acid-based hydrogels HyStemC (Sigma Aldrich), HyStem + PEGSSDA (BioTime Inc) and the peptide-based HydroMatrix (Sigma Aldrich). Each of these products has different attributes for handling (mixing the hydrogel precursors) during the initiation of polymerisation, at the embedding stage, as well as hydrogel concentration and dissociation, thus allowing assessment of a broad range of these parameters in order to try and identify an improved hydrogel for culturing micro-lenses.

3.1.2 More efficient generation of micro-lenses

In addition to finding an alternate 3D growth environment, the methods associated with purification of the ROR1$^+$ cells retained some inefficiencies. While the published E3 Medium stimulates proliferation of the ROR1$^+$ cells (108), large numbers of cells are lost through the (relatively time and cost intensive) MACS procedure. In assessing ways to further improve the cost effectiveness of obtaining ROR1$^+$ cells, it was noticed that the cell filtration step immediately prior to antibody staining resulted in significant enrichment of ROR1$^+$ cells (on average 80%) (108). This raised the possibility that the time and cost of MACS might be avoided to generate enriched (but not pure) populations of ROR1$^+$ cells for laboratory (but not clinical) applications. Accordingly, this chapter investigates possible improvements to micro-lens production by culturing aggregates of ROR1-enriched cells in alternative growth environments such as agarose or commercially-available hydrogels.

3.2 Methods

3.2.1 Reagents and consumables

General cell culture reagents and consumables were as described in 2.2.1. Additionally, the following reagents were used in the following experiments: HyStemC with PEGSSDA linker kit (comprising EsiBio PEGSSDA 0.5 mL, HyStem Glycosil, HyStem Gelin-S and Degassed (DG) water) (EsiBio, Alameda CA, USA), HydroMatrixTM (Sigma Aldrich, Castle Hill NSW, Australia), *N*-acetyl-L-cysteine (Sigma-Aldrich, Cat no. A7250-5G).

3.2.2 Human PS cell and ROR1$^+$ cell culture

Human PS cell culture methods used were as described in 2.2.2. Differentiation to heterogeneous populations containing lens cells was performed as described in 2.2.3, up to and including the 40 μm cell filtration step. After that, the ROR1-enriched cells were cultured until confluent in E3 medium (i.e., approximately 7 days from filtration) as described for the purified ROR1$^+$ cells.

3.2.3 Commercial hydrogel assessment

The selected hydrogels were prepared in accordance with the manufacturer's specifications and variations in the final hydrogel concentration concomitant with published data (156,157). The assessment process for the hydrogels is outlined in Figure 3.1.

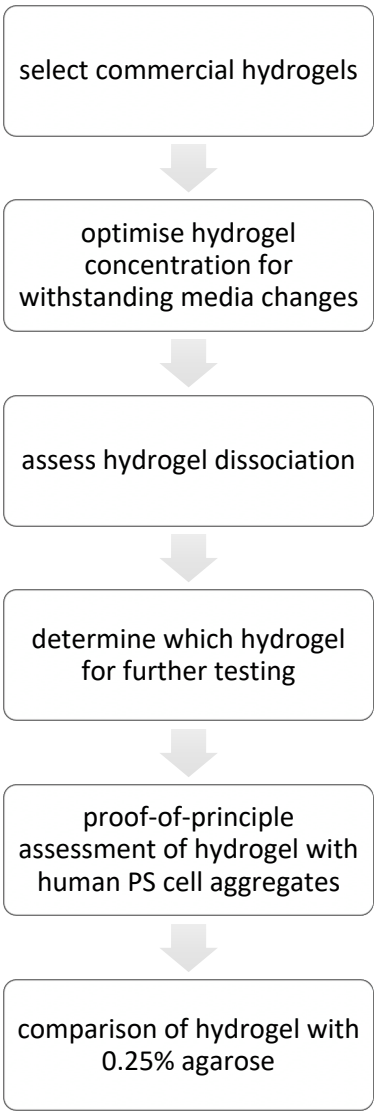

Figure 3.1 Assessment of commercial hydrogels for culture of ROR1-enriched aggregates

Flow chart depicting the process to determine whether hydrogels met the requirements for culture and retrieval of ROR1-enriched aggregates. A number of candidate products were selected on the basis that they would support 3D culture of cells. The products could be used at varying concentrations, therefore the hydrogel concentration at which stiffness properties were compatible with daily media changes was determined. The suitable candidate hydrogel or hydrogels were dissociated following the recommended method. The hydrogel or hydrogels that met the selection criteria were selected for further testing with human PS cell aggregates and finally compared to 0.25% (w/v) agarose with ROR1-enriched aggregates.

The commercial hydrogels were prepared as described (Table 3.2, Table 3.3) and subjected to the following assessment criteria (Table 3.1) to determine suitability for use with aggregated lens cells. The assessment criteria were scored as per Table 3.1. The methods used to test key hydrogel properties were:

Time to polymerise: after mixing the hydrogel components, each well was checked every 5 min to determine whether the hydrogel had set. Hydrogel polymerisation time (at room temperature) over 20 to 25 min was unsuitable due to the potential for aggregates to settle out of the hydrogel solution and attach to the culture plastic.

Rigidity of hydrogel: the rigidity was checked by tilting the 24 well plate and observing the level line at the top of the hydrogel to determine whether the hydrogel had set, then gently shaking the 24 well plate while observing under the microscope. The rigidity was checked immediately after gelling and 24 h later, after medium had been removed.

Hydrogel resistance after contact: the hydrogel surface was touched with a blue tip and it was noted whether the blue tip penetrated and/or left a mark on the hydrogel surface.

Ability to change media: to simulate cell culture medium, 500 µL of PBS was layered on top of a hydrogel without aggregates and incubated overnight. The following day, 500 µL of PBS was removed and it was noted whether complete medium removal occurred without disrupting the hydrogel surface.

Hydrogel dissociation: each hydrogel was dissociated according to the manufacturer's protocol. Once the hydrogels were dissociated, they were removed and placed into an adjacent well of a 24 well plate to assess the completeness of dissociation by noting number and size of hydrogel lumps present, if any.

Table 3.1 Assessment criteria for commercial hydrogel

Score	Time to polymerise	Rigidity of hydrogel	Ability to change medium without disrupting gel integrity	Dissociation of hydrogel
+++	5-10 min	most rigid	gel integrity retained	complete dissociation in <30 min
++	10 – 20 min	moderately rigid	some disruption to edges of gel	complete dissociation in 30-60 min
+	20-30 min	rigid	significant disruption to edges of gel	incomplete or partial dissociation requiring additional PBS rinse
-	>30 min or did not set	did not gel	could not change media without removing significant amount of gel	no dissociation or incomplete dissociation after additional PBS rinse

3.2.4 Preparation of HydroMatrix Peptide Cell Culture Scaffold

HydroMatrix has a pH of 2.5 when in aqueous solution (1% w/v). Consequently, isometric (20% w/v) sucrose is needed to be added to the cells to be encapsulated to protect the cells until physiological pH is obtained. Therefore, a 20% (w/v) sucrose solution was prepared by weighing 2.0 g of sucrose and dissolving in 10 mL of sterile water. The sucrose solution was filter sterilized using a 0.22 μm filter and syringe.

To generate the hydrogel, 0.5 mL sterile water was added to lyophilized HydroMatrix in an attempt to make a 2% (w/v) solution. The product did not disperse in this volume; therefore, a further 0.5 mL was added. Reconstituted HydroMatrix was kept on ice to prevent premature formation of the hydrogel. Gels were prepared at 1% (w/v), 0.5% (w/v) and 0.25% (w/v) concentration, according to the manufacturers protocol, in separate wells of a 24-well plate as per Table 3.2. Then 500 μL PBS (+Ca/+Mg) was added to each well and gently triturated, to initiate gelation. The 24 well plate was placed in an incubator at 37^{o}C, 5% (vol/vol) CO_2, and checked at 5 min intervals for gelling as described in Table 3.4.

Table 3.2 Preparation of HydroMatrix hydrogel

	0.25%	0.5%	1%
HydroMatrix™ stock solution (1% w/v)	75 uL	150 uL	300 uL
water	225 uL	150 uL	-
20% (w/v) sucrose solution	50 uL	50 uL	50 uL

Dissociation of the HydroMatrix hydrogel was achieved by trituration with a P1000 micropipette until liquefied, as per manufacturer's instructions.

3.2.5 Preparation of HyStem + PEGSSDA hydrogel

HyStemC + PEGSSDA was prepared at concentrations recommended by the manufacturer and at those found in literature for recovery of cells for metabolic analysis and CHiP sequencing (158). Following the manufacturer's protocol, the Glycosil, and Gelin-S solution were prepared by dissolving the lyophilized solid in 1 mL de-gassed (DG) water, using a syringe. The vials were vortexed then placed horizontally on a shaker for approximately 40 min for the solids to disperse. 250 µL DG water was added to PEGSSDA to make a 2x concentrated solution. All solutions were kept on ice and used within 2 h of reconstitution. Gelin-S, Glycosil and PEGSSDA were combined directly in wells of a 24 well plate in the amounts stated in Table 3.3. The HyStem+PEGSSDA solutions were triturated and immediately placed in the incubator at 37^{o}C, 5% (vol/vol) CO_2, and checked at 5 min intervals for setting as described in section 3.2.3.

Table 3.3 Preparation of HyStem + PEGSSDA hydrogel

The HyStem + PEGSSDA was prepared to produce a range of concentrations. The amounts of each component used for each concentration is indicated below.

	softest		standard		stiffest	
HyStemC with PEGSSDA	A	B	C	D	E	F
gel concentration (%)(w/v)	0.25	0.5	1	2	4	6
Glycosil (µL)	120	120	120	120	120	100
Gelin-S (µL)	120	120	120	120	120	100
DG water (µL)	56.25	52.5	45	30	0	0
PEGSSDA (µL) 2x concentrate	3.75	7.5	15	30	60	100

For dissociation of the HyStem + PEGSSDA hydrogels, 5.45 g *N*-acetyl-L-cysteine was dissolved in 100 mL sterile M199 medium, filtered with a 0.22 µm filter and stored in sterile tubes at -30^{o}C. Following this, 1 mL of 40 mM *N*-acetyl-L-cysteine solution was added to the top of each hydrogel in the 24-well plate and gently triturated 8 times. The plate was incubated at 37^{o}C, 5% (vol/vol) CO_2 for 1 h. Dissociation was confirmed by triturating with a 2 mL pipette. If intact hydrogel was observed, then the plate was incubated a further 30 min. Once the hydrogel was dissociated, it was removed and placed in 1 well of a 24-well plate to assess the completeness of dissociation by inspecting for presence and size of hydrogel lumps present, if any.

3.2.6 Assessment of human ES cell aggregates in hydrogel

The HyStem + PEGSSDA was trialled at 4% (w/v) and 6% (w/v), for culture of human ES cell line CA1 aggregates. The CA1 aggregates were prepared as per 2.2.6, replacing ROR1^{+} cells with CA1 human PS cells. The harvested aggregates (section 2.2.6) were embedded in 300 µL HyStem + PEGSSDA in a 24-well plate.

3.2.7 Time course assessment of ROR1-enriched aggregates

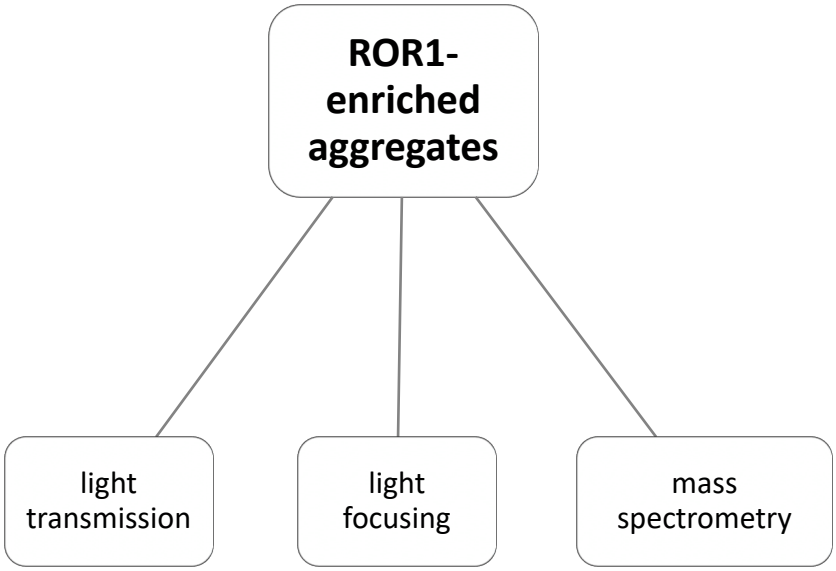

Figure 3.2 Experiment plan for assessing micro-lenses derived from ROR1-enriched cell populations

Three biological replicate cultures of ROR1-enriched cells were separately aggregated and plated in each 0.25% (w/v) agarose and hydrogel before being exposed to Stage 3 medium (90) for 35 days. Aggregates were harvested on or near day 3, day 7, day 14 and day 35 for analysis by mass spectrometry. Light transmission and light-focusing measurements were taken on or near days 3, 7, 14, 28 and 36. Aggregates were harvested on or near day 3, day 7, day 14 and day 35 for analysis by mass spectrometry.

3.2.7.1 Preparation of ROR1-enriched lens cell aggregates in HyStem + PEGSSDA hydrogel

ROR1-enriched lens cell aggregates were prepared as described in section 2.2.6**,** and plated in between 2 layers of 6% (w/v) HyStem + PEGSSDA with added concentrated E3 medium mixture. The E3 concentrate was added to yield a final concentration in the hydrogel equivalent to E3 ROR1^{+} cell maintenance medium (section 2.2.5). GelinS and Glycosil were made with 1 mL of DG water. PEGSSDA was made to a 2x concentration with 250 µL DG water. The GelinS, Glycosil and PEGSSDA hydrogel components were mixed to prepare a 6% (w/v) solution (Table 3.3). GelinS and Glycosil were combined in a tube with E3 super concentrated medium, then PEGSSDA added. Immediately upon addition of PEGSSDA, a 150 µL base layer was added to the required wells of a 24-well plate. The 24-well plate was placed in an incubator for 60 min at 37°C, 5% (vol/vol) CO_2 in order for the base layer to completely polymerise.

ROR1-enriched aggregates were prepared as described in section 2.2.6. Using a 2 mL pipette, aggregates were removed from the AggreWell and left in a loosely capped 15 mL tube to settle for 15 min. The supernatant was removed and 40 µL containing aggregates was added to each well, on the surface of the base layer.

A second batch of GelinS, Glycosil and PEGSSDA hydrogel components were mixed to prepare a 6% (w/v) solution (Table 3.3). GelinS and Glycosil were combined in a tube with E3 super concentrated medium, then PEGSSDA added. Immediately upon addition of PEGSSDA, 200 µL was added to the wells of the 24 well plate to make a 200 µL overlay of hydrogel. The overlay method was described in (129) whereby one layer was allowed to set then a second hydrogel and cell layer added. The 24 well plate was placed in an incubator for 30 min at 37°C, 5% (vol/vol) CO_2 to allow the top layer to polymerise. 500 µL of Yang stage 3 (DMEM:F12 medium with 100 ng/mL FGF2 and 20 ng/ mL Wnt3a) medium was added to each well, on top of the hydrogel.

3.2.7.2 Preparation of ROR1-enriched aggregates in 0.25% agarose

ROR1-enriched aggregates were prepared as described in section 2.2.5. Samples were collected on or near days 3, 7, 14 and 36 for analysis by mass spectrometry. The collected samples of 0.25% (w/v) agarose containing the aggregates were homogenized with a plastic micro-pestle, directly in a 1.5 mL Eppendorf tube before addition of Rapi-Gest and the samples were processed for mass spectrometry as described in section 2.2.11. Light focusing and light transmittance data were collected as described in section 2.2.10.

3.3 Results

3.3.1 Assessment of commercial hydrogel physical properties

As a first step to determining the suitability of the 3 hydrogels for micro-lens culture, their aggregation and dissociation characteristics were assessed. Dissociation of HyStemC hydrogel required overnight incubation with collagenase or hyaluronidase, raising the possibility that this would result in significant changes in micro-lens gene expression profile (a key desired downstream analysis method for micro-lens samples). On this basis, HyStemC was excluded from further assessment.

According to manufacturer instructions, both HyStem + PEGSSDA and HydroMatrix were recommended for use at varying concentrations. Therefore, the hydrogel concentration at which stiffness properties of these two hydrogels were compatible with daily media changes was determined. As aggregates take approximately 10-20 min to settle in a 15 mL tube immediately after harvesting from the AggreWell plates 25 min was chosen as the maximal allowed time for hydrogel setting. HyStem + PEGSSDA at concentrations at or lower than 3% (w/v) did not set, either at all, or within the 25 min timeframe. HydroMatrix did not gel at any concentration within the 25 min timeframe. Accordingly, HydroMatrix was excluded from further testing, as were concentrations of HyStem+ PEGSSDA below 3% (w/v).

As micro-lens culture currently requires daily medium changes, both HyStem+ PEGSSDA concentrations were assessed for their mechanical strength via their ability to withstand medium changes. This involved looking under the microscope and tilting or shaking the 24 well plate in addition to determining whether a blue tip would leave a mark on the surface of the polymerized hydrogel. The 6% (w/v) HyStem + PEGSSDA hydrogel withstood media change without loss or damage to the gel, and the 4% (w/v) HyStem + PEGSSDA hydrogel sustained some minor loss and damage during the test media change.

Table 3.4 Assessment of commercial hydrogels at varying concentrations

The hydrogels were assessed according to the criteria described in (3.2.3).

	HyStem + PEGSSDA							HydroMatrix		
hydrogel % (vol/vol)	0.25	0.5	1	2	3	4	6	0.25	0.5	1
Time taken to polymerise (min)	>45	>45	>45	>45	>45	25	10	>30	>30	>30
Rigidity of hydrogel day 0	-	-	-	-	+	++	+++	-	-	-
Rigidity of hydrogel day 1	-	-	-	-	-	+	++	-	-	-
Ability to change media without disrupting hydrogel integrity	-	-	-	-	+	+	++	-	-	-
Dissolution of hydrogel	-	-	-	-	++	++	+++	-	-	-
Proceed to further testing	no	no	no	no	no	**yes**	**yes**	no	no	no

An additional desirable hydrogel property is the capacity to easily, quickly and cleanly dissociate and release the micro-lens tissues. This would facilitate downstream analyses such as mass spectrometry and gene expression analysis without interference by matter from the growth environment and decrease the sectioning time required for immunofluorescence or electron microscopy analysis. Therefore, the final physical parameter tested involved the ease of dissociation of the hydrogels. To simplify the cost and time required for this testing, ROR1-enriched cell aggregates were initially omitted from the testing. Based on the rigidity testing, only the 4% and 6% (vol/vol) HyStem + PEGSSDA were tested for dissociation using *N*-acetyl-L-cysteine. This assessment showed that both concentrations of HyStem + PEGSSDA dissociated after incubation and trituation with *N*-acetyl-L-cysteine. On the basis of these data, 4% and 6% (vol/vol) HyStem + PEGSSDA were the commercially available hydrogels chosen for subsequent experiments.

3.3.2 Assessment of human PS cell aggregates in hydrogel

To test the permeability of the 4% and 6% (w/v) HyStem + PEGSSDA of hydrogels for embedding aggregates, a pilot test using human PS aggregates was performed (as they did not require the lengthy 3-stage differentiation prior to aggregation). Embedding human PS cell aggregates in 4% (w/v) HyStem + PEGSSDA resulted in aggregates settling from the gel and attaching to the culture plastic. Attachment of aggregates to the culture plastic was undesirable for the production of micro-lenses, therefore 4% (w/v) HyStem + PEGSSDA was deemed unsuitable for culture of aggregates. In contrast, the human PS cell aggregates embedded in 6% hydrogel remained suspended in the hydrogel. As the 6% (w/v) HyStem + PEGSSDA hydrogel withstood media changes, inhibited aggregate attachment to the culture surface and enabled survival in culture, for at least 24 h, of the human PS cell aggregates, the 6% (w/v) HyStem + PEGSSDA was assessed to have the most suitable properties for continuing with the time course experiments using ROR1-enriched cells.

3.3.3 Comparison of hydrogel and 0.25% agarose with ROR1-enriched cell aggregates

In order to adequately compare the 6% (w/v) HyStem + PEGSSDA hydrogel to agarose for micro-lens culture, aggregates of ROR1-enriched cells (rather than MACS-purified ROR1$^+$ cells) were embedded in both 3D growth environments and cultured in parallel. Three biological replicate experiments were completed and compared under the same incubation conditions and media changes. The aggregates and micro-lenses were assessed using light microscopy to measure light transmission and focusing, and by mass spectrometry to compare the development of crystallin proteins in each 3D growth environment.

The morphology of the ROR1-enriched cells obtained directly after 40 μm filtering and no MACS displayed a homogeneous distribution of polygonal shaped cells, consistent with the phenotype of purified ROR1$^+$ cells (Figure 3.3) and primary human fetal LECs (143). Furthermore, no spontaneous appearance of lentoids was noted using E3 Medium (108) prior to aggregate formation (similar to ROR1$^+$ cell cultures).

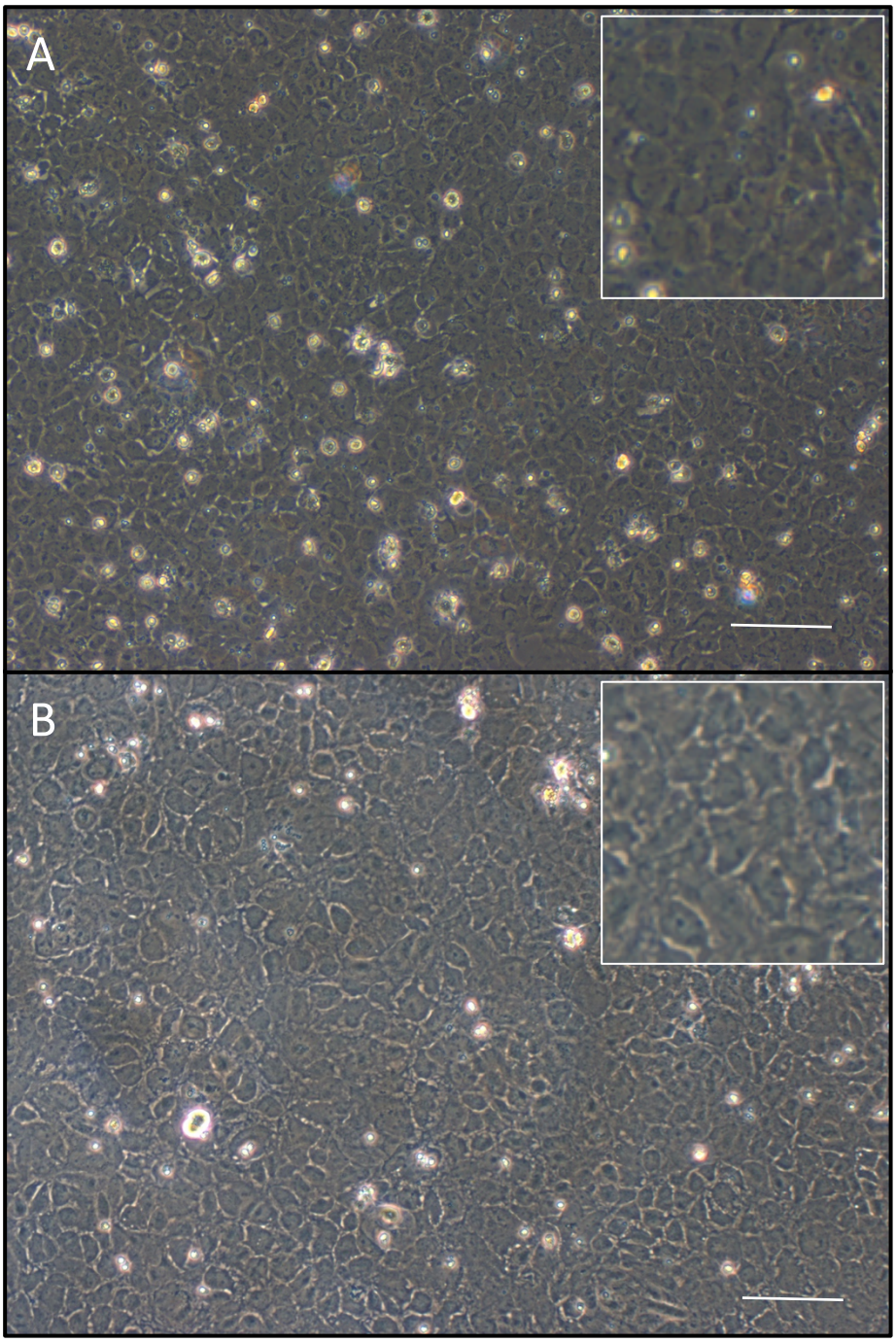

Figure 3.3 ROR1-enriched cells are morphologically similar to ROR1^{+} cells

Day 7 (A) ROR1-enriched cells in a confluent monolayer appear homogeneous and possess the polygonal lens epithelial cell phenotypically similar to purified ROR1^{+} cells (B) (Figure 2.3). Scale bar 50 µm

The day after embedding, the appearance of the aggregates in HyStem + PEGSSDA was similar to those in agarose. The aggregates in both 3D growth environments at this early stage had low light transmission compared to their respective 3D matrices (Figure 3.6, Figure 3.7). In some instances, this included dead cells surrounding the aggregates as previously noted (108). Strikingly, there was a sharp decline in the number of intact aggregates by the third day after embedding in HyStem + PEGSSDA. The previously defined-edged aggregates had lost edge definition and formerly aggregated cells appeared to detach from one another (Figure 3.4B, E, G). By day 7 (Figure 3.4F) no aggregates in HyStem + PEGSSDA remained intact. This loss of aggregates was repeatable, and was observed in all three biological replicate experiments performed using HyStem + PEGSSDA (Figure 3.4G). Ultimately, the HyStem + PEGSSDA cultured ROR1-enriched aggregates were discarded on day 7 after embedding as there were no viable aggregates remaining by that time. Consequently, no further analyses were able to be performed on the HyStem + PEGSSDA aggregates. In contrast, the majority of ROR1-enriched aggregates cultured in agarose retained their defined edges throughout the culture period (Figure 3.4A-C). Furthermore, these aggregates were typically not surrounded by dead cells.

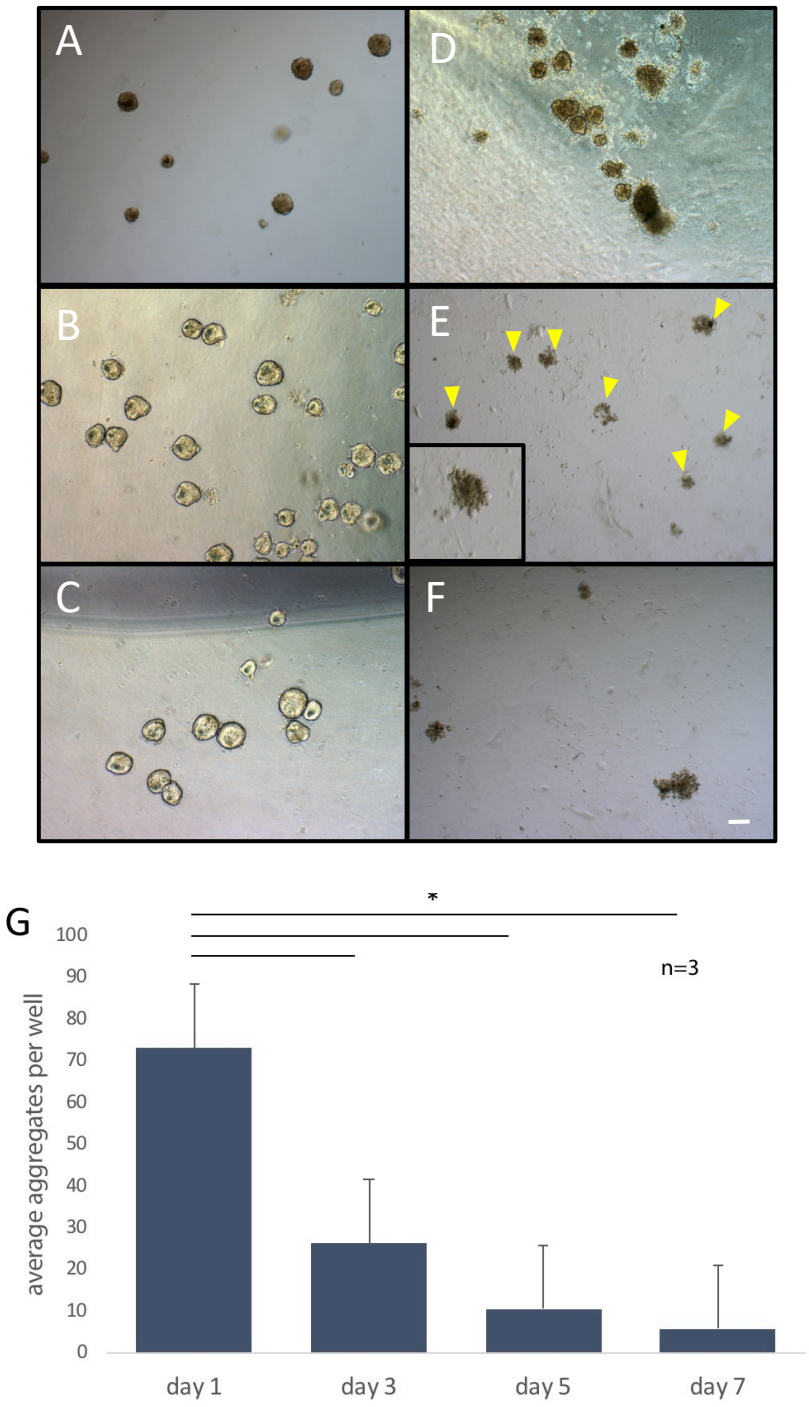

Figure 3.4 ROR1-enriched aggregates did not survive in HyStem + PEGSSDA hydrogel

(A-C) ROR1-enriched aggregates embedded in 0.25% agarose at day 1 (A), day 3 (B) and day 7 (C) retained defined edges throughout the culture period indicative of live cells being present up to (and beyond) day 7 (C). (D-F) ROR1-enriched aggregates embedded in HyStem + PEGSSDA hydrogel at day 1 had defined edges. By day 3, the aggregates appeared as clusters of dead cells (E, arrowheads, inset) and aggregate loss continued through to day 7 (F). (G) The loss of aggregates over this time was significant at each time point, with an almost total loss of aggregates in hydrogel by day 7, $p<0.05$. Scale bar 100 µm

3.3.4 Aggregated ROR1-enriched cells developed lens-like properties, earlier than ROR1$^+$ purified micro-lenses

The ROR1-enriched aggregates developed lens-like properties in the same manner seen with the purified ROR1$^+$ micro-lenses. By day 28, the light transmission of the micro-lens had at least reached that of the surrounding medium (Figure 3.6K). The light transmission and light focusing data were analysed using the Kolmogorov-Smirnov test and were found to be normally distributed then analysed using the Student's t-test. In some cases it was higher, likely due to the size of the aggregates causing a focusing effect beginning when the micro-lens periphery was in focus. Additionally, by day 28 the ROR1-enriched micro-lenses had developed significant focusing ability (Figure 3.6L).

Interestingly, by 7 days after embedding, the agarose-cultured ROR1-enriched aggregates had started to develop light transmission levels close to the surrounding culture medium (Figure 3.4B, C and Figure 3.7K). This was earlier than the purified ROR1$^+$ aggregates described in Chapter 2, where the light transmission reached background levels by day 24 in culture (Figure 2.5). Additionally, by day 7, the ROR1-enriched aggregates had developed obvious light-focusing (Figure 3.7L), also much earlier than the micro-lenses derived from purified ROR1$^+$ cells in Chapter 2.

In addition to noting the faster development of light transmission and light focusing, the ROR1-enriched aggregates were observed to develop irregular protrusions around day 14 of culture (Figure 3.5). Light microscopy showed that in some cases the protrusions appeared to mask the defined edges of the micro-lens (Figure 3.6F and G).

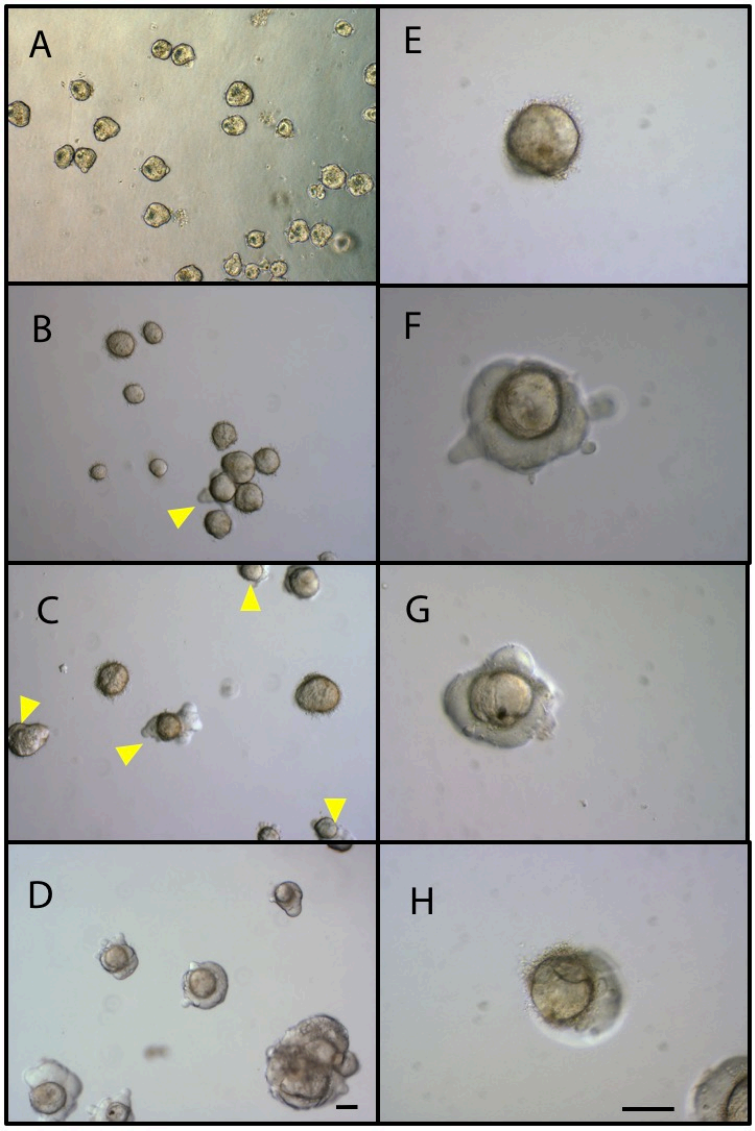

Figure 3.5 ROR1-enriched micro-lenses developed protrusions

Light microscopy images showed that ROR1-enriched cell aggregates had clearly defined edges at day 3 (A). On day 14 there was evidence of formation of small protrusions on some aggregates (arrowhead, B). By day 28 numerous aggregates had formed protrusions (arrowheads, C). The majority of micro-lenses had formed protrusions by day 36. Day 28 micro-lenses retained their defined-edge core regardless of protrusion development (E-H). Protrusions were variable in size and position relative to the micro-lens. Scale bar (A-H) 100 µm

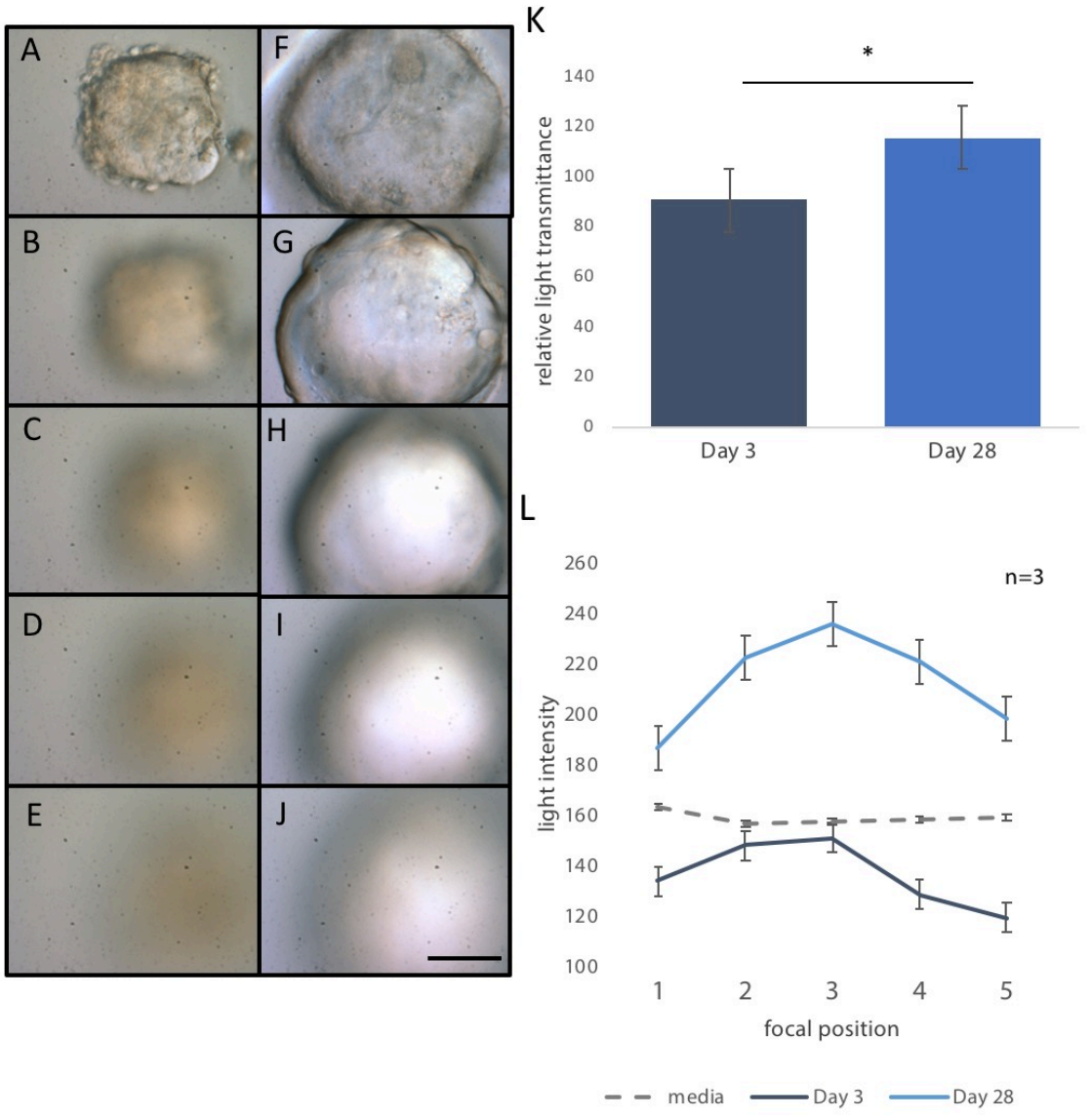

Figure 3.6 Aggregated ROR1-enriched cells develop micro-lens properties

Light microscopy images taken at increasing distances below the aggregates (A to E) on day 3 of culture show the initial low light transmission properties of the aggregates (A) and inability to focus light (C). (B to E) By day 28, the agarose-embedded ROR1-enriched micro-lenses transmitted light at least equal to the surrounding culture medium (F) and also had developed significant light-focusing ability (H). (K) Developing micro-lenses initially transmitted less light relative to the background medium at day 3, then more by day 28 ($p<0.05$). (L) The micro-lenses gain light focusing ability (position 3) and transmitted increased light (position 1) at day 28 compared to day 3 of culture and the surrounding culture medium. Scale bar 50 µm

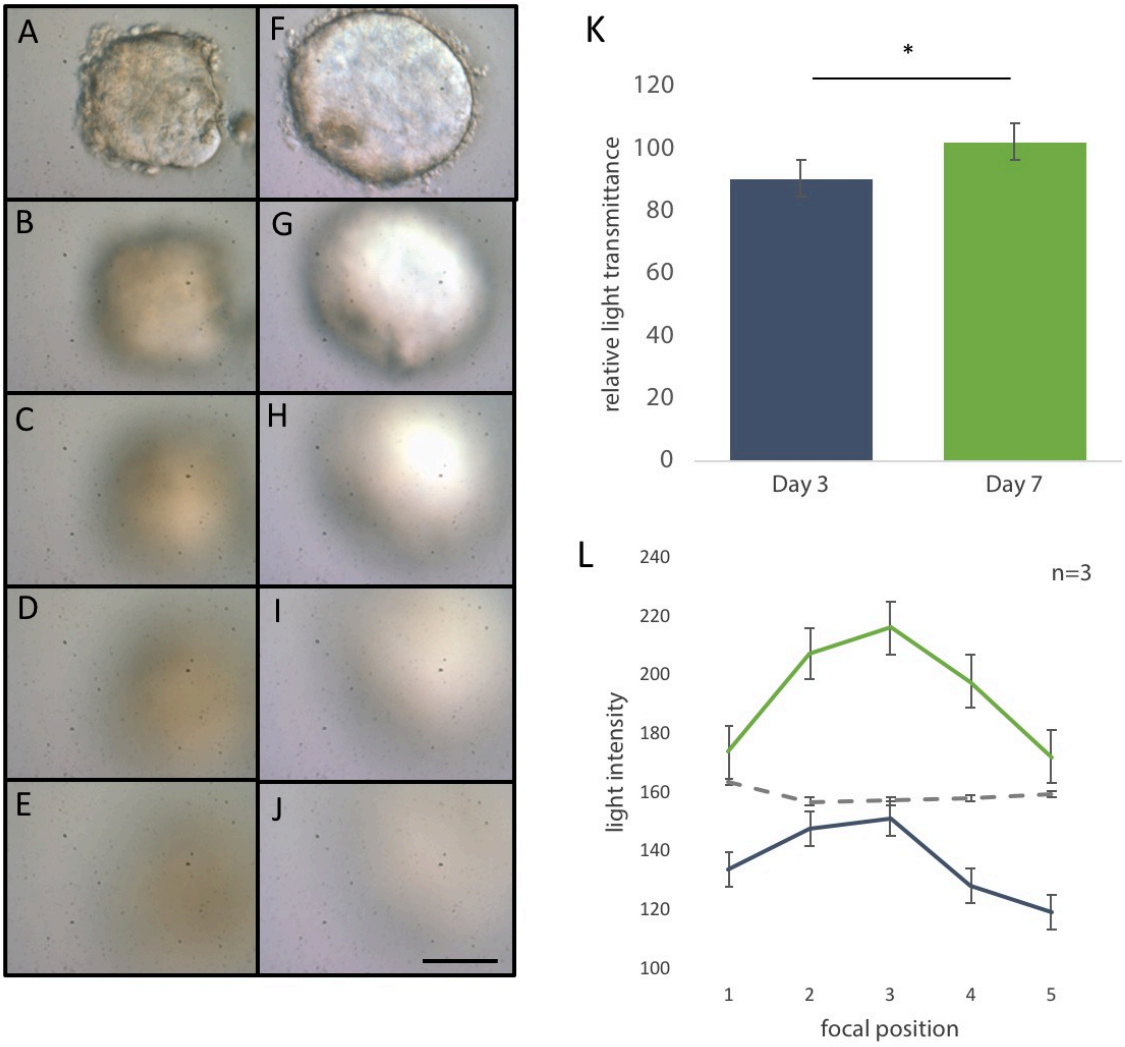

Figure 3.7 ROR1-enriched aggregates focus light 7 days after embedding in agarose

Light microscopy images taken at incrementally increasing distances below the aggregates (A to E) on day 3 of culture showed the initial low light transmission properties of the aggregates (A) and inability (C) to focus light. (F to J). By day 7, the micro-lens transmitted more light (F) and became able to focus light to a point (H). (K) Developing micro-lenses initially transmitted less light relative to the background medium at day 3, then equal to the background from day 7 onwards ($p<0.05$). (L) By day 7, the micro-lenses gain light focusing ability (position 3) and could transmit similar levels of light compared to the background culture medium (position 1). Scale bars (A-J) 50 µm

3.3.5 Aggregated ROR1-enriched cells expressed crystallin proteins

To assess the molecular changes occurring in the ROR1-enriched aggregates, the presence and abundance of lens proteins was ascertained by mass spectrometry (Figure 3.8, Figure 3.9). β-crystallin was detected at all time points, suggesting that immature LF-like cells were present in the ROR1-enriched lens cell culture. In contrast, micro-lenses at day 8 from purified ROR1$^+$ cells did not express β-crystallin (Section 2.3.4). The mass spectrometry analysis also revealed a trend of increasing sequence coverage of the crystallin proteins with increasing culture time (Figure 3.8) – suggesting the abundance of CRYAA, CRYBA1, CRYBA4, CRYBB2, and CRYBB3 significantly increased during the culture of the ROR1-enriched cell aggregates.

Notably, CRYGC that is normally present at high concentrations (>400 mg/mL) in the lens nucleus (formed during the pre-natal lens development period) (159) was identified in the ROR1-enriched micro-lens samples taken at days 7, 14 and 36. Additionally, CRYGS was detected in the later stages of culture. Together, detection of the β- and γ-crystallins indicated that mature LF-like cells, similar to those found in the lens nucleus, were present in the ROR1-enriched aggregates but at earlier tie-points compared to micro-lenses derived from purified ROR1$^+$ cells.

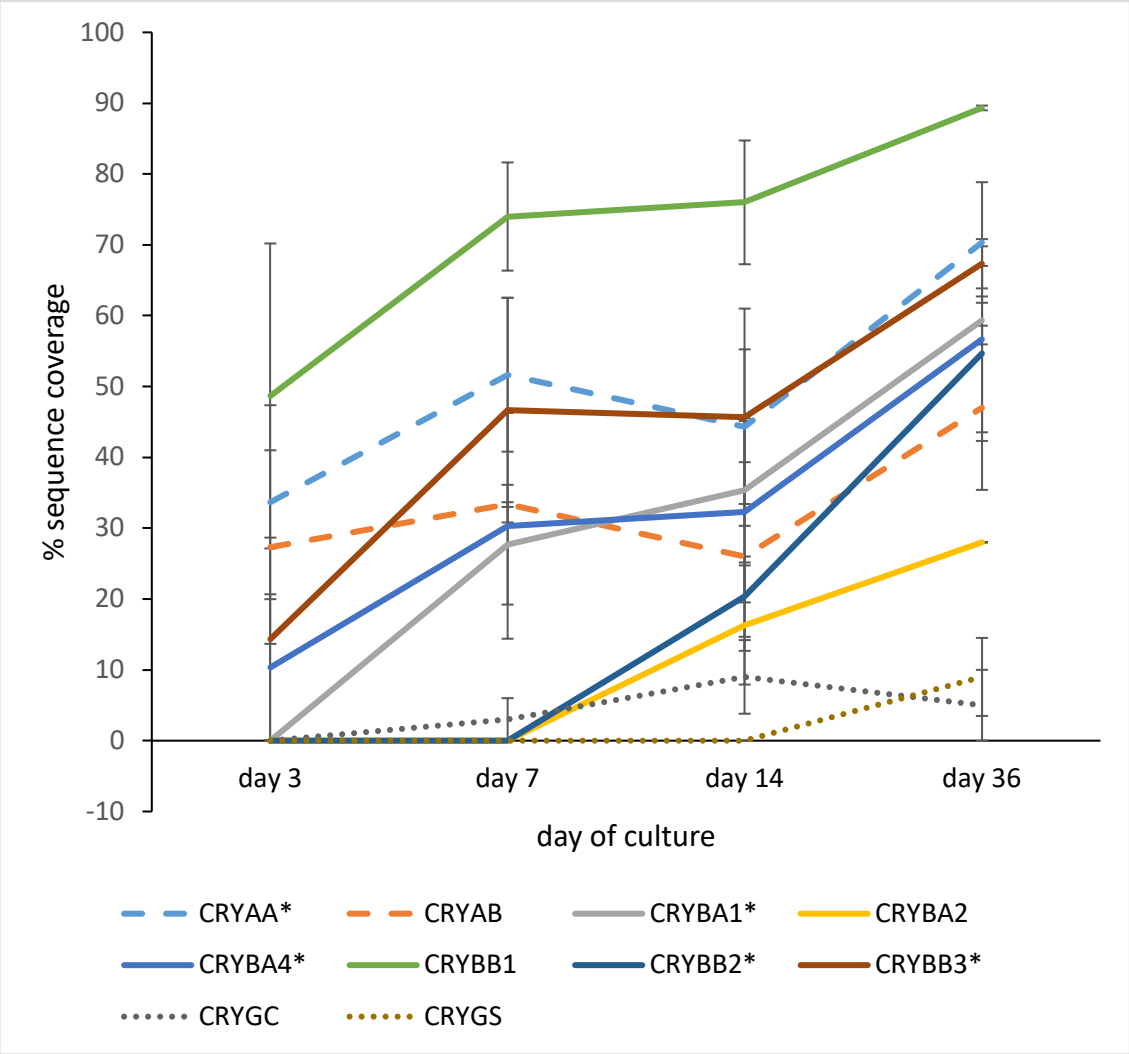

Figure 3.8 Sequence coverage of lens proteins identified by mass spectrometry

All proteins had greater sequence coverage on day 36 than day 3. All identified crystallins demonstrated a greater sequence coverage at day 36 than on day 3 after embedding. The increase in sequence coverage was significant (asterisk) for CRYAA, CRYBA1, CRYBA4, CRYBB2, and CRYBB3 ($p<0.05$). Interestingly, CRYGC was detected from day 7 onwards.

A

```
  1 MDVTIQHPWF KRTLGPFYPS RLFDQFFGEG LFEYDLLPFL SSTISPYYRQ
 51 SLFRTVLDSG ISEVRSDRDK FVIFLDVKHF SPEDLTVKVQ DDFVEIHGKH
101 NERQDDHGYI SREFHRRYRL PSNVDQSALS CSLSADGMLT FCGPKIQTGL
151 DATHAERAIP VSREEKPTSA PSS
```

B

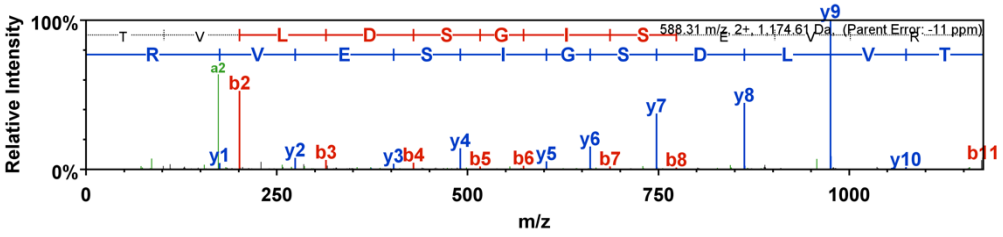

C

```
  1 MSQAAKASAS ATVAVNPGPD TKGKGAPPAG TSPSPGTTLA PTTVPITSAK
 51 AAELPPGNYR LVVFELENFQ GRRAEFSGEC SNLADRGFDR VRSIIVSAGP
101 WVAFEQSNFR GEMFILEKGE YPRWNTWSSS YRSDRLMSFR PIKMDAQEHK
151 ISLFEGANFK GNTIEIQGDD APSLWVYGFS DRVGSVKVSS GTWVGYQYPG
201 YRGYQYLLEP GDFRHWNEWG AFQPQMQSLR RLRDKQWHLE GSFPVLATEP
251 PK
```

D

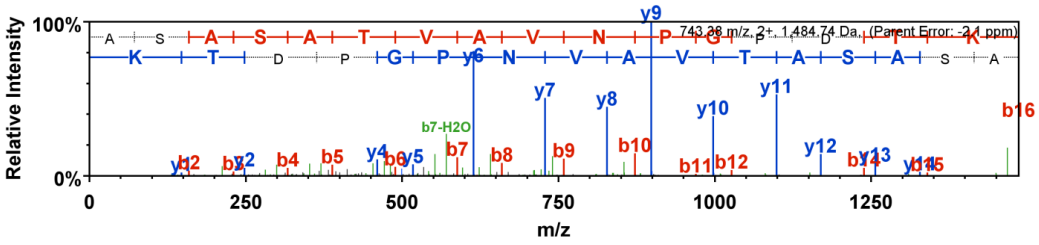

Figure 3.9 Proteins identified in ROR1- enriched micro-lenses by mass spectrometry

(A) MS/MS analysis showed 30% sequence coverage of CRYAA at day 36, with (B) example raw data peptide identification of sequence TVLDSGISEVR (A, underlined). (C) MS/MS analysis showed 89% sequence coverage of CRYBB1 at day 7, with example raw data peptide identification sequence ASASATVAVNPGPDTK (C, underlined).

3.4 Discussion

3.4.1 Evaluation of agarose and hydrogel 3D growth environments

This chapter aimed to further improve the culture parameters of the ROR1-based micro-lens system. Desirable properties of an embedding material were identified as permeability to nutrients and growth factors, polymerization at 37^{o}C, mechanical strength and the ability to dissociate to release micro-lenses with minimal potential alteration of transcription. Evaluation of 3 commercially-available hydrogels identified 6% HyStem + PEGSSDA as the only one with this range of required properties. Despite this testing, including overnight assessment of CA1 cell aggregates, 6% HyStem + PEGSSDA did not support longer-term survival of ROR1-enriched aggregates.

This failure of the HyStem + PEGSSDA occurred despite identical incubation and media conditions used for the embedded aggregates set up and cultured alongside the HyStem + PEGSSDA aggregates. The manufacturer's highest recommended concentration was 4% (w/v); however, this hydrogel was successfully used at 6% (w/v) for 3D culture of stromal cell spheroids (158). The 6% (w/v) HyStem + PEGSSDA was the only hydrogel concentration that met the mechanical requirements for daily media changes; however, the permeability of the hydrogel to nutrients and growth factors may have been reduced, potentially due to a high degree of cross-linking within the gel. In other hydrogel systems, in particular the PEG-peptide based hydrogels, cells can have the ability to locally break down the gel structure by the action of matrix metalloproteinase (MMP), allowing contraction of the hydrogel to allow cell expansion (153,154,160). Restriction of aggregate expansion or lack of access to growth factors in the HyStem + PEGSSDA hydrogel are potential causes of the aggregates' failure to develop micro-lens characteristics.

3.4.2 ROR1-enriched cells produced light-focusing micro-lenses at an early time point

ROR1-enriched cells appeared to be a phenotypically homogeneous population of cells, phenotypically similar to purified ROR1$^+$ cells. Despite the failure of the 6% HyStem + PEGSSDA to support micro-lens development, the agarose-based data demonstrates that ROR1-enriched aggregates develop micro-lens properties. Moreover, aggregated ROR1-enriched cells developed into micro-lenses albeit within a shorter timeframe compared to the purified ROR1$^+$ cells. The development of these lens-like properties at an earlier stage might be attributed to the presence of immature LF cells within the ROR1-enriched cell population, as suggested by the identification of β-crystallin much earlier in the ROR1-enriched aggregate cultures, (i.e., by day 3). This suggests that the 40 μm cell strainer step is sufficient to remove the majority of LF cells and non-lens cells, and in doing so generates sufficiently pure LEC populations for research applications. Notably, ROR1-enriched cells are unlikely to be suitable for clinical applications due to their reduced homogeneity compared to purified ROR1$^+$ cells.

The use of ROR1-enriched cells makes generation of tens-of-thousands of light-focusing micro-lenses simpler and more cost-effective compared to purified ROR1$^+$ cells for laboratory-only investigation of cataract and for drug-toxicity assays. However, the ROR1-enriched aggregates frequently developed protrusions after 14 days in culture (Figure 3.5B). While some minor bleb-like protrusions were observed in purified ROR1$^+$ micro-lenses produced in our laboratory (108), the protrusions in ROR1-enriched micro-lenses appeared more frequently and were larger than those in purified ROR1$^+$ micro-lenses. While the micro-lenses retained their core spheroidal shape and defined edge and the protrusions did not appear to be due to attachment to the cell culture plastic, it would be interesting to determine whether the protrusions are due to an inability for lens capsule production to keep pace with the growing size of the ROR1-enriched aggregates.

3.4.3 Future directions using ROR1-enriched micro-lenses

The ROR1-enriched micro-lens culture was more efficient and less expensive to produce than purified ROR1$^+$ micro-lenses. The MACS process yielded an average 10 to 20% of purified ROR1$^+$ cells from a starting ROR1-enriched (strained cell) population e.g., 30 x 10^6 ROR1-enriched cells would produce 3 to 6 x 10^6 purified ROR1$^+$ cells. The ROR1-enriched cell yield was typically 80% ROR1-positive cells post-filtration (108), with a consistent ROR1$^+$ cell morphology after one week of culture in E3 medium. Therefore, up to 8 times as many ROR1-enriched aggregates could be produced per differentiation experiment than purified ROR1$^+$ aggregates. Furthermore, purifying the ROR1$^+$ cells with MACS requires the use of an expensive anti-ROR1 antibody as well as other MACS reagents – thereby making ROR1-enriched micro-lens production more cost-effective. Overall, efficiency is increased and the ROR1-enriched aggregates enable less expensive and larger-scale micro-lens production compared to the same timeframe using purified ROR1$^+$ cells, yet while still retaining key lens properties of light transmission and light focusing ability. Furthermore, light focusing develops sooner in ROR1-enriched micro-lenses further decreasing costs by reducing growth factor requirements and time in micro-lens culture (albeit with the possibility that the ROR1-enriched micro-lenses at this point in time may not be able to be cultured as long before developing significant protrusions). This suggests that ROR1-enriched micro-lenses could be an effective tool for large-scale anti-cataract drug or lens toxicity screening.

Chapter 4

General discussion

4.1 Overview of thesis outcomes: Generation of functional *in vitro* human micro-lenses for investigating cataract

Cataract is a widespread issue and leading cause of low vision and blindness, decreasing the quality of life for tens-of-millions of people worldwide (2). Treatment for cataract involves removal of cataractous lens cells, followed by implantation of an IOL to replace lens function. With millions of cataract surgeries performed worldwide each year, the overall cost of current surgical treatment of cataract is expensive. It also requires highly specialized equipment that can be difficult to access for millions of cataract sufferers in developing countries (7,9). Clinical trials are yet to identify any effective drug or vitamin capable of delaying cataract (161). In order to develop alternative treatments for cataract, the underlying molecular mechanisms of cataract formation must be identified and understood. Animal lens models have assisted in understanding some aspects of cataract; however, they do not truly represent the human lens in terms of cell membrane composition or protein expression.

Previously published research demonstrated that heterogeneous cultures containing lens cells and non-lens cells can be generated from human PS cells, with lens cells randomly organized in microscopic (90) or macroscopic (91) structures called 'lentoids'. However, these approaches had significant limitations including the inability to produce uniformly-sized lens-like structures and limited or no demonstration of measurable light focusing or light transmission capability. Furthermore, these 'lentoids' were either abnormally adherent to the culture plastic or were lost to the culture medium preventing quantitative assessment of key lens properties.

The human micro-lenses produced through this project were obtained by mimicking *in vitro* aspects of embryonic teleost lens development. The micro-lenses expressed a variety of lens-required crystallin proteins. Parallel studies in our laboratory have shown that development of LF cells within the micro-lenses included morphologically recognizable milestones including organelle loss and denucleation (108). These results suggest that mimicking non-human development patterns might be a useful way of generating other tissue types from human PS cells.

As noted in the thesis, there were limitations to culturing the ROR1$^+$ LECs on chitosan film and with embedding the ROR1$^+$ aggregates in agarose (the temperature issues, potential for contamination and removal issues from samples for downstream analyses). Chitosan film remains worthwhile to consider for future applications using LECs, perhaps as a substrate for lens cell transplantation for *in vivo* lens regeneration studies. Additionally, purification of ROR1$^+$ cell populations by MACS requires an expensive anti-ROR1 antibody and associated processing time and decreases ROR1$^+$ yield, both of which significantly adds to the cost of the micro-lens assay. Greater efficiency in terms of both lower cost and higher cell number yield in a given timeframe was achieved through use of ROR1-enriched cells (obtained via filtration through a 40 μm cell strainer without MACS).

An attempt to further simplify the micro-lens system by assessment of several commercially-available hydrogels as potential agarose replacements was unsuccessful. This is perhaps unsurprising given that the field of embedding materials for organoid cultures is itself at the edge of scientific knowledge and technical capabilities (115,153,162).

Importantly, exposure of the micro-lenses to the emerging cystic fibrosis drug Vx-770 (suspected of causing cataract in cystic fibrosis patients) (134) resulted in loss of light transmission and/or focusing ability, suggesting the micro-lenses are suitable for clinically-relevant studies of the mechanism of cataract formation and as a tool for investigating lens toxicity. Moreover, the equipment required for micro-lens generation is simple and readily available – indicating the technique can be used in almost any tissue culture laboratory.

4.2 General implications and contribution to lens research

4.2.1 Investigation of risk factors

The ability to detect Vx-770-induced cataract suggests that exposure of human micro-lenses to known cataract risk factors could reveal some of the molecular mechanisms of cataract. Changes previously associated with different types of cataractous human or animal lenses, include abnormal cellular morphologies (e.g., swelling), proliferation, migration and/or differentiation; multi-lamellar bodies; as well as breakdown, proteolysis and/or PTM of crystallin proteins (e.g., non-enzymatic methylation of cysteine and arginine residues from the metabolic by-product S-adenosyl methionine, isomerization, cross-linking, oxidation, advanced glycemic end-products, deamidation, racemization and isomerization) (31,149,163,164). A variety of cataract risk factors have also been identified; however, the molecular mechanisms which lead to any particular type of cataractous change listed above is poorly understood. Each risk factor represents the potential of specific compounds or environments to cause cataract. The micro-lenses can be exposed to such risk-factors, either singularly or in combination, and should a cataractous change occur (as it does with Vx-770 treatment), the micro-lenses can be used to elucidate the molecular mechanism involved. Critically, micro-lens light transmission and focusing before and after exposure can be measured and used to guide time-point collection for molecular analyses (e.g., genomics, transcriptomics, proteomics, metabolomics etc.).

For example, diabetes is associated with up to five-fold increased cataract risk (46). Diabetic cataract can present as cortical and/or posterior subcapsular cataract (46,165); however, increased light scatter has been observed in human lenses of diabetic patients in the absence of visually observable cataract (166). A range of changes thought to be related to diabetes have been noted in the lenses of various species and include: osmotic swelling, decreased glutathione levels, increased levels of oxidized glutathione, increased lipid peroxidation and PTM of crystallins, including advanced glycation end-products (some of which may result in brunescence) (23,29,46) (166-168). Notably, while an aldose reductase inhibitor (Kinostat) has recently been approved as an effective treatment of cataract in dogs

(169), it appears unlikely to be a successful treatment for human cataract. The micro-lens system may therefore provide an opportunity to understand whether these and/or other molecular mechanisms occur in human lenses exposed to diabetes-like conditions. Exposure of micro-lenses to a range of concentrations of glucose or its metabolic products (e.g. sorbitol) in culture medium could determine whether, and at which concentration, there is an opacifying effect (166,168). Mass spectrometry analysis of the control and opacified micro-lenses might then reveal,

for example, when/how crystallin PTM/glycation occurs.

Additional risk factors of cataract could be tested in a similar manner. Other proposed cataract risk factors include exposure to hyperbaric oxygen. This is speculated to result in glutathione and protein thiol group loss, leading to insolubility of crystallin and nuclear cataract (170,171). Another risk factor arises from the lens being thought to have a protective effect on the retina by preventing UV light from reaching it and exposure to UVB is associated with cortical cataract in rats (38,172). Micro-lenses could be exposed to different wavelengths of UV light to determine if changes occur. Smoking is associated with cataract (33,45). Analysis of lenses from smokers vs non-smokers has shown a significant increase in Al and V ions in smokers; however, the relationship these have to cataract is unknown (33,173) but could be investigated using the micro-lens systems. Significant increases in Cd, Se and a reduction in Cu ions are age-related (33) and Cd is an inducer of oxidative stress (23). Exposing micro-lenses to these metal ions, at relevant concentrations, may be utilized to investigate their relationships to cataract. An alternative hypothesized mechanism for smoking-related cataract is by accumulation of p-benzoquinone (a compound associated with cigarette smoke-related pathogenesis) in the lens that may induce αA-crystallin aggregation (173). Finally, cholesterol-lowering statin use has a controversial association with cataract risk (39,174,175) and controlled *in vitro* assessment could assist determining whether there is an association between statin exposure and cataract.

Should cataract within the micro-lenses be induced by any of the above risk factors, then targeted analyses could be performed throughout onset and progression of cataract to define how cataract formation occurs. Once the molecular mechanisms are elucidated for cataract risk factors, this could lead to i) identification of non-invasive biomarkers of diabetic (or other) cataract (that precede vision loss), ii) identification of drug-able targets for diabetic (or other) cataract, and iii) a screening system for identification of candidate anti-cataract drugs. Widespread access to risk factor-specific drugs that reverse (in some, though not likely all cases) or delay cataract could overcome some of the issues of cataract-related impacts on health and lower the blindness rate for people in developing countries who do not have the access to cataract surgery that those in the developed world enjoy.

4.2.2 Toxicity screening

The exposure of developing micro-lenses to the drug Vx-770 demonstrated a dose-dependent effect on cataract formation. Future studies to define the molecular mechanism of Vx-770 induced cataract will be needed. However, these Vx-770 data also suggest the micro-lens system can be used to investigate other drugs that can affect the lens, either in a targeted or inadvertent manner. As with the assessment of cataract risk factors, micro-lenses can be exposed to substances to assess their cataract potential, by measuring changes in micro-lens light transmission and focusing. For example, drugs that have previously demonstrated formation of cataract such as corticosteroids (39), or are associated with cataract like antipsychotics, such as clozapine (176,177) may be screened using human micro-lenses to determine whether these drugs induce cataract in human lens tissue. Importantly, the use of micro-lenses for drug toxicity screening would enable investigation of drug effects on human tissue, eliminating any inter-species variance that may differ to human lens tissue. These micro-lenses have greater relevance to the human condition than those from other species.

4.2.3 Investigation of genetic causes of cataract

The micro-lens system could be applied using ROR1^{+} cells derived from disease-specific ES or iPS cells. This would allow production of micro-lenses for investigation of genetic cataract (32) or other diseases that affect the lens, for example Alport syndrome (74). Mutations can occur in crystallin genes, lens cytoskeletal genes, lens membrane protein genes, or genes for lens transcription factors such as PAX6 (178). Production of thousands of uniform human micro-lenses could transform future cataract research by providing an investigative platform for research into these genetic sight-affecting diseases of the lens by producing a disease-in-a-dish model to both investigate the molecular mechanisms of the disease and test proposed therapeutic agents.

4.3 Summary

The establishment of the ROR1 micro-lens system provides numerous opportunities to start to further understand lens-specific questions. Lens development, including which genes are switched on and switched off during early lens development, commencement of the OFZ in humans and the key time points in which the stages occur can be examined. Risk factors for cataract can be tested and molecular mechanisms elucidated, in a human-specific model. Likewise, preventative and/or curative treatments of cataract can be tested. Drugs can be identified that have human cataract as side effects, or alternatively drugs that caused cataract in animal tissue could be tested to see if they likewise cause cataract in human lens tissue. A human lens, along with other organoids, can form a toxicity screening panel as part of pre-clinical drug trialling. ROR1-enriched micro-lenses might be suitable/more cost-effective for this, as they are higher yielding without the need for ROR1-cell passaging (and thus are also quicker to obtain), and they appear to mature earlier than purified ROR1^{+} micro-lenses. Human ES or iPS cell generated micro-lenses that express genetic diseases of the eye can now be investigated using our micro-lens system. As a result of developing this human PS cell-derived micro-lens system, the means to examine in detail human lens development, disease, and lens drug screening with a large scale reproducible *in vitro* functional human lens system, is now possible.

Chapter 5

References

1. Taylor HR. The economic impact and cost of visual impairment in Australia. Brit J Ophthalmol. 2006;90(3):272–5.

2. Flaxman SR, Bourne RRA, Resnikoff S, Ackland P, Braithwaite T, Cicinelli MV, et al. Global causes of blindness and distance vision impairment 1990-2020: a systematic review and meta-analysis. Lancet Glob Health. 2017;5(12):e1221–34.

3. Rochtchina E, Mukesh BN, Wang JJ, McCarty CA, Taylor HR, Mitchell P. Projected prevalence of age-related cataract and cataract surgery in Australia for the years 2001 and 2021: pooled data from two population-based surveys. Clin Experiment Ophthalmol. 2003 Jun;31(3):233–6.

4. Wang W, Yan W, Fotis K, Prasad NM, Lansingh VC, Taylor HR, et al. Cataract surgical rate and socioeconomics: a global study. Invest Ophth Vis Sci. 2016;57(14):5872–81.

5. World Health Organization - AP2014_19_English. pdf, (null). Universal eye health: a global action plan 2014-2019 http://www. who. int/blindness [Internet]. [cited 2018 Mar 5]. Available from: http://scholar.google.comjavascript:void(0)

6. Wang W, Yan W, Müller A, He M. A global view on output and outcomes of cataract surgery with national indices of socioeconomic development. Invest Ophth Vis Sci. 2017 Jul 1;58(9):3669–76.

7. Hashemi H, Yekta A, Jafarzadehpur E, Doostdar A, Ostadimoghaddam H, Khabazkhoob M. The prevalence of visual impairment and blindness in underserved rural areas: a crucial issue for future. Eye (Lond). 2017 Aug;31(8):1221–8.

8. Venkatesh R, van Landingham SW, Khodifad AM, Haripriya A, Thiel CL, Ramulu P, et al. Carbon footprint and cost-effectiveness of cataract surgery. Curr Opin Ophthalmol. 2016 Jan;27(1):82–8.

9. Danquah L, Kuper H, Eusebio C, Rashid MA, Bowen L, Foster A, et al. The long term impact of cataract surgery on quality of life, activities and poverty: results from a six year longitudinal study in Bangladesh and the Philippines. PLoS ONE. 2014;9(4):e94140.

10. Rein DB, Zhang P, Wirth KE, Lee PP, Hoerger TJ, McCall N, et al. The economic burden of major adult visual disorders in the United States. Arch Ophthalmol. 2006 Dec;124(12):1754–60.

11. Polack S. Restoring sight: how cataract surgery improves the lives of older adults. Community Eye Health. 2008 Jun;21(66):24–5.

12. Wormstone IM, Wang L, Liu CSC. Posterior capsule opacification. Exp Eye Res. Elsevier Ltd; 2009 Feb 2;88(2):257–69.

13. Wormstone IM. Posterior capsule opacification: a cell biological

perspective. Exp Eye Res. 2002 Mar;74(3):337–47.

14. Zhao Y, Yang K, Li J, Huang Y, Zhu S. Comparison of hydrophobic and hydrophilic intraocular lens in preventing posterior capsule opacification after cataract surgery: An updated meta-analysis. Medicine (Baltimore). 2017 Nov;96(44):e8301.

15. Elkin ZP, Piluek WJ, Fredrick DR. Revisiting secondary capsulotomy for posterior capsule management in pediatric cataract surgery. J AAPOS. 2016 Dec;20(6):506–10.

16. Medsinge A, Nischal KK. Pediatric cataract: challenges and future directions. Clin Ophthalmol. 2015;9:77–90.

17. Kossack N, Schindler C, Weinhold I, Hickstein L, Lehne M, Walker J, et al. German claims data analysis to assess impact of different intraocular lenses on posterior capsule opacification and related healthcare costs. Z Gesundh Wiss. 2018;26(1):81–90.

18. Solebo AL, Teoh L, Rahi J. Epidemiology of blindness in children. Arch Dis Child. 2017;102(9):archdischild–2016–310532–857.

19. Churchill A, Graw J. Clinical and experimental advances in congenital and paediatric cataracts. Philos Trans R Soc Lond, B, Biol Sci. 2011 Apr 27;366(1568):1234–49.

20. Chougule P, Murat S, Mohamed A, Kekunnaya R. Follow-up patterns and associated risk factors after paediatric cataract surgery: observation over a 5-year period. Br J Ophthalmol. 2018 Jan 31.

21. Truscott RJW. Age-related nuclear cataract-oxidation is the key. Exp Eye Res. 2005 May;80(5):709–25.

22. Lim JC, Umapathy A, Donaldson PJ. Tools to fight the cataract epidemic: A review of experimental animal models that mimic age related nuclear cataract. Exp Eye Res. 2016 Apr;145:432–43.

23. Michael R, Bron A. The ageing lens and cataract: a model of normal and pathological ageing. Philos Trans R Soc Lond, B, Biol Sci. 2011 Apr 27;366(1568):1278–92.

24. Moreau KL, King JA. Protein misfolding and aggregation in cataract disease and prospects for prevention. Trends Mol Med. 2012 May;18(5):273–82.

25. Yang J, Zhou S, Guo M, Li Y, Gu J. Different alpha crystallin expression in human age-related and congenital cataract lens epithelium. BMC Ophthalmol. 2016;16(1):67.

26. Peschek J, Braun N, Franzmann TM, Georgalis Y, Haslbeck M, Weinkauf S, et al. The eye lens chaperone alpha-crystallin forms defined globular assemblies. Proc Natl Acad Sci USA. 2009 Aug 11;106(32):13272–7.

27. Bloemendal H, de Jong W, Jaenicke R, Lubsen NH, Slingsby C, Tardieu A.

Ageing and vision: structure, stability and function of lens crystallins. Prog Biophys Mol Biol. 2004 Nov;86(3):407–85.

28. Al-Ghoul KJ, Lane CW, Taylor VL, Fowler WC, Costello MJ. Distribution and type of morphological damage in human nuclear age-related cataracts. Exp Eye Res. 1996 Mar;62(3):237–51.

29. Nagaraj RH, Linetsky M, Stitt AW. The pathogenic role of Maillard reaction in the aging eye. Amino Acids. 2010 Oct 21;42(4):1205–20.

30. Pendergrass SA, Verma SS, Holzinger E, (null). Next-generation analysis of cataracts: determining knowledge driven gene-gene interactions using Biofilter, and gene-environment interactions using the PhenX Toolkit. 2015.

31. Tweeddale HJ, Hawkins CL, Janmie JF, Truscott RJW, Davies MJ. Cross-linking of lens crystallin proteins induced by tryptophan metabolites and metal ions: implications for cataract development. Free Radic Res. 2016 Oct;50(10):1116–30.

32. Shiels A, Hejtmancik JF. Genetics of human cataract. Clin Genet. 2013 Aug;84(2):120–7.

33. Langford-Smith A, Tilakaratna V, Lythgoe PR, Clark SJ, Bishop PN, Day AJ. Age and smoking related changes in metal ion levels in human lens: implications for cataract formation. PLoS ONE. 2016 Jan 21;11(1):e0147576–16.

34. Lim SA, Joo C-K, Kim MS, Chung SK. Expression of p53 and caspase-8 in lens epithelial cells of diabetic cataract. J Cataract Refract Surg. 2014 Jul;40(7):1102–8.

35. Moghadam SS, Oryan A, Kurganov BI, Tamaddon A-M, Alavianehr MM, Moosavi-Movahedi AA, et al. The structural damages of lens crystallins with peroxynitrite and methylglyoxal, two causative players in diabetic complications and preventive role of lens antioxidant components. Int J Biol Macromol. 2017 May 1;103:74–88.

36. Shore RE. Radiation and cataract risk: Impact of recent epidemiologic studies on ICRP judgments. Mutat Res. 2016 Dec;770(Pt B):231–7.

37. Ainsbury EA, Barnard S, Bright S, Dalke C, Jarrin M, Kunze S, et al. Ionizing radiation induced cataracts: Recent biological and mechanistic developments and perspectives for future research. Mutat Res. 2016 Dec;770(Pt B):238–61.

38. Löfgren S. Solar ultraviolet radiation cataract. Exp Eye Res. 2017 Mar;156:112–6.

39. Liu Y-C, Wilkins M, Kim T, Malyugin B, Mehta JS. Cataracts. Lancet. 2017 Aug 5;390(10094):600–12.

40. Gong Y, Feng K, Yan N, Xu Y, Pan C-W. Different amounts of alcohol

consumption and cataract: a meta-analysis. Optom Vis Sci. 2015 Apr;92(4):471–9.

41. Costello MJ, Burette A, Weber M, Metlapally S. Electron tomography of fiber cell cytoplasm and dense cores of multilamellar bodies from human age-related nuclear cataracts. Exp Eye Res. 2012;101:72–81.

42. Truscott RJW, Mizdrak J, Friedrich MG, Hooi MY, Lyons B, Jamie JF, et al. Is protein methylation in the human lens a result of non-enzymatic methylation by S-adenosylmethionine? Exp Eye Res. Elsevier Ltd; 2012 Dec 6;99(C):48–54.

43. Wu C, Liu Z, Ma L, Pei C, Qin L, Gao N, et al. MiRNAs regulate oxidative stress related genes via binding to the 3' UTR and TATA-box regions: a new hypothesis for cataract pathogenesis. BMC Ophthalmol. 2017 Aug 14;17(1):142.

44. Zhao Z, Fan Q, Zhou P, Ye H, Cai L, Lu Y. Association of alpha A-crystallin polymorphisms with susceptibility to nuclear age-related cataract in a Han Chinese population. BMC Ophthalmol. 2017 Jul 29;17(1):133.

45. Ye J, He J, Wang C, Wu H, Shi X, Zhang H, et al. Smoking and risk of age-related cataract: a meta-analysis. Invest Ophth Vis Sci. 2012 Jun;53(7):3885–95.

46. Vinson JA. Oxidative stress in cataracts. Pathophysiology. 2006 Aug;13(3):151–62.

47. Elbay A, Ozer OF, Altinisik M, Elbay AE, Sezer T, Bayraktar H, et al. A novel tool reflecting the role of oxidative stress in the cataracts: thiol/disulfide homeostasis. Scand J Clin Lab Invest. 2017 May;77(3):223–7.

48. Henderson MA, Valluri S, Desrosiers C, Lopez JT, Batuello CN, Caperell-Grant A, et al. Effect of gender on radiation-induced cataractogenesis. Radiat Res. 2009 Jul;172(1):129–33.

49. Chylack LT, Feiveson AH, Peterson LE, Tung WH, Wear ML, Marak LJ, et al. NASCA report 2: Longitudinal study of relationship of exposure to space radiation and risk of lens opacity. Radiat Res. 2012 Jul;178(1):25–32.

50. Dynlacht JR, Valluri S, Lopez JT, Greer F, Desrosiers C, Caperell-Grant A, et al. Estrogen protects against radiation-induced cataractogenesis. Radiat Res. 2008 Dec;170(6):758–64.

51. Clark JI. Self-assembly of protein aggregates in ageing disorders: the lens and cataract model. Philos Trans R Soc Lond, B, Biol Sci. 2013 May 5;368(1617):20120104.

52. Bloemendal H. The vertebrate eye lens. Science. 1977 Jul 8;197(4299):127–38.

53. Bassnett S, Šikić H. The lens growth process. Prog Retin Eye Res. 2017 Sep;60:181–200.

54. Sharma KK, Santhoshkumar P. Lens aging: effects of crystallins. Biochim Biophys Acta. Elsevier B.V; 2009 Oct 1;1790(10):1095–108.

55. Audette DS, Scheiblin DA, Duncan MK. The molecular mechanisms underlying lens fiber elongation. Exp Eye Res. 2017 Mar;156:41–9.

56. Kuszak JR, Mazurkiewicz M, Jison L, Madurski A, Ngando A, Zoltoski RK. Quantitative analysis of animal model lens anatomy: accommodative range is related to fiber structure and organization. Vet Ophthalmol. Blackwell Publishing Inc; 2006 Sep;9(5):266–80.

57. Garland DL, Duglas-Tabor Y, Jimenez-Asensio J, Datiles MB, Magno B. The nucleus of the human lens: demonstration of a highly characteristic protein pattern by two-dimensional electrophoresis and introduction of a new method of lens dissection. Exp Eye Res. 1996 Mar;62(3):285–91.

58. Costello MJ, Brennan LA, Basu S, Chauss D, Mohamed A, Gilliland KO, et al. Autophagy and mitophagy participate in ocular lens organelle degradation. Exp Eye Res. 2013 Nov;116:141–50.

59. De Maria A, Bassnett S. Birc7: A late fiber gene of the crystalline lens. Invest Ophth Vis Sci. 2015 Jul;56(8):4823–34.

60. Costello MJ, Brennan LA, Mohamed A, Gilliland KO, Johnsen S, Kantorow M. Identification and ultrastructural characterization of a novel nuclear degradation complex in differentiating lens fiber cells. PLoS ONE. 2016;11(8):e0160785.

61. Rowan S, Chang M-L, Reznikov N, Taylor A. Disassembly of the lens fiber cell nucleus to create a clear lens: the p27 descent. Exp Eye Res. Elsevier Ltd; 2016 Apr 2;:1–7.

62. Khan SY, Hackett SF, Lee M-CW, Pourmand N, Talbot CC Jr, Riazuddin SA. Transcriptome profiling of developing murine lens through RNA sequencing. Invest Ophth Vis Sci. 2015 Jul 1;56(8):4919–8.

63. Bassnett S, Beebe DC. Coincident loss of mitochondria and nuclei during lens fiber cell differentiation. Dev Dyn. Wiley Subscription Services, Inc., A Wiley Company; 1992 Jun;194(2):85–93.

64. Bassnett S. Lens organelle degradation. Exp Eye Res. 2002 Jan;74(1):1–6.

65. Counis MF, Chaudun E, Arruti C, Oliver L, Sanwal M, Courtois Y, et al. Analysis of nuclear degradation during lens cell differentiation. Cell Death Differ. 1998 Apr;5(4):251–61.

66. National Eye Institute. Eye Health: Anatomy of the Eye [Internet]. Duffy MA, editor. visionaware.org. [cited 2017 Jun 29]. Available from: http://www.visionaware.org/info/your-eye-condition/eye-health/anatomy-of-the-eye/125

67. van Rens GL, de Jong WW, Bloemendal H. A superfamily in the mammalian eye lens: the beta/gamma-crystallins. Mol Biol Rep. 1992 Feb;16(1):1–10.

68. Wang X, Garcia CM, Shui Y-B, Beebe DC. Expression and regulation of alpha-, beta-, and gamma-crystallins in mammalian lens epithelial cells. Invest Ophth Vis Sci. 2004 Oct;45(10):3608–19.

69. Augusteyn RC. Growth of the lens: in vitro observations. Clin Exp Optometry. 2008 May;91(3):226–39.

70. van Rens GL, de Jong WW, Bloemendal H. A superfamily in the mammalian eye lens: the beta/gamma-crystallins. Mol Biol Rep. 1992 Feb;16(1):1–10.

71. Slingsby C, Wistow GJ, Clark AR. Evolution of crystallins for a role in the vertebrate eye lens. Protein Sci. 2013 Apr;22(4):367–80.

72. Toyama BH, Hetzer MW. Protein homeostasis: live long, won't prosper. Nature Rev Mol Cell Bio. Nature Publishing Group; 2013 Jan 1;14(1):55–61.

73. Danysh BP, Duncan MK. The lens capsule. Exp Eye Res. 2009 Feb;88(2):151–64.

74. Kelley PB, Sado Y, Duncan MK. Collagen IV in the developing lens capsule. Matrix Biol. 2002 Aug;21(5):415–23.

75. McAvoy JW, Dawes LJ, Sugiyama Y, Lovicu FJ. Intrinsic and extrinsic regulatory mechanisms are required to form and maintain a lens of the correct size and shape. Exp Eye Res. 2017 Mar;156:34–40.

76. Uechi G, Sun Z, Schreiber EM, Halfter W, Balasubramani M. Proteomic view of basement membranes from human retinal blood vessels, inner limiting membranes, and lens capsules. J Proteome Res. 2014 Jul 17;(13):3693–705.

77. Danysh BP, Patel TP, Czymmek KJ, Edwards DA, Wang L, Pande J, et al. Characterizing molecular diffusion in the lens capsule. Matrix Biol. 2010 Apr;29(3):228–36.

78. Cvekl A, Ashery-Padan R. The cellular and molecular mechanisms of vertebrate lens development. Development. 2014 Dec;141(23):4432–47.

79. Chamberlain CG, McAvoy JW. Evidence that fibroblast growth factor promotes lens fibre differentiation. Curr Eye Res. 1987 Sep;6(9):1165–9.

80. McAvoy JW, Chamberlain CG. Fibroblast growth factor (FGF) induces different responses in lens epithelial cells depending on its concentration. Development. 1989 Oct;107(2):221–8.

81. Charlton-Perkins M, Brown NL, Cook TA. The lens in focus: a comparison of lens development in Drosophila and vertebrates. Mol Genet Genomics. 2011 Oct;286(3-4):189–213.

82. Cvekl A, Duncan MK. Genetic and epigenetic mechanisms of gene regulation during lens development. Prog Retin Eye Res. 2007 Nov;26(6):555–97.

83. Zou P, Wu S-Y, Koteiche HA, Mishra S, Levic DS, Knapik E, et al. A conserved role of αA-crystallin in the development of the zebrafish embryonic lens. Exp Eye Res. 2015 Sep;138:104–13.

84. Cvekl A, McGreal R, Liu W. Chapter Ten-Lens Development and Crystallin Gene Expression. Progress in Molecular Biology and …. Elsevier; 2015;134:129–67.

85. Cvekl A, Zhang X. Signaling and Gene Regulatory Networks in Mammalian Lens Development. Trends Genet. 2017 Oct;33(10):677–702.

86. Greiling TMS, Clark JI. Early lens development in the zebrafish: a three-dimensional time-lapse analysis. Dev Dyn. 2009 Sep;238(9):2254–65.

87. Dahm R, Schonthaler HB, Soehn AS, van Marle J, Vrensen GFJM. Development and adult morphology of the eye lens in the zebrafish. Exp Eye Res. 2007 Jul;85(1):74–89.

88. O'Rahilly R. The prenatal development of the human eye. Exp Eye Res. 1975 Aug;21(2):93–112.

89. O'Connor MD, McAvoy JW. *In vitro* generation of functional lens-like structures with relevance to age-related nuclear cataract. Invest Ophth Vis Sci. 2007 Mar 1;48(3):1245–8.

90. Yang C, Yang Y, Brennan LA, Bouhassira EE, Kantorow M, Cvekl A. Efficient generation of lens progenitor cells and lentoid bodies from human embryonic stem cells in chemically defined conditions. FASEB J. Federation of American Societies for Experimental Biology; 2010 Sep;24(9):3274–83.

91. Fu Q, Qin Z, Jin X, Zhang L, Chen Z, He J, et al. Generation of functional lentoid bodies from human induced pluripotent stem cells derived from urinary cells. Invest Ophth Vis Sci. 2017 Jan 1;58(1):517–27.

92. Qiu X, Yang J, Liu T, Jiang Y, Le Q, Lu Y. Efficient generation of lens progenitor cells from cataract patient–specific induced pluripotent stem cells. PLoS ONE. 2012 Mar 5;7(3):e32612–10.

93. Li D, Qiu X, Yang J, Liu T, Luo Y, Lu Y. Generation of human lens epithelial-like cells from patient-specific induced pluripotent stem cells. J Cell Physiol. 2016 Dec;231(12):2555–62.

94. Thomson JA, Itskovitz-Eldor J, Shapiro SS, Waknitz MA, Swiergiel JJ, Marshall VS, et al. Embryonic stem cell lines derived from human blastocysts. Science. 1998 Nov 6;282(5391):1145–7.

95. Zdravkovic T, Nazor KL, Larocque N, Gormley M, Donne M, Hunkapillar N, et al. Human stem cells from single blastomeres reveal pathways of embryonic or trophoblast fate specification. Development. 2015 Dec 1;142(23):4010–25.

96. Giritharan G, Ilic D, Gormley M, Krtolica A. Human embryonic stem cells derived from embryos at different stages of development share similar

transcription profiles. PLoS ONE. 2011;6(10):e26570.

97. Mitalipova MM, Rao RR, Hoyer DM, Johnson JA, Meisner LF, Jones KL, et al. Preserving the genetic integrity of human embryonic stem cells. Nat Biotechnol. 2005 Jan;23(1):19–20.

98. Klimanskaya I, Chung Y, Becker S, Lu S-J, Lanza R. Human embryonic stem cell lines derived from single blastomeres. Nature. 2006 Nov 23;444(7118):481–5.

99. Ho R, Chronis C, Plath K. Mechanistic insights into reprogramming to induced pluripotency. J Cell Physiol. 2011 Apr;226(4):868–78.

100. Takahashi K, Yamanaka S. Induction of pluripotent stem cells from mouse embryonic and adult fibroblast cultures by defined factors. Cell. 2006 Aug 25;126(4):663–76.

101. Liu C, Oikonomopoulos A, Sayed N, Wu JC. Modeling human diseases with induced pluripotent stem cells: from 2D to 3D and beyond. Development. 2018 Mar 8;145(5).

102. Lovicu FJ, McAvoy JW, de Iongh RU. Understanding the role of growth factors in embryonic development: insights from the lens. Philos Trans R Soc Lond, B, Biol Sci. 2011 Apr 27;366(1568):1204–18.

103. Chen Y, Stump RJW, Lovicu FJ, Shimono A, McAvoy JW. Wnt signaling is required for organization of the lens fiber cell cytoskeleton and development of lens three-dimensional architecture. Dev Biol. 2008 Dec 1;324(1):161–76.

104. de Iongh RU, Abud HE, Hime GR. Frizzled signaling in eye development and disease. Front Biosci. 2006 Sep 1;11:2442–64.

105. Tholozan FMD, Quinlan RA. Lens cells: more than meets the eye. Int J Biochem Cell Biol. 2007;39(10):1754–9.

106. Qiu X, Yang J, Liu T, Jiang Y, Le Q, Lu Y. Efficient generation of lens progenitor cells from cataract patient-specific induced pluripotent stem cells. Public Library of Science; 2012;7(3):e32612.

107. Mengarelli I, Barberi T. Derivation of multiple cranial tissues and isolation of lens epithelium-like cells from human embryonic stem cells. Stem Cells Trans M. 2013 Feb 13;2(2):94–106.

108. Murphy P, Kabir MH, Srivastava T, Mason ME, Dewi CU, Lim S, et al. Light-focusing human micro-lenses generated from pluripotent stem cells model lens development and drug-induced cataractin vitro. Development. 2018 Jan 9;145(1):dev155838.

109. Lancaster MA, Knoblich JA. Organogenesis in a dish: modeling development and disease using organoid technologies. Science. 2014 Jul 18;345(6194):1247125.

110. Dekkers JF, Berkers G, Kruisselbrink E, Vonk A, de Jonge HR, Janssens HM, et al. Characterizing responses to CFTR-modulating drugs using rectal organoids derived from subjects with cystic fibrosis. Sci Transl Med. 2016 Jun 22;8(344):344ra84.

111. Dutta D, Heo I, Clevers H. Disease modeling in stem cell-derived 3D organoid systems. Trends Mol Med. 2017 May;23(5):393–410.

112. Spence JR, Mayhew CN, Rankin SA, Kuhar MF, Vallance JE, Tolle K, et al. Directed differentiation of human pluripotent stem cells into intestinal tissue in vitro. Nature. 2011 Feb 3;470(7332):105–9.

113. McCracken KW, Howell JC, Wells JM, Spence JR. Generating human intestinal tissue from pluripotent stem cells in vitro. Nat Protoc. 2011 Nov 10;6(12):1920–8.

114. Broutier L, Andersson-Rolf A, Hindley CJ, Boj SF, Clevers H, Koo B-K, et al. Culture and establishment of self-renewing human and mouse adult liver and pancreas 3D organoids and their genetic manipulation. Nat Protoc. 2016 Sep;11(9):1724–43.

115. Huch M, Knoblich JA, Lutolf MP, Martinez-Arias A. The hope and the hype of organoid research. Development. 2017 Mar 15;144(6):938–41.

116. Sachs N, Tsukamoto Y, Kujala P, Peters PJ, Clevers H. Intestinal epithelial organoids fuse to form self-organizing tubes in floating collagen gels. Development. 2017 Mar 15;144(6):1107–12.

117. Choi J, Iich E, Lee J-H. Organogenesis of adult lung in a dish: differentiation, disease and therapy. Dev Biol. 2016 Dec 15;420(2):278–86.

118. Takasato M, Little MH. A strategy for generating kidney organoids - recapitulating the development in human pluripotent stem cells. Dev Biol. Elsevier; 2016 Dec 15;420(2):210–20.

119. Morizane R, Bonventre JV. Kidney organoids: a translational journey. Trends Mol Med. Elsevier Ltd; 2017 Mar 1;23(3):246–63.

120. Schutgens F, Verhaar MC, Rookmaaker MB. Pluripotent stem cell-derived kidney organoids_ An in vivo-like in vitro technology. Eur J Pharmacol. Elsevier; 2016 Nov 5;790(c):12–20.

121. Nakano T, Ando S, Takata N, Kawada M, Muguruma K, Sekiguchi K, et al. Self-formation of optic cups and storable stratified neural retina from human ESCs. Cell Stem Cell. 2012 Jun 14;10(6):771–85.

122. Finkbeiner SR, Zeng X-L, Utama B, Atmar RL, Shroyer NF, Estes MK. Stem cell-derived human intestinal organoids as an infection model for rotaviruses. MBio. 2012;3(4):e00159–12.

123. Qian X, Nguyen HN, Jacob F, Song H, Ming G-L. Using brain organoids to understand Zika virus-induced microcephaly. Development. 2017 Mar 15;144(6):952–7.

124. Wang Q, McAvoy JW, Lovicu FJ. Growth factor signaling in vitreous humor-induced lens fiber differentiation. Invest Ophth Vis Sci. 2010 Jul;51(7):3599–610.

125. O'Connor MD, Wederell ED, de Iongh RU, Lovicu FJ, McAvoy JW. Generation of transparency and cellular organization in lens explants. Exp Eye Res. 2008 May;86(5):734–45.

126. Wang E, Wang D, Geng A, Seo R, Gong X. Growth of hollow cell spheroids in microbead templated chambers. Biomaterials. 2017 Oct;143:57–64.

127. Wages P, Horwitz J, Ding L, Corbin RW, Posner M. Changes in zebrafish (Danio rerio) lens crystallin content during development. Mol Vis. 2013;19:408–17.

128. Bibliowicz J, Tittle RK, Gross JM. Toward a better understanding of human eye disease insights from the zebrafish, Danio rerio. Prog Mol Biol Transl Sci. 2011;100:287–330.

129. Ryan S-L, Baird A-M, Vaz G, Urquhart AJ, Senge M, Richard DJ, et al. Drug discovery approaches utilizing three-dimensional cell culture. Assay Drug Dev Technol. 2016 Jan;14(1):19–28.

130. Breslin S, O'Driscoll L. Three-dimensional cell culture: the missing link in drug discovery. Drug Discov Today. 2013 Mar;18(5-6):240–9.

131. Loessner D, Stok KS, Lutolf MP, Hutmacher DW, Clements JA, Rizzi SC. Bioengineered 3D platform to explore cell-ECM interactions and drug resistance of epithelial ovarian cancer cells. Biomaterials. 2010 Nov;31(32):8494–506.

132. Ravi M. Applications of three-dimensional cell cultures in the early stages of drug discovery, focusing on gene expressions, drug metabolism, and susceptibility. Crit Rev Eukaryot Gene Expr. 2017;27(1):53–62.

133. McColley SA. A safety evaluation of ivacaftor for the treatment of cystic fibrosis. Expert Opin Drug Saf. 2016 May;15(5):709–15.

134. Talamo Guevara M, McColley SA. The safety of lumacaftor and ivacaftor for the treatment of cystic fibrosis. Expert Opin Drug Saf. 2017 Nov;16(11):1305–11.

135. Dryden C, Wilkinson J, Young D, Brooker RJ, Scottish Paediatric Cystic Fibrosis Managed Clinical Network (SPCFMCN). The impact of 12 months treatment with ivacaftor on Scottish paediatric patients with cystic fibrosis with the G551D mutation: a review. Arch Dis Child. 2018 Jan;103(1):68–70.

136. Davies JC, Wainwright CE, Canny GJ, Chilvers MA, Howenstine MS, Munck A, et al. Efficacy and safety of ivacaftor in patients aged 6 to 11 years with cystic fibrosis with a G551D mutation. Am J Respir Crit Care Med. 2013 Jun 1;187(11):1219–25.

137. Davies JC, Cunningham S, Harris WT, Lapey A, Regelmann WE, Sawicki GS,

et al. Safety, pharmacokinetics, and pharmacodynamics of ivacaftor in patients aged 2-5 years with cystic fibrosis and a CFTR gating mutation (KIWI): an open-label, single-arm study. Lancet Respir Med. Elsevier Ltd; 2016 Jan 20;4(2):1–9.

138. Zhao L, Chen X-J, Zhu J, Xi Y-B, Yang X, Hu L-D, et al. Lanosterol reverses protein aggregation in cataracts. Nature. 2015 Jul 30;523(7562):607–11.

139. Makley LN, McMenimen KA, DeVree BT, Goldman JW, McGlasson BN, Rajagopal P, et al. Pharmacological chaperone for α-crystallin partially restores transparency in cataract models. Science. 2015 Nov 6;350(6261):674–7.

140. O'Connor MD, Kardel MD, Iosfina I, Youssef D, Lu M, Li MM, et al. Alkaline phosphatase-positive colony formation is a sensitive, specific, and quantitative indicator of undifferentiated human embryonic stem cells. Stem Cells. 2008 May;26(5):1109–16.

141. cdn.stemcell.com [Internet]. [cited 2018 Mar 30]. Available from: https://cdn.stemcell.com

142. Shainhouse JZ, Grierson LM, Naseer Z. A long-term, open-label study to confirm the safety of topical diclofenac solution containing dimethyl sulfoxide in the treatment of the osteoarthritic knee. Am J Ther. 2010 Nov;17(6):566–76.

143. Andley UP, Rhim JS, Chylack LT, Fleming TP. Propagation and immortalization of human lens epithelial cells in culture. Invest Ophth Vis Sci. 1994 Jun;35(7):3094–102.

144. Taylor DL, Thevarajah JJ, Narayan DK, Murphy P, Mangala MM, Lim S, et al. Real-time monitoring of peptide grafting onto chitosan films using capillary electrophoresis. Anal Bioanal Chem. 2015 Mar;407(9):2543–55.

145. Suzuki S, Dawson RA, Chirila TV, Shadforth AMA, Hogerheyde TA, Edwards GA, et al. Treatment of silk fibroin with poly(ethylene glycol) for the enhancement of corneal epithelial cell growth. J Funct Biomater. 2015;6(2):345–66.

146. Madden PW, Lai JNX, George KA, Giovenco T, Harkin DG, Chirila TV. Human corneal endothelial cell growth on a silk fibroin membrane. Biomaterials. 2011 Jun;32(17):4076–84.

147. Deeley JM, Mitchell TW, Wei X, Korth J, Nealon JR, Blanksby SJ, et al. Human lens lipids differ markedly from those of commonly used experimental animals. Biochim Biophys Acta. 2008 Jun;1781(6-7):288–98.

148. Slingsby C, Wistow GJ. Functions of crystallins in and out of lens: roles in elongated and post-mitotic cells. Prog Biophys Mol Biol. 2014 Jul;115(1):52–67.

149. Kyselova Z. Different experimental approaches in modelling cataractogenesis: An overview of selenite-induced nuclear cataract in rats.

Interdiscip Toxicol. 2010 Mar;3(1):3–14.

150. Truscott RJW, Friedrich MG. The etiology of human age-related cataract. Proteins don't last forever. Biochim Biophys Acta. 2016 Jan;1860(1 Pt B):192–8.

151. Srivastava OP, Srivastava K, Chaves JM, Gill AK. Post-translationally modified human lens crystallin fragments show aggregation in vitro. Biochem Biophys Rep. 2017 Jul;10:94–131.

152. Asthana A, Kisaalita WS. Biophysical microenvironment and 3D culture physiological relevance. Drug Discov Today. 2013 Jun;18(11-12):533–40.

153. Gjorevski N, Sachs N, Manfrin A, Giger S, Bragina ME, Ordóñez-Morán P, et al. Designer matrices for intestinal stem cell and organoid culture. Nature. Nature Publishing Group; 2016 Nov 16;:1–17.

154. Ehrbar M, Rizzi SC, Schoenmakers RG, San Miguel B, Hubbell JA, Weber FE, et al. Biomolecular hydrogels formed and degraded via site-specific enzymatic reactions. Biomacromolecules. 2007 Oct;8(10):3000–7.

155. Zhang J, Skardal A, Prestwich GD. Engineered extracellular matrices with cleavable crosslinkers for cell expansion and easy cell recovery. Biomaterials. 2008 Dec;29(34):4521–31.

156. WEB_Rev_C_PEGSSDA_Vial_Datasheet.pdf [Internet]. esibio.com. [cited 2017 Dec 12]. Available from: https://www.esibio.com/media/wysiwyg/esibio/documents/WEB_Rev_C_PEGSSDA_Vial_Datasheet.pdf

157. a6982bul.pdf [Internet]. http://www.sigmaaldrich.com/catalog/product/aldrich/757845?lang=en&region=AU. [cited 2017 Dec 12]. Available from: https://www.sigmaaldrich.com/content/dam/sigma-aldrich/docs/Sigma/Bulletin/a6982bul.pdf

158. Sherman MH, Yu RT, Tseng TW, Sousa CM, Liu S, Truitt ML, et al. Stromal cues regulate the pancreatic cancer epigenome and metabolome. Proc Natl Acad Sci USA. 2017 Jan 31;114(5):1129–34.

159. Vendra VPR, Khan I, Chandani S, Muniyandi A, Balasubramanian D. Gamma crystallins of the human eye lens. Biochim Biophys Acta. 2016 Jan;1860(1 Pt B):333–43.

160. Bott K, Upton Z, Schrobback K, Ehrbar M, Hubbell JA, Lutolf MP, et al. The effect of matrix characteristics on fibroblast proliferation in 3D gels. Biomaterials. 2010 Nov;31(32):8454–64.

161. Mathew MC, Ervin A-M, Tao J, Davis RM. Antioxidant vitamin supplementation for preventing and slowing the progression of age-related cataract [Internet]. Cochrane Eyes and Vision Group, editor. Vol. 90, Cochrane Database of Systematic Reviews. 2012 [cited 2018 Mar 27]. p. 847. Available from:

http://doi.wiley.com/10.1002/14651858.CD004567.pub2

162. Cruz-Acuña R, Quirós M, Farkas AE, Dedhia PH, Huang S, Siuda D, et al. Synthetic hydrogels for human intestinal organoid generation and colonic wound repair. Nat Cell Biol. 2017 Oct 23;19(11):1326–35.

163. Fujii N, Takata T, Fujii N, Aki K. Isomerization of aspartyl residues in crystallins and its influence upon cataract. Biochim Biophys Acta. 2016 Jan;1860(1 Pt B):183–91.

164. Lampi KJ, Wilmarth PA, Murray MR, David LL. Lens β-crystallins: the role of deamidation and related modifications in aging and cataract. Prog Biophys Mol Biol. 2014 Jul;115(1):21–31.

165. Thompson J, Lakhani N. Cataracts. Prim Care. 2015 Sep;42(3):409–23.

166. Obrosova IG, Chung SSM, Kador PF. Diabetic cataracts: mechanisms and management. Diabetes Metab Res Rev. 2010 Mar;26(3):172–80.

167. Kato S, Shiokawa A, Fukushima H, Numaga J, Kitano S, Hori S, et al. Glycemic control and lens transparency in patients with type 1 diabetes mellitus. Am J Ophthalmol. 2001 Mar;131(3):301–4.

168. Pollreisz A, Schmidt-Erfurth U. Diabetic cataract-pathogenesis, epidemiology and treatment. J Ophthalmol. 2010;2010:608751.

169. Kador PF, Wyman M, Oates PJ. Aldose reductase, ocular diabetic complications and the development of topical Kinostat(®). Prog Retin Eye Res. 2016 Sep;54:1–29.

170. Gesell LB, Trott A. De novo cataract development following a standard course of hyperbaric oxygen therapy. Undersea Hyperb Med. 2007 Nov;34(6):389–92.

171. Freel CD, Gilliland KO, Mekeel HE, Giblin FJ, Costello MJ. Ultrastructural characterization and Fourier analysis of fiber cell cytoplasm in the hyperbaric oxygen treated guinea pig lens opacification model. Exp Eye Res. 2003 Apr;76(4):405–15.

172. Löfgren S. Lenses from Brown-Norway pigmented rats are more tolerant to in vitro ultraviolet irradiation than lenses from Fischer-344 albino rats. Acta Ophthalmol. 2012 Mar;90(2):179–83.

173. Chowdhury A, Choudhury A, Chakraborty S, Ghosh A, Banerjee V, Ganguly S, et al. p-Benzoquinone-induced aggregation and perturbation of structure and chaperone function of α-crystallin is a causative factor of cigarette smoke-related cataractogenesis. Toxicology. 2018 Feb 1;394:11–8.

174. Barnes S, Quinlan RA. Small molecules, both dietary and endogenous, influence the onset of lens cataracts. Exp Eye Res. 2017 Mar;156:87–94.

175. Yu S, Chu Y, Li G, Ren L, Zhang Q, Wu L. Statin use and the risk of cataracts: a systematic review and meta-analysis. J Am Heart Assoc. 2017 Mar

20;6(3).

176. Souza VBNE, Moura Filho FJR de, Souza FG de ME, Rocha CF, Furtado FAML, Gonçalves TBA, et al. Cataract occurrence in patients treated with antipsychotic drugs. Rev Bras Psiquiatr. 2008 Sep;30(3):222–6.

177. Alam MS, Praveen Kumar KV. Clozapine-induced cataract in a young female. J Pharmacol Pharmacother. 2016 Oct;7(4):184–6.

178. Li J, Xia C-H, Wang E, Yao K, Gong X. Screening, genetics, risk factors, and treatment of neonatal cataracts. Birth Defects Res. 2017 Jun 1;109(10):734–43.

Appendix A Publication

Light-focusing human micro-lenses generated from pluripotent stem cells model lens development and drug-induced cataract in vitro

Patricia Murphy*, Md Humayun Kabir*, Tarini Srivastava*, Michele E. Mason*, Chitra U. Dewi, Seakcheng Lim, Andrian Yang, Djordje Djordjevic, Murray C. Killingsworth, Joshua W. K. Ho, David G. Harman and Michael D. O'Connor.

*equally contributing authors